University of Alberta

Investigation of osteogenic and adhesive properties of Rosette nanotubes

by

Rahul Agrawal

A thesis submitted to the Faculty of Graduate Studies and Research
in partial fulfillment of the requirements for the degree of

Master of Science
in
Biomedical Sciences

Department of Biomedical Engineering

Fall 2013, Edmonton, Alberta

ABSTRACT

This thesis is focussed on bone tissue engineering for improving the osseointegration of joint implants. We have incorporated nano-scaled materials called as Rosette Nanotubes (RNTs) which mimic the geometry of the natural components of bone with the growth factor, Bone Morphogenetic Protein-7 (BMP-7). In particular, short peptide sequences were identified from BMP-7 (SNVILKKYRN, KPSSAPTQLN, and KAISVLYFDDS) and were linked with Twin K1 RNTs. The first stage of our study was focused on the purification and characterization of these short peptides co-assembled with RNTs using HPLC (High Performance Liquid Chromatography) and their characterization by SEM (Scanning Electron Microscopy) respectively. The Second stage involved cyto-compatibility studies of the RNTs. The third stage involved the adhesion studies of RNTs coated on different substrates. The fourth and final stage was the osteogenic differentiation studies of these materials. Results have shown that the HPLC purification yield was 12-20% and SEM characterization showed the presence of successfully assembled nanotubes. Coating of RNTs on different substrates has shown a significant increase in adhesion of human Bone Marrow Stromal Cells (hBMSCs) on tissue culture treated plates and non-tissue culture treated plates. Moreover, peptide co-assemblies with Twin K1 RNTs have shown a significant increase in specific ALP (Alkaline phosphatase) activity. In summary, Twin K1 RNTs and peptide co-assembled RNTs have shown promising results for improving the cell adhesion on plastic substrates (treated and non-treated plates). Moreover, peptide co-assembled RNTs have shown early signs of osteogenic differentiation.

Acknowledgements

I would like to thank my examination committee members Drs. Hasan Uludağ, Nadr Jomha, Robert Burrell and Hicham Fenniri.

I would like to thank Dr. Mounir-El-Bakkari for synthesizing Twin K1; Dr. Jae-Young Cho for performing the Scanning Electron Microscopy studies; Alaaeddin Alsbaiee for synthesizing the peptide and Mono K1; Dr. Takeshi Yamazaki for performing the modeling studies; Dr. Rachel Beingessner for suggestions in thesis writing, Dr. Mike Xia for training the HPLC, Laura Rose and Cezary Kucharski for training me.

I was fortunate to work in the labs of Drs. Hicham Fenniri and Hasan Uludağ. I would like to thank the members of both the research groups for their kindness, assistance and friendship: Zhimin Yan, Wei-Zheng Shen, Venkatakrishnan Paramasarthi, Liang Shuai, Belete Legesse, Mohammad R. Hassan, Uyen Ho, Kumakshi Sharma, Zhaoyi Qin, Abdullah Alshememry, Hamidreza Aliabadi, Charlie Hsu, Breanne Landry, Perveen Mehdipoor, Basak Sahin, Juliana Valencia and Hilal Gul-Uludag

Most of all, I wish to express my gratitude towards my Supervisor, Dr. Hicham Fenniri and my Co-supervisor, Dr. Hasan Uludağ for their assistance and kind guidance.

Being a firm believer of God, I offer my great regards to the almighty who has helped me to reach this stage in life.

Last but much importantly, I would like to thank my most sincere heart-filled respect and regards to my elder brother, Kapil Agrawal and my parents, Dr. Mahesh Agrawal and Mrs. Shail Agrawal.

Rahul Agrawal

TABLE OF CONTENTS

LIST OF TABLES

Page No.

LIST OF FIGURES

Page No.

List of abbreviations

AB	aminobutyl
AFM	Atomic Force Microscopy
ALP	Alkaline phosphatase
AVN	Avascular Necrosis
BMP-7	Bone Morphogenetic Protein-7
CDH	Congenital dislocation of the hip joint
CNF	Carbon Nanofibres
CNT	Carbon Nanotubes
CoCrMo	Cobalt-chromium-molybdenum
HA	Hydroxyapatite
hBMSCs	Human Bone Marrow Stromal Cells,
HPLC	High Performance Liquid Chromatography
K	Lysine
KRSR	Lysine-arginine-serine-arginine
LC-MS	Liquid chromatography-mass spectroscopy
OA	Osteoarthritis
ON	Osteonecrosis
PGA	Polyglycolide
pHEMA	Poly(2-hydroxyethylmethacrylate)
PLA	Polylactide
PLGA	Poly-lactide-co-glycolide
PMMA	Polymethylmethacrylate

RA	Rheumatoid Arthritis
RNT	Rosette Nanotubes
rhBMP-7	recombinant human Bone Morphogenetic Protein-7
SEM	Scanning Electron Microscopy
SWCNTs	Single-wall Carbon Nanotubes
MWCNTs	Multi-wall Carbon Nanotubes
TCP	Tricalcium Phosphate
TGF- β	Transforming Growth Factors-β
Ti	Titanium
UV-Vis	Ultraviolet-Visible spectroscopy
ZnO	Zinc oxide
μg	microgram

1) INTRODUCTION

The painful and crippling disability caused by bone defects has been a problem on a global level. Mal-aligned defects can be due to numerous causes such as traumatized and maligned joints, osteoarthritis (OA), rheumatoid arthritis (RA), avascular necrosis (AVN) or osteonecrosis (ON), congenital dislocation of the hip joint (CDH), joint stiffness and osteoporosis. If possible, doctors prescribe less painful non-invasive techniques. However, when such non-invasive techniques are unable to alleviate the severe joint pain of the dysfunctional joint, a joint replacement surgery is carried out.

It is more commonly carried out with knees and hip-joints. In some cases shoulder and ankle replacements (though far less common as compared to knee and hip-replacements) are carried out. Joint replacement involves replacement anthroplasty, which is an orthopaedic procedure in which the arthritic or dysfunctional joint surface is replaced with an orthopaedic prosthesis.

In order to fairly assess the wide-spread nature of the problem, we begin with some statistical data of the yearly joint-replacement surgeries within Canada.

1.1) STATISTICS OF HIP AND KNEE REPLACEMENT SURGERIES IN CANADA

According to the Canadian Joint Replacement Registry, 13,900 total knee replacements and 10,044 total hip replacement surgeries were performed in 2003-04. These numbers rose to 22,545 total knee replacements and 15,953 total hip replacements in 2009-10 (Joint replacements, 2000)). These figures suggest that the number of patients undergoing knee and hip

replacement surgeries have been increasing over time. In addition, with the aging population these numbers are projected to rise in the near future.

1.2) HISTORY OF JOINT REPLACEMENT SURGERY

The earliest records of a hip replacement surgery were accounted in 1891 by Dr. T Gluck who used ivory to replace a femoral head (Gomez PF, 2005). Later, Maurice Down introduced a variety of titanium orthopaedic fracture devices such as plates and screws in the 1950s (Historical Perspective of Metallic Implants, 2010). A significant breakthrough occurred in 1960s after the introduction of the ultra-low friction cemented arthroplasty by John Charnley (Charnley J, 1960). Since then, titanium has been extensively used in biomedical implants owing to its biocompatibility and surface energy (Raines AL, 2010).

Although joint replacement surgeries improve the quality of life for patients, traditional implant materials like titanium and titanium alloys used for joint replacement have certain shortcomings such as the lifespan of current artificial joint implants is about 10~15 years on average (Emery DFG, 1997) and thus younger and more active patients such as men under 60 years of age and women under 55 years of age receiving joint replacements will inevitably need more than one revision surgery in their lifetime. For example, in 2009-10, among the 15,953 total hip replacement surgeries reported in Canada; 10.8% of these were revision surgeries. In addition, among the 22,545 total knee replacement surgeries, 6.2% of these were revision surgeries (Joint replacements, 2000)). Moreover, joint replacement surgery is a costly affair; a total knee replacement is $18,000-$20,000 or more (Desai A, 2013). Overall, due to higher number of elderly patients and the relatively high percentage of revision procedures performed around the world, it is vital to develop a new class of bone substituting materials which can

restore bone functions with lengthening the lifetime of current implants while speeding the recovery and minimizing the revision procedures. However, before we discuss about the bone substitutes, it is important to understand the structure of bone.

1.3) STRUCTURE OF BONE

The structure of natural bone has been shown in Figure 1.1. Bone is composed of tissues that have micron-structured features as well as nano-features (Huinan L, 2007). Bone tissue is a type of dense connective tissue. The hierarchical structure of human bone has three levels. First, the macrostructure includes cancellous bone as well as cortical bone. Second, the microstructure includes lamellae, cells, osteons and harvesian systems. Last, nanostructure level includes non-collagenous proteins, fibrillar collagens and embedded calcium phosphate minerals. The contents of bone in terms of their weigh percentage are summarized in Table 1.1 (Ji B, 2004)(Bhowmik R, 2007). Table 1.1 shows that hydroxyapatite constitutes the greater proportion of a bone's weight followed by collagen, water, ions and non-collagenous proteins.

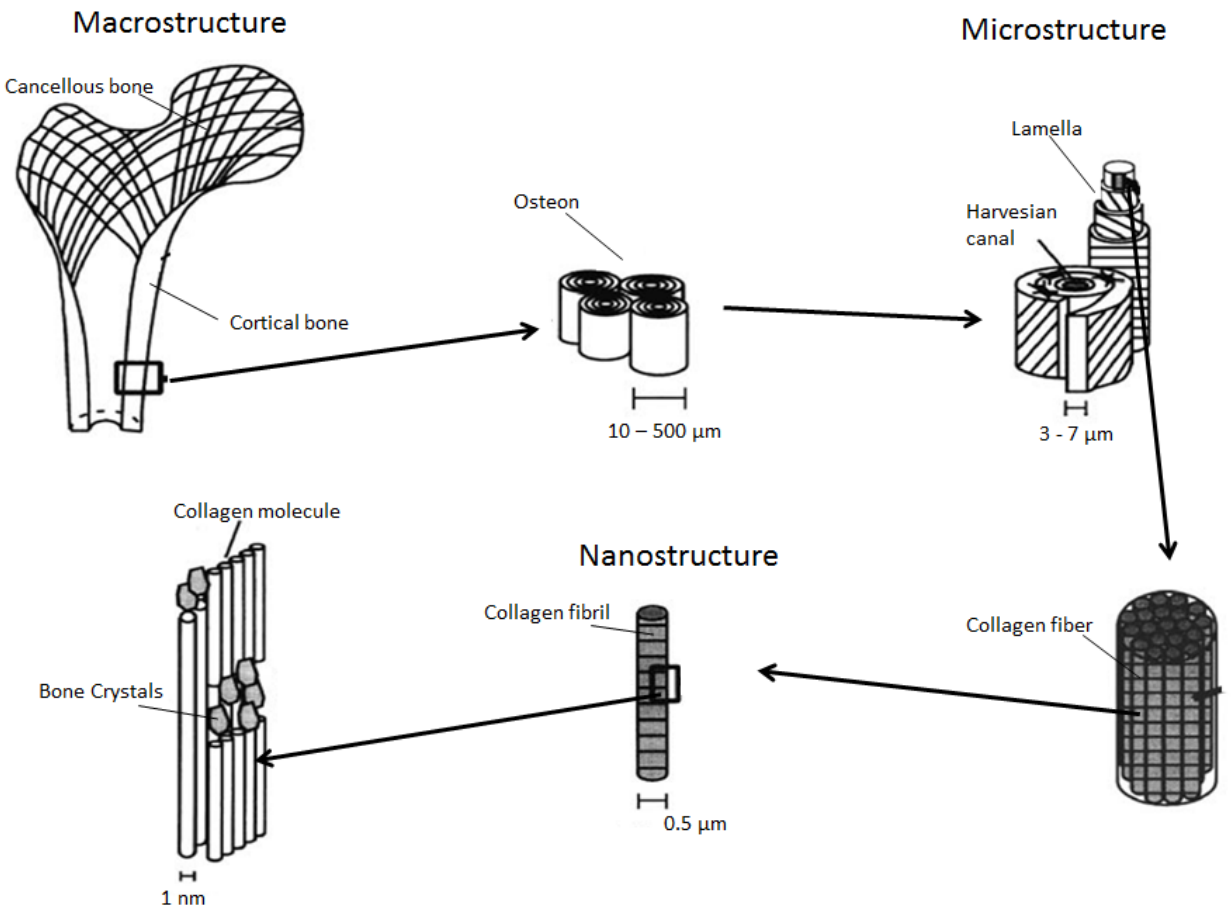

Figure 1.1 Schematic structure of a human femur, adapted and redrawn from (Liu H, 2007) License number 3214940709553 © Elsevier publications.

Components	Weight percentage
Hydroxyapatite (Inorganic)	60
Collagen (Organic)	20
Water	9

Ions and Non-collagenous proteins	11

Table 1.1 Bone Composition (adapted and redrawn from reference (Ji B, 2004)(Bhowmik R, 2007))

Vascular network in the bone marrow supply the mesenchymal stem cells or hematopoietic cells which have the capacity to differentiate into osteoblasts, osteocytes, endothelial cells, fibroblasts and osteoclasts (Webster TJ, 2001). Under the influence of growth factors, cytokines and proteins present in the physiological bone matrix, cells can be activated for bone regeneration. Bone and cartilage are living systems and thus a variety of cells such as osteoblasts in the bone and chondrocytes in the cartilage grow in the extracellular matrix. In this manner, the extracellular matrix supports mechanical forces, provides space for cells, and provides an environment suitable for cell attachment and nutrition exchange. In addition, osteoblasts and chondrocytes must adhere to a surface in order to generate cell migration, proliferation, differentiation and long-term functions (Dunn GA, 1982)(Mizuno K, 2008)(Lu H, 2009). With the growing knowledge of bone's structure and nanomaterials, researchers have become successful in making materials with at least one dimension lesser than 100 nanometer having unique physical, chemical, mechanical and biological properties which can mimic the properties of natural bone.

1.4) IDEAL REQUIREMENTS OF IMPLANT MATERIALS

An ideal implant should replace the bone defects and provide a framework to regenerate and heal host bone and orthopaedic soft tissue around it. Implants should also have sufficient mechanical strength to connect severed fractured bone segments, severed cartilage, blood vessels, nerves and other soft tissue to eventually support physiological loads. Moreover,

implants should have a suitable surface chemistry to successfully integrate into the host tissue. In other words, they should be biocompatible and encourage new tissue growth, not just bone and cartilage, but also blood vessels, nerves, etc (Balasundaram G, 2007).

1.5) COMPLICATIONS LEADING TO IMPLANT FAILURE

Potential reasons for joint-implant revision surgeries can be broadly divided into three major categories: patient-related factors, implant-related factors and failures related to inadequate surgical technique (Wroblewski B M, 1984)(Berry DJ, 2002)(Ong A, 2002). In regards to the limitations of implant materials, there are many complications that may results in a failure. In the following sections, complications leading to implant failures are discussed in greater detail.

Osseointegration is the formation of direct structural and functional bone-to-implant contact area under load and is critical to preventing implant failure (Branemark PI, 1983). Insufficient osseointegration can be caused by many reasons such as the formation of fibrous tissue capsule due to the excessive secretion of fibrous tissue from inflammatory cells (Ratner, 2002)(Webster TJ, 2001)(Castner DG, 2002). Figure 1.2 shows the cascade of cellular events that occur after inserting a biomaterial into a surgical site which could lead to inflammation and infection (Ratner BD, 2002). As shown in the Figure 1.2, neutrophils and macrophages arrive at the injury site and begin to attempt to phagocytize the implanted material. When they fail to engulf the large mass, they fuse together to form giant cells and seperatethe biomaterial from the neighbouring tissues. At the same time, these giant cells send out chemical messengers such as cytokines to recruit other cells. Right after, fibroblasts secrete collagen which comprises the

extra-cellular matrix of the soft tissue. The final stage is the complete encapsulation of the implant in an acellular, avascular collagen bag about 50-200 micrometers thick (Castner DG, 2002). The fibrous capsule prevents sufficient bonding between an implant surface, juxtaposed bone and frequently leads to clinical failure of orthopaedic implants. Consequently, repelling fibroblasts cause an inflammatory reaction at the surface of the newly implanted orthopaedic device (Webster TJ, 2001).

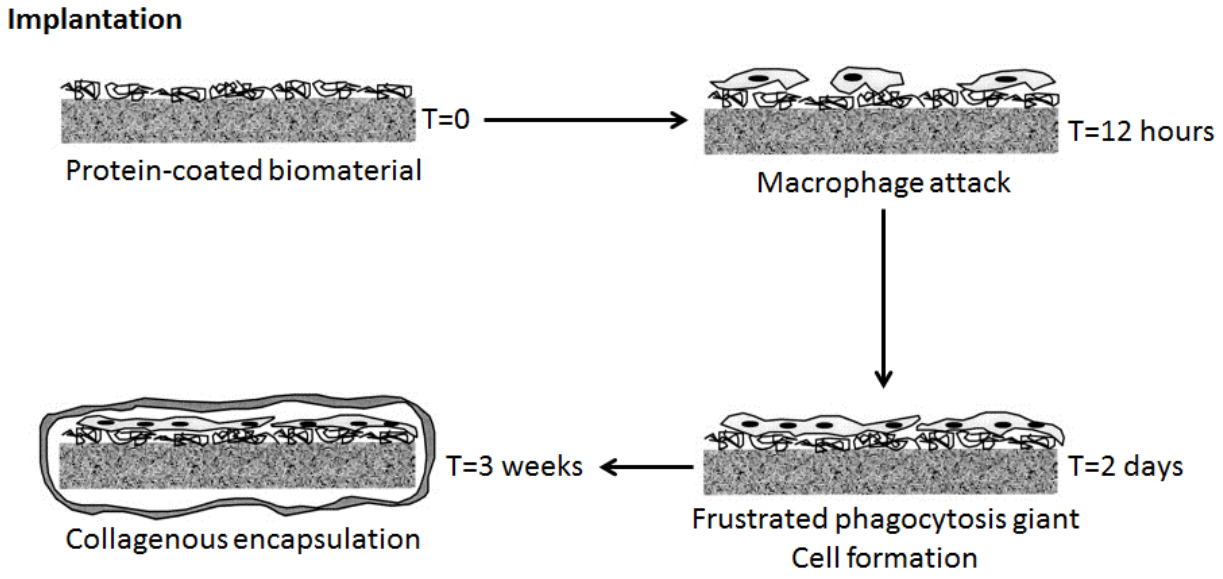

Figure 1.2) The time course and generalized reactions that comprise the foreign body reaction adapted and redrawn from (Ratner BD, 2002) license number 3214950159707 © Elsevier publications.

Another factor influencing osseointegration is material surface roughness (Esposito M, , 1998) (Esposito M, 1998). Recent studies have shown that the surface roughness affect the rate of osseointegration and biomechanical fixation (Wennerberg A, 1998) (Webster TJ, 1999). Since

traditional orthopaedic implant materials like metals, ceramics, polymers and composites have only been chosen for implantation based on their mechanical properties and biological inertness, there has not been a large emphasis concerning biomaterial chemical and surface properties to date. Therefore, a variety of implant failures originating from insufficient osseointegration and stress-strain imbalances have frequently taken place when using such conventional materials in orthopaedic applications.

Osteolysis refers to an active resorption of bone matrix by osteoclasts as part of an ongoing disease process which can result in implant instability and failure. Sometimes osteolysis can be induced by the wear particles from implant materials (Zhu YH, 2001) (Harris WH, 1995) (David V, 2007) (Bronson JG, 1999). Generally, the wear debris originates from implant materials like metals, ceramics and polymers like polyethylene. These wear particles appear most commonly at the bearing implant surface but are also at the host-implant or implant-implant interfaces. Figure 1.3 gives a schematic diagram of wear debris leading to implant loosening and its failure (Musib MK, 2011). Eileen Inghama *et al* have proposed that macrophages could be responsible for stimulating osteolysis as shown in Figure 1.4 (Inghama E, 2005). Figure 1.4 shows the formation of inflamed periprosthetic membrane rich in macrophages, cytokines and implant-derived wear particles which lead to the activation of osteoclats (Inghama E, 2005).

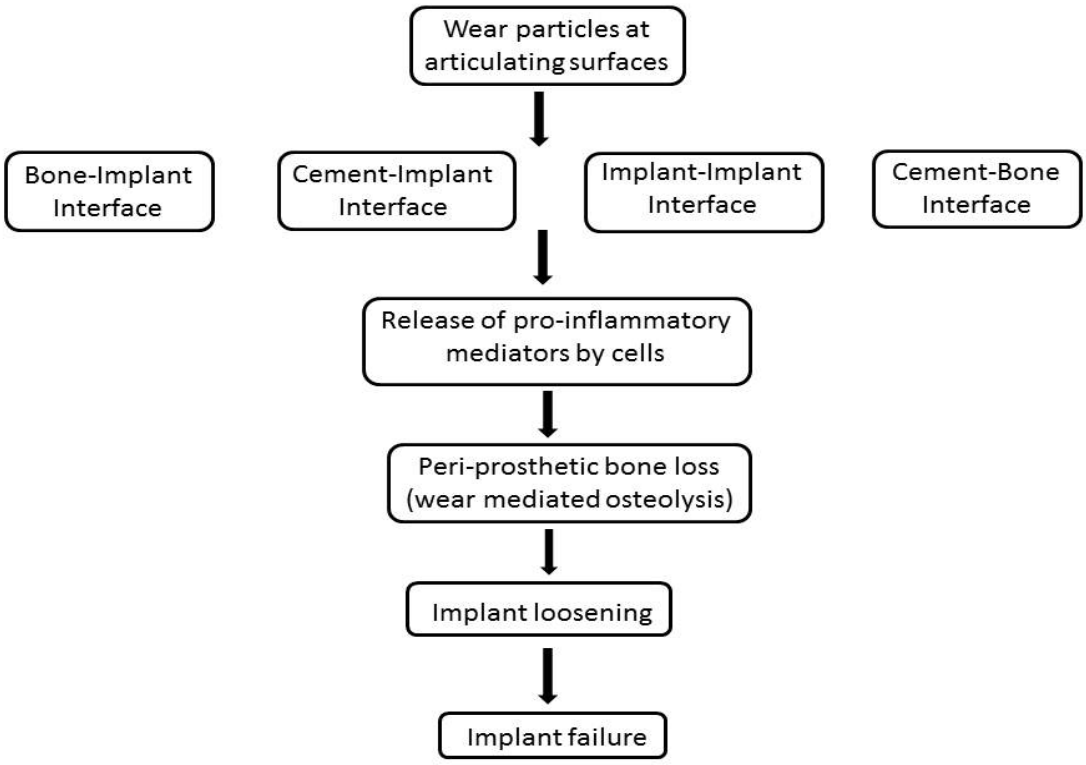

Figure 1.3) Schematic showing the generation and release of wear debris at the articulating surface and the cascade of events at the periprosthetic region eventually leading to wear-mediated osteolysis and implant failure, adapted and redrawn from (Musib MK, 2011)

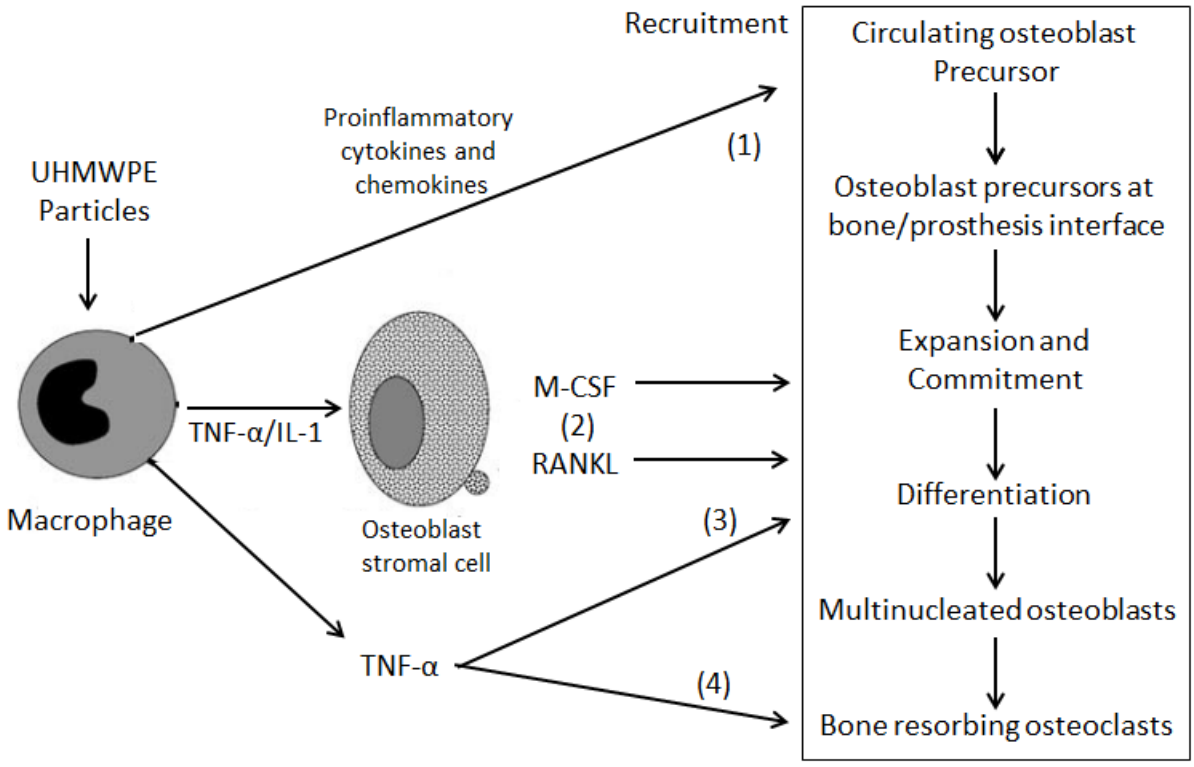

Figure 1.4 Potential mechanisms whereby UHMWPE particle-stimulated macrophages may stimulate osteolysis in total joint replacement. There are several potential pathways whereby macrophages, activated by particles in the periprosthetic membrane may contribute to osteolysis. (1) The milieu of inflammatory cytokines and chemotactic factors generated may lead to an increased recruitment of haematopoietic osteoclast precursors from the vasculature. (2) Macrophage TNF-α/IL-1 production may lead to enhanced M-CSF and RANKL expression by osteoblasts/ stromal cells leading to the expansion, commitment and differentiation of osteoclast precursors into mature osteoclasts. (3) TNF- α may augment the differentiation of osteoclast precursors in the presence of basal levels of RANKL-signalling by stromal cells. (4) TNF- α may activate mature osteoclasts to resorb bone. It is possible that all of these mechanisms are relevant *in vivo*. The evidence for a role for TNF- α is substantial. (This figure was adapted and redrawn from (Ingham E, 2005)) License number 3214890826237 © Elsevier publications.

One of the approaches to prevent osteolysis is to reduce the generation of wear particles. Recently, scientists have investigated wear-resistant bearing implant materials in order to reduce the production of wear particles such as metal-on-metal, ceramic-on-ceramic or ceramic-or-polyethylene implant (D'Antonio J, 2005) (Learmonth ID, 2007).

In addition to these conventional materials, researchers have started exploring materials with natural chemistries and structural similarities to bone and cartilage to develop a new generation of biocompatible and bio-integrated implants which can restore tissue growth as occurs in a natural process.

Moreover, to improve cellular adhesion, proliferation and long-term functions at orthopaedic implantation sites researchers have started immobilizing recombinant proteins or peptides onto nanostructured implants (Simank HG, 2006) (Balasundaram G, 2006) (Gavenis K, 2006) (Abarrategi A, 2008) (Shi X H. J., 2006).

In this manner, several bone-related growth factors (which are produced by bone cells and stored in the bone matrix) have been used to induce bone formation either through injection or implant surface medication. These include fibroblast growth factors, insulin-like growth factors I and II, platelet-derived growth factors and TGF- β (Transforming Growth Factors-β) and bone morphogenetic proteins (Harris WV, 1996) (Lind M, 1995) (Wang JS, 1996).

1.6) BONE MORPHOGENETIC PROTEIN SHORT PEPTIDES

Transforming growth factor beta (TGF-β) is a protein that controls proliferation, cellular differentiation, and other functions in most cells. It is a type of cytokine which plays a role in immunity, cancer, heart disease, Diabetes, Marfan syndrome, Loeys-Dietz syndrome,

Parkinson's disease and AIDS (Schoenhoff FS, 2009). The TGF-β family is part of a superfamily of proteins which includes inhibins, activin, anti-müllerian hormone, bone morphogenetic protein, decapentaplegic and Vg-1. Among many sub-classes of BMPs, BMP-7 (Bone morphogenetic protein 7 also known as osteogenic protein-1 or OP-1) is a protein that is encoded by the *BMP7* gene in humans. It plays a key role in the transformation of mesenchymal cells into bone and cartilage. It is inhibited by noggin and a similar protein, chordin, which are expressed in the Spemann-Mangold Organizer. BMP-7 may be involved in bone homeostasis. It is expressed in the brain, kidneys and bladder. BMP-7 induces the phosphorylation of SMAD1 and SMAD5, which in turn induce transcription of numerous osteogenic genes. It has been demonstrated that BMP-7 treatment is sufficient to induce all of the genetic markers of osteoblast differentiation in many cell types (Hahn GV, 1992) (Chen D, 2004) (Itoh F, 2001).

BMPs possess several hundred amino acids which make them too large and complex to chemically functionalize onto nano-structured materials. Therefore, it is important to identify smaller bioactive regions of BMPs. Some researchers have found that short peptide sequences of BMPs also improve osteoblast growth. For example, a synthetic peptide (KIPKASSVPTELSAISTLYL) derived from "knuckle epitope" in BMP-2 has increased alkaline phosphatase activity in osteoblasts (Saito A, 2003). Moreover, a short sequence of BMP-7 (AISVLYFDDSSNVILKKYRN) improves the mineralization process in osteoblasts. Therefore, when the structures of BMP-2 and BMP-7 were compared, certain bioactive areas were similar in function with the BMP type II receptor and amino acid sequence as shown in Figure 1.5 (Chen Y, 2009)

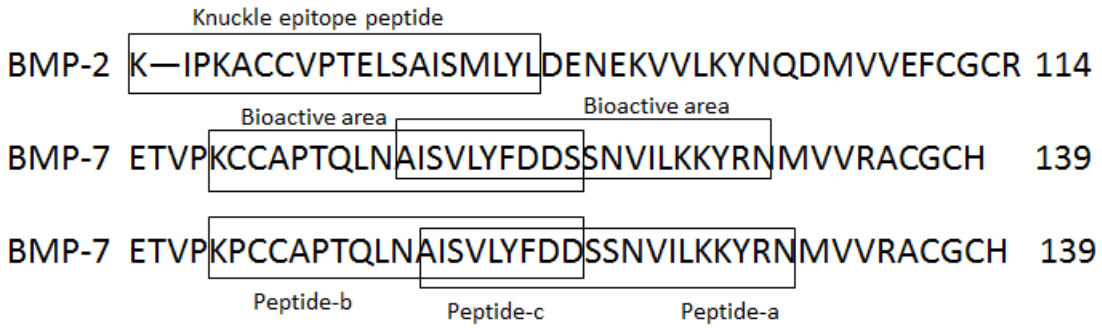

Figure 1.5 The comparison of the bioactive areas in BMP-2 and BMP-7 (adapted and redrawn from (Chen Y, 2009) Licencse number 3214931144003 © John Wiley and Sons.

In addition, BMPs form dimers and bind to receptor type I and II on the cell surfaces to initiate cellular activities (J M., 1998). Studies have determined that the region around the "knuckle epitope" (KIPKASSVPTELSAISTLYL) of BMP-2 binds the receptor type II complex with receptor type I on osteoblasts, to initiate signal transduction (Saito A, 2003). After making a comparison of the structures of BMP-2 and BMP-7, peptide A, B, C is at a similar region in BMP-7 as the knuckle epitope in BMP-2 as shown in Figure 1.6 (Chen Y, 2009). Webster *et al* have demonstrated that osteoblasts treated with BMP-7 short peptides like peptide A, B and C have similar alkaline phosphatase, total protein content but significantly higher calcium concentration compared with BMP-7 (Chen Y, 2009). Because of the prospective utility of short peptides in bone regeneration they could be physisorbed on implants materials to improve their properties.

Figure 1.6 Comparison of BMP-2 (left) and BMP-7 (right) structures (adapted from (Chen Y, 2009) License No. 3212730287691 © John Wiley and Sons

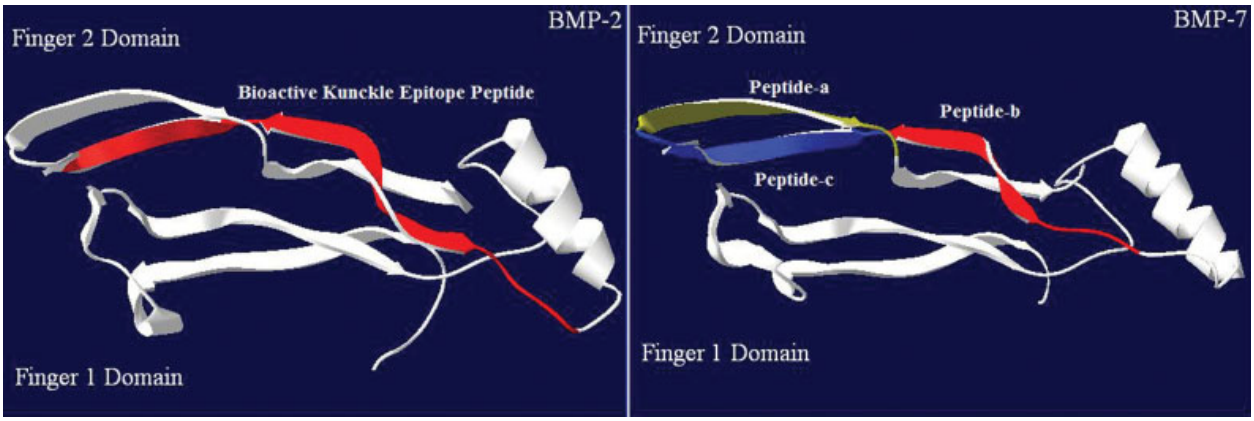

1.7) MATERIALS USED AS IMPLANTS

Since natural bone has nanostructured features, nano-featured biomaterials are expected to represent biomimetic features and suitable physiochemical properties in promoting bone cell functions as well as guiding tissue regeneration. Figure 1.7 shows the representation of events at the bone implant interface (Puleo DA, 1999). In the following paragraphs, the various materials used as implants are described.

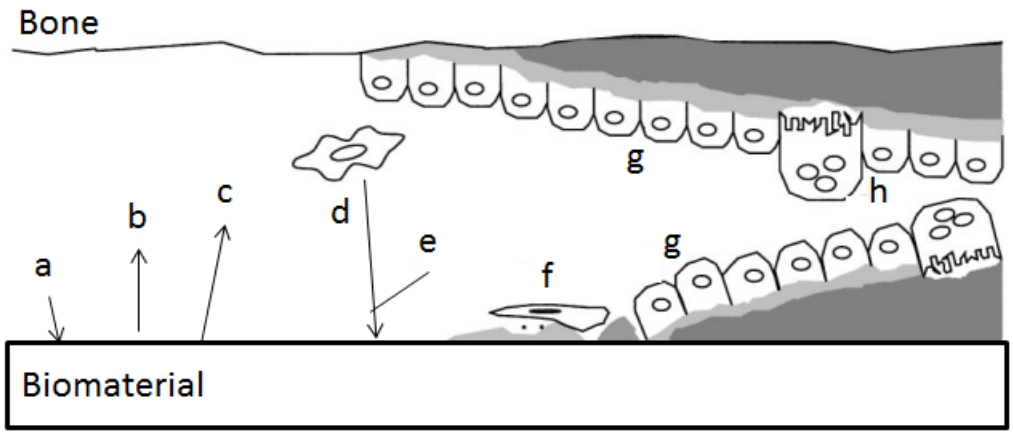

Figure 1.7) Representation of events at the bone implant interface. (a) Protein adsorption from blood and tissue fluids, (b) protein desorption, (c) surface changes and material release, (d) inflammatory and connective tissue cells approach the implant, (e) possible targeted release of matrix proteins and selected adsorption of proteins such as BSP and OPN, (f) formation of *lamina limitans* and adhesion of osteogenic cells, (g) bone deposition on both the exposed bone and implant surfaces, (h) remodeling of newly formed bone (adapted and redrawn from (Puleo DA, 1999) License number 3212680003116 © Elsevier publications.

Materials for bone tissue engineering and orthopaedic applications can be made of ceramics, polymers, metals, organic materials and composites. In regards to nanomaterials synthesis, numerous top-down and bottom-up nanofabrication technologies (such as electrospinnig, phase separation, self-assembly processes, thin film deposition, chemical vapor deposition, chemical etching, nano-imprinting, photolithography, electron beam or nanosphere lithographies) have been used to create ordered or random nanotopographies (Freeman JW, 2008). By synthesizing materials at the nanoscale, it dramatically increases the surface area, surface roughness or surface area to volume ratios which may lead to higher surface reactivity with many superior physicochemical properties like mechanical, electrical, optical, catalytic and magnetic properties (Fahlman BD, 2007).

1.7.1) METALS AND METAL ALLOYS

Metals and alloys offer extremely strong mechanical properties. Most common materials used are titanium and CoCrMo. Titanium and titanium based alloys are highly biocompatible

with little toxicity due to the natural formation of an oxide layer. Therefore, a few methods have been employed by researchers to transform current titanium into that which increases tissue growth by possessing nano-features. One of the common ways is via chemical etching which is a process of treating titanium with strong acids. It has been found that chemical etching dramatically improves the bioactivity of typical adhesive proteins like fibronectin and vitronectin to accelerate cell attachment and proliferation (Raimondo T, 2010) (Bosco R, 2012). Although the etching produces nano-rough features on titanium at low cost with little equipment, the process and resulting surface features are not controllable and are often quite random. In contrast, using Temescal Electron Beam Evaporator is a complex system that produces desirable thickness and exact nano-rough morphologies on metals (Raimondo T, 2010).

Another emerging and promising technique to create nano-features on titanium is anodization. Anodization is an electrochemical method and is widely used as a surface modification technique for metals to produce protective oxidative layers under acidic conditions (Siegel RW, 1995). An *in vitro* study provided evidence of enhanced adhesion of mesenchymal stem cells cultured on anodized titanium compared with unanodized titanium (Bertoncini P, 2012) (Webster BE, 2007). Moreover, *in vivo* studies have also demonstrated the use of anodized titanium for orthopaedic applications. For example, anodized titanium screws have been inserted into rabbit tibia and allowed to penetrate one cortical layer. After 6 weeks, histology stains showed bone tissue formation on the nanostructured titanium implant surfaces that had an oxide thickness of more than 600 nm (Sul YT J. C., 2002). A set of similar experiments were conducted in sheep and rat using anodized screws or rods inserted for 4 to 12 weeks and showed that the anodized titanium implants had excellent cytocompatibility properties and an ability to quickly grow bone next to the implant (Ishizawa H, 1995) (Giavaresi GFM, 2003). Moreover, no

infection or inflammatory responses were observed around the anodized nanotubular titanium screws. In addition, anodization takes less than an hour and is an inexpensive technique to modify the surfaces of titanium for improving bone cell functions for orthopaedic applications. Since the nano-modification of metals occurs only on the surface of metals, the mechanical properties of metals remain a concern. Although the bulk metal will not degrade, ion release or the degradation of the modified surface could create a toxic environment. For example, anodized titanium surface increases the fluoride content which could be detrimental to neighbouring cartilage cells (Gong D, 2001).

1.7.2) NANOCOMPOSITES AND NANOCERAMICS

Ceramics are non-metallic inorganic materials which have excellent cytocompatibility properties and a high degree of biodegradability in the physiological environment. According to the tissue response in an osseous environment, ceramics can be classified into three groups: bioactive ceramics (such as HA (hydroxyapatite), tricalcium phosphate (TCP), bioglasses, HA/TCP bi-phase ceramics, and glass-ceramics), biopassive ceramics (such as alumina, titania and zirconia), and biodegradable ceramics (such as TCP). As the grain size and the pore diameter are reduced, nanoceramics possess increased surface area, surface roughness and number of grain boundaries at the surface. For example, increased surface roughness and improved surface wettability are found in the material characterization studies of HA compared with conventional alumina and titania (Webster TJ, 2000). In zinc oxide (ZnO), atomic force microscopy (AFM) root-mean-square roughness values of nanophase and microphase ZnO were 32 and 10 nm respectively (TiO_2, 2006). In addition, 23 nm grain size alumina had

approximately 50% more surface area for cell adhesion than 177 nm grain size alumina; similarly, a 32 nm grain size titania had nearly 35% more surface area than that of a 2.12 μm grain size titania (Webster TJ, 1999). A nanophase ZnO compact had 25% more surface area than that of microphase ZnO (Colon G, 2006).

Furthermore, nanoceramics show excellent cytocompatibility. For example, nanophase hydroxyapatite has demonstrated increased adhesion and proliferation of bone marrow derived mesenchymal stem cells compared with conventional hydroxyapatite *in vitro* (Zhou GS, 2007). In addition, a nanophase hydroxyapatite and poly(lactide-co-glycolide) composite promotes human mesenchymal stem cell adhesion and osteogenic differentiation *in vitro* (Lock J, 2012). Recently, *in vivo* studies also demonstrated that a bioresorbable nanocrystalline HA was used as a valuable addition to TCP-HA (tricalciumphosphate-Hydroxyapatite) for acetabular bone grafting in animal models. In this study, HA paste resulted in better acetabular cup stability than pure allografts and at the same time did not cause adverse biological activity (Chris AJJ, 2006). Moreover, Desai *et al* have showed that nanophase alumina surfaces cause a 45% increase in marrow stromal cells adhesion, proliferation, viability, a 35% increase in alkaline phosphatase activity and a 50% increase in matrix production when compared with amorphous alumina (Ketul CP, 2007). A similar trend is observed with zinc oxide and titania. Overall, the wettability and special surface topography of nanophase ceramics could be the main reason for the observed promoted bone cell functions on nanoceramics. At the tissue-implant interface, the necessary step for success is the adsorption of specific proteins onto biomaterial surfaces (Webster TJ, 2001). Many researchers have demonstrated that the protein adsorption process depends on the surface properties such as hydrophilicity, charge density roughness and surface energy (Webster TJ, 2000).

Importantly, the mechanical properties of biomaterials should be considered as they play a critical role in the long-term success of orthopedic implants. A variety of nanocomposites such as zirconia-toughened alumina nanocomposites, ceria-stabilized tetragonal zirconia-alumina nanocomposites have been shown to promise as bearing materials with excellent cytocompatibility and low wear rates in order to prevent osteolysis. Overall, nanoceramics can offer significantly improved mechanical properties, good wear properties as well as excellent cytocompatibility compared to conventional ceramics (Affatato S, 2006) (Tanaka K, 2002) (Takemoto M, 2006).

1.7.3) NANO-FEATURED POLYMERS AND HYDROGELS

Both natural and synthetic polymers have been widely explored as biodegradable scaffold materials (Agrawal CM, 2001). Moreover, polymers also offer the advantage of having a tunable chemical composition, crytallinity, molecular weight, molecular weight distribution, controlled microstructure and macrostructure (Thomson RC, 1999) (Boccaccini AR, 2003) (Liu X, 2004). For example, PLGA (Poly-lactide-co-glycolide) is one of the most popular FDA approved polymers for orthopedic applications. Following that, there has been intensive development of medical devices composed of PGA (polyglycolide), PLA (polylactide) and their copolymers (Boccaccini AR, 2003).

Usually polymers that degrade via hydrolysis have a close relationship with molecular weight and degree of polymerization. Generally, a low molecular weight, higher surface area and surface energy allow nanostructured hydrogels to have better hydrolysis rates (Cooper SL, 2004).

However, weaker mechanical properties of PLGA and its acidic degradation by-products limit the applications of PLGA for tissue engineering.

Polymethylmethacrylate (PMMA) is another popular polymer used in orthopaedic applications as bone cements. Usually, it is injected into a line of the acetabular cups for smooth articulation with metallic femoral head components. At the same time, PMMA has some disadvantages too. PMMA suffers from fatigue-related cracking and impact induced breakage due to its poor setting and fixation (Unwin PS, 2001). PMMA also releases toxic monomers and causes osteolysis of the surrounding tissue by exothermic polymerization *in vivo* (Davidson JA, 1994) (Dunn MG, 1994). Another related polymer, poly(2-hydroxyethylmethacrylate) (pHEMA) was reported as a biocompatible polymer for tissue repair surgery, drug delivery and corneal implants (AS, Hydrogels for biomedical applications, 2002) (Schiraldi C, 2004) (Filmon RBM, 2002). pHEMA has suitable mechanical properties and ease of modification for diverse applications. In terms of its method of preparation, when pHEMA is bulk polymerized with low water content, a material with hardness similar to natural bone can be created (Filmon R G. F., 2002). In 2012, Ji Soo Choi *et al* have demonstrated that a polymer, BD™ PuraMatrix™ Peptide Hydrogel was used with human mesenchymal stem cells for functional recovery of following spinal cord hemisection in rats (Ji SC, 2012). Generally, for orthopedic applications, nano-featured, low water content and biocompatible polymers with good mechanical properties are the most suitable candidate such as pHEMA and nano-hydroxyapatite composites.

1.7.4) CARBON NANOTUBES AND NANOFIBERS

Carbon Nanotubes (CNTs) and Carbon Nanofibres (CNFs) have an excellent property of tenability. They can be synthesized from nanometer to millimeter lengths and 1-100 nanometer widths (Hata K, 2004) (Harrison BS, 2007). Moreover, CNTs and CNFs offer superior cytocompatibility, mechanical and electrical properties and they have been incorporated into natural and synthetic polymers as well as ceramics scaffolds for orthopaedic applications (Harrison BS, 2007) (Wei W, 2007) (Cui D, 2007) (Saito N, 2008) (Abarrategi A, 2008) (Shi XHJ, 2006). The CNTs and CNFs composites overcome poor mechanical properties of polymer or ceramic scaffolds, have improved electrical conductive properties which contribute to new bone formation under electrical stimulation and promising cytocompatibility (Elias KL, 2002) (Price RL W. M., 2003) (Zanello LP, 2006) (Sitharaman B, 2008) (Webster TJ, 2004) (Price RL E. K., 2004). CNTs and CNFs are known as one of the strongest while light-weight materials to reinforce bone tissue engineering scaffolds. For example, Joseph *et al* have shown that carbon nanotube based poly(lactic acid) nanofiber scaffold showed no adverse toxic effects when mesenchymal stem cells were cultured with the scaffold after 28 days at 37^{o}c (Joseph NM, 2011). In a similar manner, CNFs have been used as bone implant material reinforcements for HA. The resulting composite exhibits bending strengths similar to cortical bone (Cooper CA, 2002). In addition, they have been recently employed to enhance the mechanical properties of other materials such as poly(propylene fumarate) (Shi X HJ, 2005). Overall, these studies indicate that the CNTs/CNFs and their composites can serve as osteogenic scaffolds with good cytocompatibility properties, reinforced mechanical properties and improved electrical conductivity to effectively enhance bone tissue growth.

1.7.5) Self-Assembled Rosette Nanotubes (RNTs)

A new class of biomaterial which is the focus of this dissertation is self-assembled Rosette Nanotubes (RNTs). RNTs are a type of soft organic nanomaterial obtained through the self-assembly of low-molecular-weight synthetic molecules when placed in water. In the design of RNTs, the DNA base pair building blocks (Guanine^Cytosine, G^C) possess key elements for their sequential self-assembly towards the formation of stable nanotubular architectures (Chun AL, 2005) (Journeay WS, 2008) (Fenniri, 2001). Figure 1.8A shows the G^C motif of one type of RNTs, Twin K1 RNTs (ChenY, 2010). An amino acid side chain (lysine, K) has been chosen to impose chirality (such as handedness) and surface chemistry on the RNTs. Importantly, lysine side chain (with an amine and carboxyl group) provide the possibility to functionalize a variety of drugs onto RNTs (for example, to attach peptide growth factors through peptide bonds). Figure 1.8B shows the simulated image of the same molecule. Furthermore, six G^C motifs undergo spontaneous self-assembly under physiological conditions first into a supermacrocycle resembling a rosette as shown in Figure 1.8C. Then, through non-covalent interactions such as hydrogen bonds, base stacking interactions and hydrophobic effects, the rosettes form a stable tubular stack with a hollow core of 1.1 nm in diameter as shown in Figure 1.8D. Twin K1 RNTs are robust, mainly due to its lower charge density, larger number of hydrogen bonds per self-assembling motif and lower steric repulsion (Moralez JG, 2005). Furthermore, RNTs possess amphiphilic character and hollow architecture therefore, RNTs can be used to encapsulate and deliver hydrophobic drugs otherwise difficult to deliver in biological systems (Chen Y, 2011).

Figure 1.8, Twin K1 structure and its self-assebly, A) Structure of Twin K1 where Twin G^C is covalently attached with a lysine unit, B) Self-assembled Rosette formed by six G^C motifs maintained by 36 H-bonds, C) Self-assembled Twin K1 RNT obtained from rosette stacking (adapted from (Zhang L, 2009) License No. 3212620618069 copyright Elsevier publications, Reprinted with permission from(Chhabra R, 2010) copyright 2013 American Chemical Society).

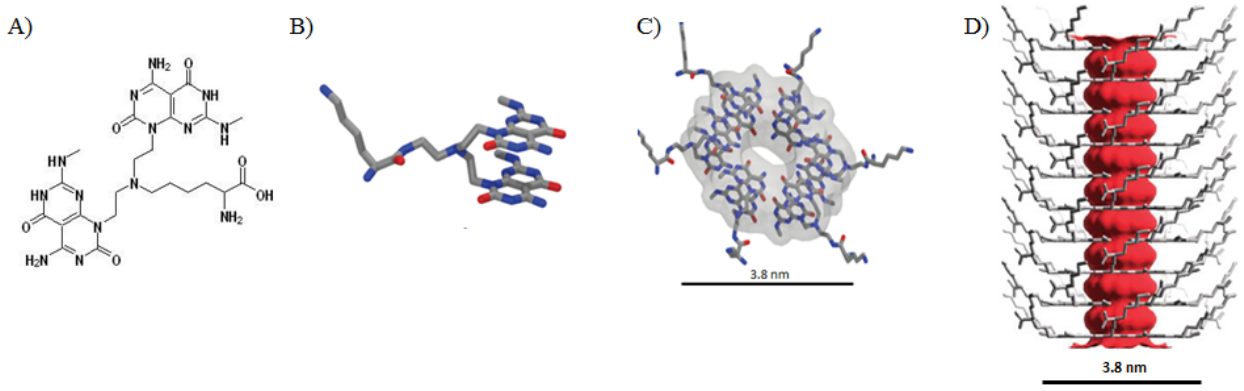

In addition, it is possible to further functionalize the outer space of the G^C motif of RNTs in order to yield predefined chemical and physical properties for specific tissue regenerations. For example, the amino acid side chain of RNTs has been successfully replaced by RGD (arginine-glycine-asparctic acid) peptide sequences which has been shown to create more favourable environment for osteoblasts than conventional non-modified implants (Zhang L, 2009). Recently, Journeay *et al*. reported an in vivo inflammatory study on the RNTs (Journeay WS, 2008). Results have demonstrated that RNTs have low acute toxicity *in vivo*: i.e., 5 µg dose of RNTs did not trigger an inflammatory response and even with a 50 µg dose, inflammation was resolved after 7 days. Therefore, with such excellent cytocompatibility, flexible design and synthetic accessibility, RNTs are very well suited for orthopaedic and bone tissue engineering applications. Moreover, RNTs have been shown to possess osteoconductive

properties. For example, Chun *et al.* have demonstrated that osteoblast (bone forming cells) adhesion was greatly enhanced by the Mono K1 RNTs coated titanium compared with uncoated titanium even at a very low concentration of 0.005 mg/mL (Chun AL, 2005). Secondly, Zhang *et al.* have shown that Mono K1 has the ability to mimic the structure of collagen in bone and therefore, has been used as a coating material with nanocrstalline HA to improve the osteoblast adhesion on Ti (Lijie Z, 2008). In addition, Chen *et al.* have demonstrated that Dexamethasone can be quickly encapsulated into RNTs and released to promote osteoblast over long periods of time (Yupeng Chen S. S., 2011). Furthermore, when Twin K1 RNTs were functionalized with KRSR (lysine-arginine-serine-arginine) and AB (aminobutyl), they have shown increased osteoblast adhesion on Ti. Additionally, AB functionalised Twin K1 RNTs have shown increased endothelial cell adhesion (Zhang L, 2010).

RNTs can be synthesized by two ways, self-assembled RNTs and co-assembled RNTs, thereby offering a general strategy for tailoring the physical and chemical properties of RNTs.

Self-assembled RNTs: When a nanotube is composed of only one kind of motif. For example, Figure 1.9C shows a self-assembled RNT of Twin K1 where each and every motif is TwinK1. Another example is Figure 1.10 which shows a unit of self-assembled RNT of Peptide B where Twin G^C is linked with the sequence of Peptide B through a lysine. The Twin G^C assembly is responsible for making the rosette and then building a tube (Suri SS, 2011).

Figure 1.9 Structure of PeptideB-TwinG^C. TwinG^C is covalently attached with Lysine. This lysine is further attached with the 11 amino acid peptide B sequence

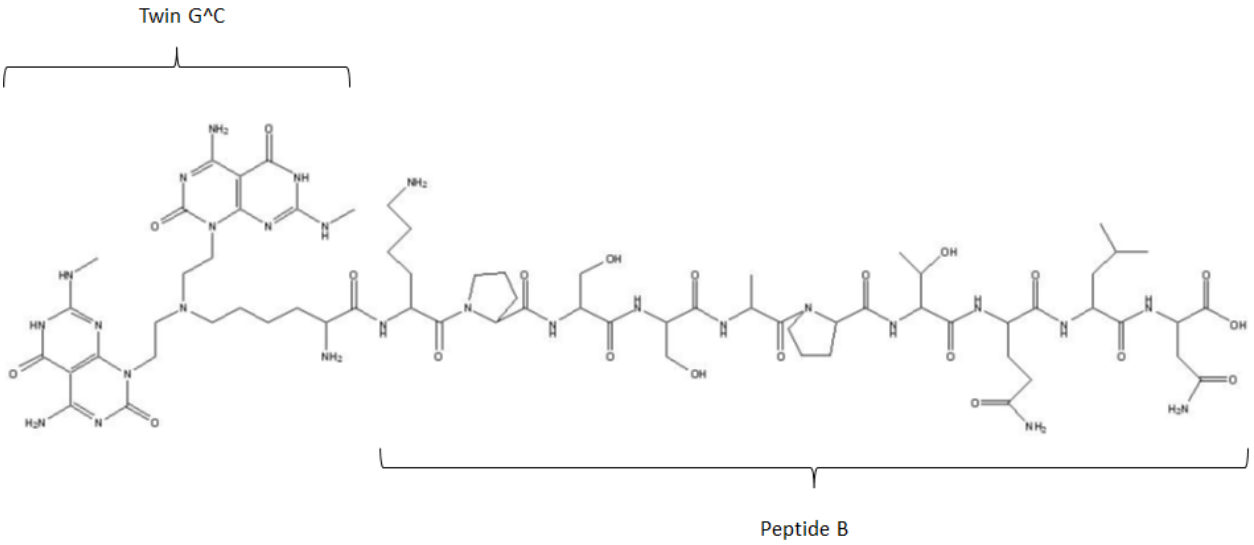

Co-assembled RNTs: When RNTs are synthesized to express more than one functional group on the outer surface, this is achieved by co-assembling two motifs in solution. For example, co-assembled nanotubes of TwinK1 and Peptide B-Twin G^C in a molar ratio of 9:1 as shown in Figure 1.10. Figure 1.11A and Figure 1.11B show the self-assembled RNTs of Twin K1 and Peptide B-Twin G^C. Figure 1.11C shows their co-assembly in a ratio of 9:1.

Figure 1.10, Modeling images of Twin K1, PepB-TwinG^C and Pep B-Twin G^C (9:1) co-assembled RNTs. A) Modeling of Twin K1 self-assembled nanotubes, B) Modeling of Peptide B-Twin G^C self-assembled nanotubes and C) Modeling of Twin K1 and Pep B-Twin G^C (9:1) co-assembled RNT.

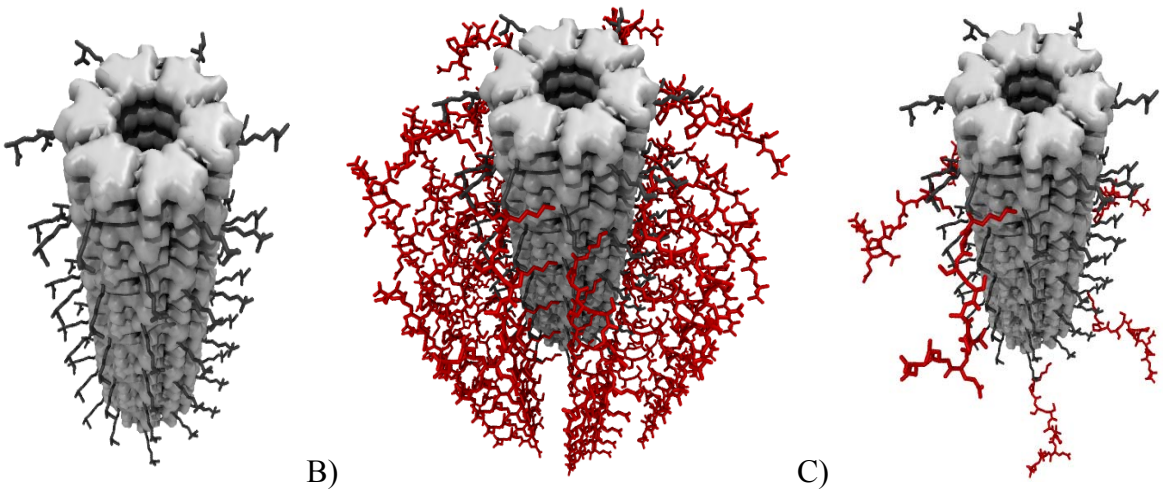

A) B) C)

Overall, RNTs have several unique features that make them attractive for orthopedic and bone tissue engineering applications: (a) rapid and quantitative preparation through self-assembly and co-assembly; (b) biomimetic nanostructured features that improve osteoblast (bone-forming cell) attachment; (c) ability to serve as calcification template (Zhang, Chen, Rodriguez, Fenniri, & Webster, 2008); (d) facile functionalization with amino acid and peptide side chains; (e) well-controlled spatial distributions of the side chains to enhance their functionality (Journeay, Suri, Moralez, Fenniri, & Singh, 2008)(Zhang L, 2009) (Lijie Zhang, 2010) (Zhang, Chen, Rodriguez, Fenniri, & Webster, 2008); and (f) synthetic accessibility, chemical tunability, and functional group tolerance which impart a broad range of tailorable chemistries and biological properties.

In summary, rosette nanotubes can serve as a biocompatible and a bioactive implant material and a linkage for both bone tissue engineering applications. However, RNTs are not as mechanically strong as a natural bone and they are not able to encapsulate cells at high concentrations as demonstrated in previous studies (Chun AL, 2005) (Chun AL, 2004).

Therefore, RNTs could be applied on metal implants on their exterior surface to overcome their disadvantages, but provide biocompatibility and bioactivity.

Furthermore, for achieving success in orthopaedic implant application, the important factors are material, biological interactions and growth factor delivery. The delivery of growth factor could expedite the process of tissue regeneration (Friedlaender GE, 2001) (Calori GM, 2009). One of the most potent inducers of bone regeneration is TGF-β family of proteins such as BMP-7 which promotes the regeneration of bone (discussed in section 1.6).

We have combined the properties of RNTs with BMP-7 short peptides together. We have designed studies where we have investigated the effects of RNTs (Twin K1) on adhesion of human bone marrow stromal cells (hBMSCs) on different substrates. In addition, next step of our study is to co-assemble BMP-7 short peptides with these RNTs and study their osteogenic differentiation using hBMSCs.

1.8) Objectives of the project

The objectives of this dissertation were to purify, characterize the RNTs and explore their utility as a biocompatible, bioactive and deliverable material for bone regeneration. Specific goals of the project can be defined as:

- Purify RNTs of Twin K1 attached with short peptides A, B & C. This was accomplished using High Performance Liquid Chromatography (HPLC)

- Characterize the RNTs using SEM showing the self-assembled nanotubes of Twin K1 and co-assembled nanotubes of Twin K1 with Peptide A-Twin G^C in a ratio of 9:1. Similar experiments were conducted for Peptide B-Twin G^C and Peptide C-Twin G^C
- Perform *in vitro* studies of cellular adhesion using hBMSCs with the materials; Twin K1 and Peptide A/B/C-Twin G^C co-assembly on substrates like tissue culture treated plastic, Non treated plastic and titanium
- Perform *in vitro* osteogenic differentiation studies of hBMSCs by treating them with Peptide A/B/C-Twin G^C

1.9) References

1. Abarrategi A, G. M.-V.-L. (2008). Multiwall carbon nanotube scaffolds for tissue engineering purposes. *Biomaterials, 29*, 94-102.

2. Affatato S, T. R. (2006). Advanced nanocomposite materials for orthopaedic applications, a long-term in vitro wear study of zirconia-toughened alumina. *J. Biomed. Mater. Res. Part B, 78B*, 76-82.

3. Agrawal CM, a. R. (2001). Biodegradable polymeric scaffolds for musculoskeletal tissue engineering. *Journal of Biomedical Materials Research, 55*(2), 141-150.

4. AS, H. (2002). Hydrogels for biomedical applications. *Advanced Drug Delivery Reviews, 43*, 3-12.

5. Balasundaram G, S. M. (2006). Using hydroxyapatite nanoparticles and decreased crystallinity to promote osteoosteoblast. *Biomaterials, 14*, 2798–2805.

6. Berry DJ, H. W. (2002). Twenty-fiveyearsurvivorship of two thousand consecutive primary Charnleytotal hip replacements: factors affecting survivorship of acetabular and femoral components. *J Bone Jnt Surg Am, 84*(A(2)), 171-177.

7. Bertoncini P, L. C. (2012). Early adhesion of human mesenchymal stem cells on TiO(2) surfaces studied by single-cell force spectroscopy measurements. *J Mol Recognit, 25*(5), 262-269.

8. BM, W. (1984). Current trends in revision of total hip arthroplasty. *Int Orthop, 8*(2), 89-93.

9. Boccaccini AR, a. M. (2003). Bioresorbable and bioactive polymer/bioglass® composites with tailored pore structure for tissue engineering applications. *Composites Science and Technology, 63*(16), 2417-2429.

10. Branemark PI, A. R. (1983). Osseointegrated titanium fixtures in the treatment of edentulousness. *Biomaterials, 4*, 25-28.

11. Calori GM, D. D. (2009). Bone morphogenetic proteins and tissue engineering: future directions. *Injury, 40*(3), S67-76.

12. Castner DG, R. B. (2002). Biomedical surface science: Foundations to frontiers. *Surface Science, 500*, 28-60.

13. Chen D, Z. M. (2004). Bone morphogenetic proteins. *Growth Factors, 22*(4), 233-241.

14. Chris Arts JJ, V. N. (2006). The use of a bioresorbable nano-crystalline hydroxyapatite paste in acetabular bone impaction grafting. *Biomaterials, 27*, 1110-1118.

15. Chun AL, M. J. (2004). Helical rosette nanotubes: A more effective. orthopaedic implant material. *Nanotechnology, 15*, s234-s239.

16. Chun AL, M. J. (2005). Helical rosette nanotubes: a biomimetic coating for orthopedics? *Biomaterials, 26*, 7304-7309.

17. Colon G, W. B. (2006). Increased osteoblast and decreased Staphylococcus epidermidis functions on nanophase ZnO and TiO2. *J Biomed Res A, 78*, 595-604.

18. Cooper CA, R. D. (2002). Distribution and alignment of carbon nanotubes and nanofibrils in a polymer matrix. *Composites Science and Technology, 62*, 105-112.

19. (2004). Polymers . In V. S. Cooper SL, & H. A. Ratner BD (Ed.), *Biomaterials Science: an Introduction to Materials in Medicine.* Boston, MA: Elsevier Academic Press.

20. D, C. (2007). Advances and prospects on biomolecules functionalized carbon nanotubes. *J Nanosci Nanotechnol, 7*, 1298-1314.

21. D.A. Puleo, A. N. (1999). Understanding and controlling the bone}implant interface. *Biomaterials, 20*, 2311-2321.

22. D'Antonio J, C. W. (2005). Alumina ceramic bearings for total hip arthroplasty. *Clinical orthopaedics and related research, 436*, 164-171.

23. David V, J. N. (2007). Periprosthetic osteolysis and its association with the molecule RANKL expression. *Physiol. Res., 56*, 455-462.

24. Davidson JA, P. R. (1994). Abrasive wear of ceramic, metal, and UHMWPE bearing surfaces from third-body bone, PMMA bone cement, and titanium debris. *Biomed Mater Eng, 4*(3), 213-29.

25. Dunn, G. (1982). Contact guidance of cultured tissue cells: a survey of potentially relevant properties of the substratum. In R. C. Bellairs, *Cell Behaviour* (pp. 247–280). Cambridge: Cambridge University Press.

26. Eileen Inghama, J. F. (2005). The role of macrophages in osteolysis of total joint replacement. *Biomaterials, 26*, 1271-1286.

27. Elias KL, P. R. (2002). Enhanced functions of osteoblasts on nanometer diameter carbon fibers. *Biomaterials, 23*, 3279-3287.

28. Emery DFG, C. H. (1997). Stanmore total hip replacement in younger patients: review of a group of patients under 50 years of age as operation. *Jounral of bone and joint surgery, 79*, 240-246.

29. Esposito M, H. J. (1998). Biological factors contributing to failures of osseointegrated oral implants (I): Success criteria and epidemiology. *European Journal of Oral Sciences, 106*, 527-551.

30. Esposito M, H. J. (1998). Biological factors contributing to failures of osseointegrated oral implants (II): Etiopathogenesis. *European Journal of Oral Sciences, 106*, 721–764.

31. Fahlman, B. D. (2007). *Materials Chemistry.* Dordrecht, Netherlands: Springer.

32. Fenniri, H., Mathivanan, P., Vidale, K. L., Sherman, D. M., Hallenga, K., Wood, K. V., et al. (2001). Helical Rosette Nanotubes: Design, Self-Assembly and Charaterization. *J. Am. Chem. Soc., 123*, 3854-3855.

33. Filmon R, B. M. (2002). Adherence of osteoblast-like cells on calcospherites developed on a biomaterial combining poly(2-hydroxyethyl) methacrylate and alkaline phosphatase. *Bone, 30*(1), 152-158.

34. Filmon R, G. F. (2002). Effects of negatively charged groups (carboxymethyl) on the calcification of poly(2-hydroxyethyl methacrylate). *Biomaterials, 23*(14), 3053-3059.

35. Franz-Xaver Huber, O. B.-J.-J. (2006). First histological observations on the incorporation of a novel nanocrystalline hydroxyapatite paste OSTIM® in human cancellous bone. *BMC Musculoskelet Disord, 7*, 50.

36. Freeman JW, W. L. (2008). In H. C. Gonsalves KE (Ed.), *Biomedical nanostructures* (pp. 3-24). New Jersey, New York, USA: John Wiley & Sons Inc.

37. Friedlaender GE, P. C. (2001). Osteogenic protein-1 (bone morphogenetic protein-7) in the treatment of tibial nonunions. *J. Bone Joint Surg Am, 83A*, 151-158.

38. Gavenis K, K. D.-P.-R. (2006). BMP-7 loaded microspheres as a new delivery system for the cultivation of human chondrocytes in a collagen type-I gel. *J Biomed Mater Res Part B: Appl Biomater, 82*, 275–283.

39. Giavaresi G, F. M. (2003). Histomorphometric and microhardness assessments of sheep cortical bone surrounding titanium implants with different surface treatments. *J Biomed Mater Res A, 67*(1), 112-120.

40. Giavaresi G, F. M. (2003). Mechanical and histomorphometric evaluations of titanium implants with different surface treatments inserted in sheep cortical bone. *Biomaterials, 24*(9), 1583-1594.

41. Gong D, G. C. (2001). Titanium oxide nanotube arrays prepared by anodic oxidation. *J. Mater. Res, 16*, 3331.

42. Hahn GV, C. R. (1992). A bone morphogenetic protein subfamily: chromosomal localization of human genes for BMP5, BMP6, and BMP7. *Genomics , 14*(3), 759-762.

43. Harrison BS, A. A. (2007). Carbon nanotube applications for tissue engineering. *Biomaterials, 28*, 344-353.

44. Hata K, F. D. (2004). Water-assisted highly efficient synthesis of impurity-free single-walled carbon nanotubes. *Science, 306*, 1362-1364.

45. Hicham Fenniri, B.-L. D. (2002). Entropically driven self-assembly of multichannel rosette nanotubes. *Proc Natl Acad Sci, 99*(Suppl 2), 6487-6492.

46. Huinan Liu, T. J. (2007). Nanomedicine for implants: A review of studies and necessary experimental tools. *Biomaterials, 28*, 354-369.

47. interface, U. a. (1999). D.A. Puleo, A. Nanci. *Biomaterials, 20*, 2311-2321.

48. Ishizawa H, F. M. (1995). Mechanical and histological investigation of hydrothermally treated and untreated anodic titanium oxide films containing Ca and P. *Biomed Mater Res, 29*(11), 1459-1468.

49. Itoh F, A. H. (2001). Promoting bone morphogenetic protein signaling through negative regulation of inhibitory Smads. *EMBO J, 20*(15), 4132–4142.

50. J, C. (1960). Anchorage of the femoral head prosthesis to the shaft of the femur. *Journal of bone joint surgery*(42B), 28-30.

51. J, C. (1960). Surgery of the hip-joint: present and future developments. *Br. Med. J*(5176), 821-826.

52. J, M. (1998). TGF-b signal transduction. *Ann Rev Biochem, 67*, 753-791.

53. Jesus G. Moralez, J. R. (2005). Hierarchy, Helical Rosette Nanotubes with Tunable Stability and. *J. Am. Chem. Soc., 127*(23), 8307-8309.

54. JG, B. (1999). Breakthrough technology: searching for artificial articular cartilage. *Orthopedic Technology Review, 1*(1).

55. Ji B, G. H. (2004). How do slender mineral crystal resist buckling in biological materials. *Phil Mag Lett, 84*, 631-641.

56. Ji Soo Choi, J. W.-S.-K. (2012). Effects of Human Mesenchymal Stem Cell Transplantation Combined with Polymer on Functional Recovery Following Spinal Cord Hemisection in Rats. *Korean J Physiol Pharmacol, 16*(6), 405-411.

57. Joseph N. Mackle, D. J.-P. (2011). In vitro Characterization of an Electroactive Carbon-Nanotube-Based Nanofiber Scaffold for Tissue Engineering. *Macromol. Biosci, 11*, 1272-1282.

58. Journeay, W. S., Suri, S. S., Moralez, J. G., Fenniri, H., & Singh, B. (2008). Novel Rosette Nanotubes Show Low Acute Pulmonary Toxicity In Vivo. *Int. J. Nanomed, 3*, 373-383.

59. JS, W. (1996). Basic fibroblast growth factor for stimulation of bone formation in osteoinductive or conductive implants. *Acta Orthop Scand Suppl, 269*, 1–33.

60. Ketul C. Popat, K.-I. C. (2007). Osteogenic differentiation of marrow stromal cells cultured on nanoporous alumina surfaces. *Journal of Biomedical Materials Research Part A, 80A*(4), 955-964.

61. Learmonth ID, Y. C. (2007). The operation of the century: total hip replacement. *Lancet, 370*, 1508–1519.

62. Lijie Zhang, U. D. (2010). Tuning Cell Adhesion on Titanium with Osteogenic Rosette Nanotubes. *J Biomed Mater Res A, 95*(2), 550-563.

63. Lind M, D. B.-P. (1995). Chemotaxis of human osteoblasts. Effects of osteotropic growth factors. *APMIS, 103*, 140–146.

64. Lock J, N. T. (2012). Nanophase hydroxyapatite and poly(lactide-co-glycolide) composites promote human mesenchymal stem cell adhesion and osteogenic differentiation in vitro. *J Mater Sci Mater Med, 23*(10), 2543-2552.

65. Lu H, G. L. (2009). Effects of poly(L-lysine), poly(acrylic acid) and poly(ethylene glycol) on the adhesion, proliferation and chondrogenic differentiation of human mesenchymal stem cells. *J Biomater Sci Polym Ed, 20*(5-6), 577-589.

66. MG, D. (1994). Biomaterials used in orthopedic surgery. In R. S. Greco (Ed.), *Implantation Biology: The Host Response and Biomedical Devices* (pp. 229-252). CRC Press.

67. Mizuno K, M. T. (2008). Exogenous synovial stem cells adhere to defect of meniscus and differentiate into cartilage cells. *J Med Dent Sci, 55*(1), 101-111.

68. Musib, M. K. (2011). A Review of the History and Role of UHMWPE as A Component in Total Joint Replacements. *International Journal of Biological Engineering, 1*(1), 6-10.

69. Ong A, W. K. (2002). Early failure of precoated femoral components in primary total hip arthroplasty. *J Bone Jnt Surg Am, 84*(A(5)), 786–792.

70. P.X., L. X. (2004). Polymeric scaffolds for bone tissue engineering. *Annals of Biomedical Engineering , 32*(3), 477-486.

71. Price RL, E. K. (2004). Nanometer surface roughness increases select osteoblast adhesion on carbon nanofiber compacts. *J Biomed Mater Res, 70A*, 129-138.

72. Price RL, W. M. (2003). Selective bone cell adhesion on formulations containing carbon nanofibers. *Biomaterials, 24*, 1877-1887.

73. PS, U. (2001). *The recent advantages in bone and joint implant technology.* New Jersey , New York, USA: John Wiley & Sons, Inc.

74. Rahul Bhowmik, K. S. (2007). Mechanics of molecular collagen is influenced by hydroxyapatite in natural bone. *NANO- AND MICROMECHANICAL PROPERTIES OF HIERARCHICAL BIOLOGICAL MATERIALS, 42*, 8795-8803.

75. Ratner, B. D. (2002). Reducing capsular thickness and enhancing angiogenesis around implant drug release systems. *Journal of Controlled Release, 78*, 211-218.

76. Reddi AH, R. A. (2009). Bone morphogenetic proteins (BMPs): from morphogens to metabologens. *Cytokine & growth factor reviews, 20*(5-6), 341-42.

77. Ruggero Bosco, J. V. (2012). Surface Engineering for Bone Implants: A Trend from Passive to Active Surfaces. *coatings, 2*, 95-119.

78. Saito A, S. Y. (2003). Activation of osteo-progenitor cells by a novel synthetic peptide derived from the bone morphogenetic protein-2 knuckle epitope. *Biochim Biophys Acta , 1651*, 60-67.

79. Saito N, U. Y. (2008). Carbon nanotubes for biomaterials in contact with bone. *Curr Med Chem, 15*(5), 523-527.

80. Sarabjeet Singh Suri, S. M. (2011). RGD-tagged helical rosette nanotubes aggravate acute lipopolysaccharide-induced lung inflammation. *Int J Nanomedicine*, 3113-3123.

81. Schiraldi C, D. A. (2004). Development of hybrid materials based on hydroxyethylmethacrylate as supports for improving cell adhesion and proliferation. *Biomaterials, 25*(17), 3645-3653.

82. Shi X, H. J. (2005). Rheological behaviour and mechanical characterization of injectable poly(propylene fumarate)/single-walled carbon nanotube composites for bone tissue engineering. *Nanotechnology, 16*, S531-S538.

83. Shi X, H. J. (2006). Injectable nanocomposites of single-walled carbon nanotubes and biodegradable polymers for bone tissue engineering. *Biomacromolecules, 7*, 2237-2242.

84. Siegel RW, F. G. (1995). Mechanical properties of nanophase metals. (6, Ed.) *Nanostruct. Mater.*, 205-216.

85. Simank HG, S. M. (2006). The influence of surface coatings of dicalcium phosphate (DCPD) and growth and differentiation factor-5 (GDF-5) on the stability of titanium implants in vivo. *Biomaterials, 27*, 3988-3994.

86. Sitharaman B, S. X. (2008). In vivo biocompatibility of ultra-short single-walled carbon nanotube/biodegradable polymer nanocomposites for bone tissue engineering. *Bone, 43*(2), 362-370.

87. Slif D. Ulrich & Thorsten M. Seyler & Derek Bennett, R. E. (2008). Total hip arthroplasties: What are the reasons for revision? *International Orthopaedics (SICOT), 32*, 597-604.

88. Sul YT, J. C. (2002). Qualitative and quantitative observations of bone tissue reactions to anodised implants. *Biomaterials, 23*(8), 1809-1817.

89. Sul YT, J. C. (2002). Resonance frequency and removal torque analysis of implants with turned and anodized surface oxides. *Clin Oral Implants Res, 13*(3), 252-259.

90. Takemoto M, F. S. (2006). Bone-bonding ability of a hydroxyapatite coated zirconia–alumina nanocomposite with a microporous surface. *J. Biomed. Mater. Res., 78A*, 693-701.

91. Tanaka K, T. J. (2002). Ce-TZP/Al2O3 nanocomposite as a bearing material in total joint replacement. *J. Biomed. Mater. Res., 63*, 262-270.

92. Theresa Raimondo, S. P. (2010). Greater osteoblast and endothelial cell adhesion on nanostructured polyethylene and titanium. *Int J Nanomedicine, 5*, 647-652.

93. Thomson RC, M. A. (1999). Guided tissue fabrication from periosteum using preformed biodegradable polymer scaffolds. *Biomaterials, 20*(21), 2007-2018.

94. TiO2, I. o. (2006). Colon G, Ward BC, Webster TJ. *J Biomed Mater Res A, 78*, 595-604.

95. TJ, W. (2001). Nanophase ceramics: the future orthopedic and dental implant. In Y. JY (Ed.), *Advances in chemical engineering* (pp. 125–166). New York: Academic Press.

96. Webster TJ, E. C. (2000). Specific proteins mediate enhanced osteoblast adhesion on nanophase ceramics. *J Biomed Mater Res, 51*, 475-483.

97. Webster TJ, S. R. (1999). Osteoblast adhesion on nanophase ceramics. *Biomaterials, 20*, 1221–1227.

98. Webster TJ, W. M. (2004). Nano-biotechnology: carbon nanofibres as improved neural and orthopaedic implants. *Nanotechnology, 15*, 48-54.

99. Webster, B. E. (2007). Titanium, Increased Stem Cell Adhesion on Carbon Nanotubes Grown from Anodized. *Mater. Res. Soc. Symp. Proc, 951*.

100. Webster, T. J. (2001). Nanophase ceramics: The future orthopedic and dental implant material. In J. Y. Ying (Ed.), *Advances in Chemical Engineering Vol. 27* (pp. 125-166). New York: Academic Press.

101. Wei W, S. A. (2007). Biological properties of carbon nanotubes. *J Nanosci Nanotechnol, 7*, 1-14.

102. Wennerberg A, H. C. (1998). A histomorphometric evaluation of screw-shaped implants each prepared with two surface roughnesses. *Clin. Oral Implants Res, 9*, 11-19.

103. WH, H. (1995). The problem is osteolysis. *Clin. Orthop., 311*, 46-53.

104. WV, G. (1996). Periodontal tissue engineering by growth factors. *Bone, 19*, 23s–37s.

105. Yupeng Chen, T. J. (2009). Increased osteoblast functions in the presence of BMP-7 short peptides for nanostructured biomaterial applications. *J Biomed Mater Res A., 91*(1), 296-304.

106. Zanello LP, Z. B. (2006). Bone cell proliferation on carbon nanotubes. *Nano Lett, 6*, 562-567.

107. Zhang L, R. F. (2009). Arginine-glycine-aspartic acid modified rosette nanotube-hydrogel composites for bone tissue engineering. *Biomaterials, 30*(7), 1309-1320.

108. Zhang, L. a. (2009). regeneration, Nanotechnology and nanomaterials: Promises for improved tissue. *nanotoday, 4*(1), 66-80.

109. Zhang, L., Chen, Y., Rodriguez, J., Fenniri, H., & Webster, T. J. (2008). Biomimetic Helical Rosette Nanotubes and Nanocrystalline Hydroxyapatite Coatings on Titanium for Improving Orthopedic Implants. *Int. J. Nanomed, 3*, 323-333.

110. Zhou GS, S. Z. (2007). Different effects of nanophase and conventional hydroxyapatite thin films on attachment, proliferation and osteogenic differentiation of bone marrow derived mesenchymal stem cells. *Biomed Mater Eng, 17*(6), 387-395.

111. Zhu YH, C. K. (2001). Review article: polyethylene wear and osteolysis in total hip arthroplasty. *Journal of Orthopaedic Surgery, 9*, 91-99.

2) Materials & Methods:

Low glucose MEM-alpha and CyQuant® Cell proliferation assay kits were purchased from Invitrogen (Burlington, ON, Canada). Ascorbic acid, dexamethasone, β-glycerol phosphate, Alkaline Phosphatase substrate (*p*-Nitrophenyl Phosphate Substrate), 2-amino-2-methylpropan-1-ol, Triton X-100, MTT (3-(4,5-Dimethylthiazol-2-yl)-2,5-diphenyltetrazolium bromide) & DMSO (Dimethyl sulfoxide) were purchased from Sigma Aldrich (St Louis, ON, USA). rhBMP-7 was purchased from Biovision (Santa Clara, CA, USA). rhFGF-2 was purchased from Humanzyme, supplied by Cedarlane (Burlington, ON, Canada). SYBR Green I, DMEM (Dubelcco's Modified Eagle Medium) (low glucose), Pen/Strep, and 0.05% trypsin/EDTA were purchased from Invitrogen (Carlsbad, CA, USA). Ti Grade II wafers were purchase from ESPI metals (Ashland, ON, USA). Patient BMSC samples were generously provided by Dr. Harry Jiang (University of Alberta, Dept. of Surgery). Peptides with or without Twin K1 were synthesized by a doctoral student of Dr. Hicham Fenniri, Alaaeeddin Alsbaiee.

2.1) Peptide Purification:

Large scale purification of peptides was done by using semi-prep HPLC after optimizing the purification conditions using analytical grade HPLC. Column specifications of analytical grade HPLC were Agilent, Zorbax S8-C18, size 4.6×250mm, 5µm. The mobile phase composed of a mixture of 2 components; A: Water + 1% Acetonitrile + 0.1% Trifluoroacetic acid and B: 100% Acetonitrile + 0.1% Trifluoroacetic acid. A flow rate of 1 mL/min was used with an injection volume of 10 µL having a sample concentration of 1 mg/mL. Gradient elution program was used consisting of 0-3 min, 100% A; 3-40 min, 0%-20% B; 41-48 min, 100% B and 49-56 min, 100%

A. Peptide A elutes at 25.8 min and stops at 26.3 min while using UV Vis detector at 220nm. Peptide A-Twin K1 elution extends from 22.5 min and stops at 23.1 min while using UV Vis detector at 220 nm. Using the same gradient elution system, Peptide B elutes at 16.3 min and stops at 16.8 min while using UV Vis detector at 254 nm. Peptide B-Twin K1 elutes at 22.1 min and stops at 22.6 min detected by UV Vis at 254 nm. After the isolation of the peptide of interest, its LC-MS was performed every time to confirm the presence of peptide.

After optimizing the purification conditions in analytical grade HPLC, Phenomenex semi-prep HPLC was used with column specifications of Gemini, C18 110A, size 250×10.00mm, 5 micron. The same mobile phase system was used however, the flow rate was raised to 2mL/min, injection volume of 100 µL with sample concentration of 10mg/mL and gradient program was modified as 0-1 min, 0-10 % B; 1-25 min, 10-20% B; 26-32 min, 100% B and 33-40 min, 0% B. Using semi prep HPLC, Peptide A elutes from 10.4 min to 10.9 min, Peptide A-Twin K1 elutes from 18.0 min to 18.7 min while using UV Vis detector at 220 nm confirmed by LC-MS. Peptide B elution time extends from 9.6 min to 10.3 min and Peptide B-Twin K1 elution time is from 9.3 min to 9.8 min using UV Vis detector at 254 nm, confirmed by LC-MS. Twin K1, Peptide C and Peptide C-Twin K1 were not purified by HPLC.

2.2) SEM characterization:

The RNT solution at a concentration 0.1 mg/mL was prepared and 50 µL of the solution was added on top of the SEM grid as allowed to stand for 5 min. The remaining solution was then wiped away using filter paper and allowed to dry for 24 hrs. The SEM grid was always prepared 24 hrs prior to its use.

2.3) Cell Culture:

hBMSCs were cultured in low glucose MEM-alpha + 10% FBS (v/v) + 100 U/mL Penicillin + 100 g/L streptomycin + 5 ng/mL bFGF. hBMSCs were extracted from bone marrow aspirate using 0.05% trypsin and adding 5mL of media . After centrifugation for 5 minutes at 600 rpm, the supernatant was discarded and the cellular pellet was re-suspended into fresh media. This passaging was done at an appropriate ratio of 1:3. hBMSCs were used till passage five.

2.3.1) Cytotoxicity assay of TwinK1, Peptide A:Twin G^C, Peptide B:Twin G^C & Peptide C:Twin G^C

hBMSCs were seeded in 24-well plates (approx. 50,000 cells/well) with 0.5 mL media (low glucose MEM-alpha + 1% Pen/Strep + 10% FBS). Peptides were added 24 hrs later at concentrations of 0.2 µg/mL to 200 µg/mL. After an incubation of 24 hrs, 100 µL of 5 mg/mL MTT was added to each well and incubated for 2 hrs, after which media was replaced with 0.5 mL DMSO. 100 µL of each sample was transferred to a 96-well plate and the absorbance was determined at 570 nm with a microplate reader (ELX 800, Bio-Tek Instruments). Relative cell viability (%) was determined by normalizing to the absorbance of untreated cells.

2.3.2) Cell Adhesion using Fluorescent Imaging:

Plastic plates were coated by adding Pep A-Twin G^C self-assembled nanotubes and Pep A-Twin G^C: Twin K1 (1:1) co-assembled nanotubes in a concentration of 50 µg/mL, 25 µg/mL, 12.5 µg/mL, 5 µg/mL and 0.5 µg/mL prepared in milliQ water, allowed to incubate for 30 minutes and the excess solution was removed from the plate. Plates were allowed to dry

overnight. BMP-7 was coated onto the plates in the similar way at concentrations of 1 µg/mL and 0.1 µg/mL. Next day, hBMSCs were added on top and incubated for 18 hrs. After incubation, the medium was removed from the wells and washed with HBSS. Then 3.7% formalin was used to fix the cells and stained with 0.3 µg/mL Hoescht 33258 stain for 15 minutes and washed. Imaging was done using a fluorescent microscope from 5 locations of the well; Center, Top, Bottom, Left and Right. After capturing images, Image J software was used for image processing to count the number of cells in each picture and statistics were done to analyze the results.

2.3.3) Cell Adhesion using Hemocytometry:

Plastic plates were coated by adding Pep A-Twin G^C self-assembled nanotubes in a concentration of 50 µg/mL, 5 µg/mL, 0.5 µg/mL and 0.05 µg/mL prepared in milliQ water, allowed to incubate for 30 minutes and the excess PepA-Twin G^C solution was removed from the plate. Plates were allowed to dry overnight. BMP-7 was coated onto the plates in the similar way at concentrations of 1 µg/mL, 0.1µg/mL and 0.01 µg/mL. Next day, hBMSCs were added on top and incubated for the next 18 hrs. After incubation, medium was removed from the well and washed twice with 1x HBSS followed by detachment with 0.05% trypsin then, 3.7% formalin was added. 10 µL of cell suspension was withdrawn and mounted on the Hemocytometer. The number of cells were counted in the 4 squares of the hemocytometer. This set of information was collected from each well (counted in duplicate) followed by multiplication with 10,000/4 to get the final cell count in a well.

2.3.4) Cell Adhesion on different substrates coated with Twin K1 using Hemocytometry & MTT

Tissue culture treated plastic plates and non-treated plastic plates were coated by TwinK1 self-assembled nanotubes in a concentration of 50 μg/mL, 5 μg/mL, 0.5 μg/mL and 0.05 μg/mL, allowed to incubate for 30 minutes and the excess TwinK1 solution was removed from the plate. Plates were allowed to dry overnight. Next day, hBMSCs in 3 different densities of 33,000/well, 50,000/well and 88,000/well were added on top and incubated for the next 18 hrs. After sterilizing the Ti wafers, they were coated with 150 μL of peptides using the Drop Casting technique. In this technique, after the addition of materials were allowed to stand for 30 minutes and the excess material was removed from the wafer. Wafers were allowed to dry overnight. Next day, hBMSCs in 3 different densities of 33,000/well, 50,000/well and 88,000/well were added in a cell suspension of 500 μL volume and incubated for 18 hrs.

2.3.5) Calibration curve of cell numbers using MTT

After sterilizing Ti wafers, they were placed in 24 well non-tissue culture treated plates. hBMSCs at 5 different cell densities of 100,000 cells/well, 50,000 cells/well, 25,000 cells/well, 12,500 cells/well and 6,250 cells/well were added in a cell suspension of 500 μL volume and incubated for 18 hrs. After incubation, 100 μL of 5 mg/mL MTT was added to each well and incubated for 2 hrs. Then, the medium was removed and 0.5 mL DMSO was added to dissolve the crystals. 100 μL of this solution was transferred to a 96-well plate and the absorbance was analyzed at 570 nm with a microplate reader (ELX 800, Bio-Tek Instruments).

2.3.6) Cell Adhesion on Ti wafers using MTT:

After sterilizing the Ti wafers, they were coated with materials as described in Section 2.3.4. The wafers were allowed to dry overnight. Next day, hBMSCs cell suspension of 500 µL volume was added on top and incubated for the next 18 hrs. In the no treatment group, cells were added without any treatment on the wafer. After 18 hrs, MTT was conducted as explained in section 2.3.5.

2.3.7) Cell Adhesion on Ti wafers by measuring the fluorescence of dissolved cellular contents using SYBR green dye:

After sterilizing the Ti wafers, they were coated with materials as described in Section 2.3.4. Next day, hBMSCs cell suspension of 500 µL volume was added on top and incubated for 18 hrs. In the no treatment group, cells were added without any treatment on the wafer. After 18 hrs, the medium was removed and the wafers were washed with HBSS. 500 µL of ALP buffer (containing 0.5 M 2-amino-2-methylpropan-1-ol and 0.1% (v/v) Triton-X100 at pH 10.5) was added and then allowed to stand for 2 hrs. 200 µL of 10X diluted SYBR green dye prepared in HBSS was added to this buffer and rested in the dark for 10 mins. Then 100 µL of this solution was added in black plates and its fluorescence was measured at 497/520 nm.

2.3.8) Calibration Curve of Cell Adhesion on Ti wafers by measuring the fluorescence of dissolved cellular contents using SYBR green dye:

After sterilizing the Ti wafers, they were placed in 24 well non-tissue culture treated plates. hBMSCs cell suspension at different cell densities 50,000 cells/well, 25,000 cells/well, 12,500 cells/well and 6,250 cells/well were added as a cell suspension in 500 µL volume and incubated for 18 hrs. The medium was then removed and the wafers were washed with HBSS. 500 µL of

ALP Buffer was added and allowed to stand for 2 hrs. 200 µL of 10x times diluted SYBR green dye prepared in HBSS was added and stored in the dark for 10 mins. Then 100 µL of this solution was added in black plates and its fluorescence was measured at 497/520 nm. In each experiment, a negative control was used where no cells were added and the fluorescence of the Ti wafer was measured and the obtained value was reduced from each data point.

2.3.9) Calibration curve of cell attachment density on Ti using fluorescent imaging

After sterilizing the Ti wafers, they were placed in 24 well non-tissue culture treated plates. hBMSCs cell suspension was added as described in the Section 2.3.5. Afterwards, the medium was removed and the wafers were washed with HBSS. Cells were stained with 10x times diluted SYBR green dye prepared in HBSS and allowed to stand in the dark for 10 mins. Then the residual dye was washed with HBSS and 3.7% formalin was added to fix the cells on the wafer. Cells were imaged using the DAPI filter of Fluorescence microscope (Zeiss LSM 710). The microscope was automated to scan the entire wafer, capture images and stitch them together. Further, Imaris software was used for image processing. Cells were counted and statistics were done. In each experiment, a negative control was used where no cells were added and the absorbance of the Ti wafer was measured and the obtained value was reduced from each data point.

2.3.10) Cell Adhesion on Ti wafers by counting cells using fluorescent imaging.

After sterilizing the Ti wafers, they were coated with materials as described in section 2.3.4. Next, the addition of cells was done same as section 2.3.7. After 18 hrs, results were analyzed and described as in the section 2.3.9

2.3.11) Comparison of Coating techniques and its influence on cell adhesion using Twin K1 & PepA:Twin K1 (1:9) co-assembly

After sterilizing the Ti wafers, they were placed in 24 well non-tissue culture treated plates. Drop casting on wafers was performed as above in section 2.3.4. For Dipping technique, the Ti wafer was submerged in nanotube solution of 400 µL volume. For spin coating, spin rotor was used at 1200 rpm for 60 sec and 20 µL of nanotube solution was added on the wafer. After coating, wafers were allowed to dry overnight. Next day, hBMSCs cell suspension of 500 µL volume was added on top and incubated for the next 18 hrs. In the no treatment group, cells were added without any treatment on the wafer. MTT assay and SYBR Green imaging assay was done as described in sections 2.3.5 and 2.3.10.

2.3.12) Comparison of cell adhesion on Ti via filling the well with hBMSCs suspension or restricting the cell spreading on Ti wafer

Method I: After sterilizing the Ti wafers, they were placed in 24 well non-tissue culture treated plates. hBMSCs cell suspension having an approximate cell density of 50 K cells in 500 µL volume were added on top and incubated for 18 hrs. The MTT assay was then performed as described in section 2.3.5

Method II: After sterilizing the Ti wafers, they were placed in 24 well non-tissue culture treated plates. hBMSCs were concentrated in a volume of 150 µL containing approx. 25,000 cells and then were carefully added on top of the wafer and incubated for 18 hrs without disturbing or shaking the plates. The medium was removed and the wafers were rinsed with HBSS. Then, 500 µL of media was added into each well. Later, 100 µL of 5 mg/mL MTT was added to each well

and incubated for 2 hrs. Media was replaced with 500 µL DMSO to dissolve the crystals. 100 µL of each sample was transferred to a 96-well plate and the absorbance was analyzed at 570 nm with a microplate reader (ELX 800, Bio-Tek Instruments).

2.3.13) Cell Adhesion on Ti wafers using MTT by restricting the cell spreading on the Ti wafer:

After sterilizing the Ti wafers, they were placed in 24 well non-tissue culture treated plates. Wafers were coated with materials by adding the RNT solution in a range of concentrations of 200 µg/mL, 50 µg/mL, 5 µg/mL and 0.5 µg/mL prepared in milli Q water, after resting for 30 minutes, the excess solution was removed from the wafer. The wafer was then allowed to dry overnight. The next day, hBMSCs were added in the same way as described in Method II of section 2.3.12. In the No Treatment group, cells were added without doing any treatment on the wafers. After 18 hrs, MTT assay was performed to as described in Method II of section 2.3.12.

2.3.14) Proliferation of hBMSCs on Ti after 1, 5 and 10 days

After sterilizing the Ti wafers, they were coated as described in Section 2.3.4 by Pep A:Twin K1 (1:9) coassembled RNTs, Pep B:Twin K1 (1:9) coassembled RNTs, Twin K1 self-assembled RNTs and Mono K1 self-assembled RNTs in concentrations of 200 µg/mL, 50 µg/mL, 5 µg/mL and 0.5 µg/mL. The next day, hBMSCs were added as described in Method II of section 2.3.12. After 24 hrs, 5 days and 10 days, the MTT assay was performed after each time interval as described in Method II of section 2.3.12.

2.3.15) Comparison of Mono K1, Twin K1, Peptide A:TwinK1(1:9), Peptide B:TwinK1(1:9) nanotube coating on Non treated plastic and its analysis by MTT & Hemocytometry

24 well Non-treated plastic plates were coated with materials as described in section 2.3.6 by adding the nanotube solutions in concentrations of 200 µg/mL, 50 µg/mL, 5 µg/mL and 0.5 µg/mL. The MTT assay and hemocytometry was done as mentioned in Section 2.3.1 and Section 2.3.3.

2.3.16) Cell adhesion of hBMSCs on Acid etched Ti coated with Twin K1

Ti wafer were etched as described in section 2.4 for 5 min. After sterilizing the Ti wafers, they were coated with materials as described in section 2.3.6 by adding nanotubes solution in a range of concentrations of 200 µg/mL, 50 µg/mL, 5 µg/mL and 0.5 µg/mL prepared in milli Q water. The next day, hBMSCs were added as described in Method II of section 2.3.12.

2.3.17) Osteogenic Differentiation of hBMSCs using Peptide assemblies:

Osteogenic differentiation studies were conducted using two techniques. In Technique1 I, the substrate (tissue culture plate) was coated with the peptides and in Technique II, the peptides were dissolved into the medium

Technique I: Tissue culture treated plastic plates were coated with Peptide B:Twin K1 (1:9) co-assembled nanotubes as described in Section 2.3.2.

Technique II: Using Tissue Culture treated plates, hBMSCs were seeded in 24-well plates. Materials were added in solution, 24 hrs later at concentrations of 0.2 µg/mL to 200 µg/mL. Plates were incubated at 37^{o}c and 5% CO_2. Time points were pre-decided to harvest the cells by

removing the medium, washing the wells with 1xHBSS and adding 500 µL of ALP buffer. After waiting for 2 hrs, cell contents dissolved in buffer were frozen in -20 ^{o}c.

Alkaline Phosphatase Assay: Frozen samples were allowed to thaw at room temperature. Fresh Alkaline phosphatase substrate solution was prepared at the concentration of 2 mg/mL in ALP buffer. 50 µL of sample was added in a 96-well plate and then using a repeating pipette alkaline phosphatase was added in the shortest duration of time possible. Right then, its absorbance at 405 nm was meausred using the microplate reader (ELX 800, Bio-Tek Instruments) at periodic intervals up to 5 min and their maximum slope values were recorded.

DNA Assay: CyQuant Dye calibration curve of different DNA concentrations were prepared using the method described in Mostafa NZ, 2009). 50 µL of samples were added in the black 96-well plate and 50 µL of dye solution was added and the fluorescence was measured at 480/520 nm. The ALP activity was presented as p-Nitro phenylphosphate formed for every minute (mmol/min/mL), and normalized by the total DNA content (µg DNA/mL) of each lysate to attain the specific ALP activity (ALP/DNA).

Calcium Deposition Assay: After reaching the pre-decided time points (14 days, 21 days and 28 days), medium was removed from the wells and 0.3 mL of 0.5 N HCl was added in each well and allowed to stay overnight. The next day, aliquots (20 µl) of each sample were added to 50 µL of a solution containing 0.028 M 8-hydroxyquinoline and 0.5% (v/v) sulfuric acid, plus 0.5 mL of a solution containing 3.7×10^{-4} M ocresolphthalein and 1.5% (v/v) 2-amino-2-methylpropan-1-ol. The absorbance was measured spectrophotometrically at 570 nm. Calcium standards were utilized to generate the standard curve and to calculate calcium concentration in each sample which was expressed in terms of mg/dL (Varkey M, 2007).

2.4. Acid Etching of Ti:

Concentrated nitric acid and concentrated sulphuric acid were mixed in a ratio of 1:3. This mixture was carefully heated to 80 ^{o}C. Wafers of Ti were dipped in this heated mixture for 5 min or 8 min. Immediately after that, the Ti wafers were withdrawn from the mixture and washed with water.

2.5. Statistical Analysis

Statistics were performed using a two-tailed heteroscedastic t-statistic test for adhesion, proliferation and long term differentiation studies where $p < 0.05$ was considered statistically significant.

3) Results & Discussion

3.1) HPLC Purification

Peptide Purification: The purification was done with the goal of extracting pure peptides out of the mixture of shorter or undesired sequences of peptides formed during the synthesis process. In order to purify peptides, they were subjected to HPLC purification with an UV-Vis detector. Table 3.1 shows the elution time of each peptide with its percentage yield.

Table 3.1) Elution times and percentage yield of peptides after HPLC purification.

Sr. No.	Compound Name	Elution time	% yield
1	Peptide A	29.5 – 29.9 min	16
2	Peptide A-Twin G^C	22.5 – 23 min	20
3	Peptide B	8.1 – 8.5 min	18
4	Peptide B-Twin G^C	21.9 – 22.5 min	11

In general, when the compounds are purified by HPLC (High Performance Liquid Chromatography), there is a lag time between their detection by UV-Vis and their collection from the column. Thus, in order to avoid the contamination of the pure peptide with the adjoining signals of other undesirable peptides, isolation of the peak was performed after the signal in UV Vis starts ascending and stopped before the signal approached the base line. This may account for some of the loss of product yield. It is important to mention that Peptide C and

Peptide C-Twin G^C were not subjected to HPLC purification as their synthesis was clean and did not require further purification. (Chromatograms are included in appendix).

3.2) SEM Characterization

The aim of this experiment was to study the morphology of PepA, PepB, PepC self-assembled RNTs, co-assembled RNTs and the surface of Ti wafers using Scanning Electron Microscopy (SEM).

A) 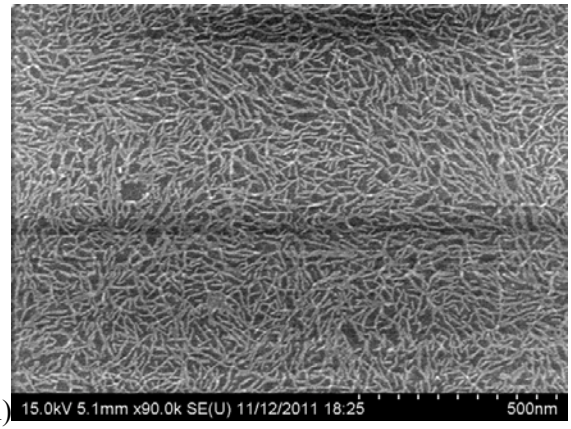

B) 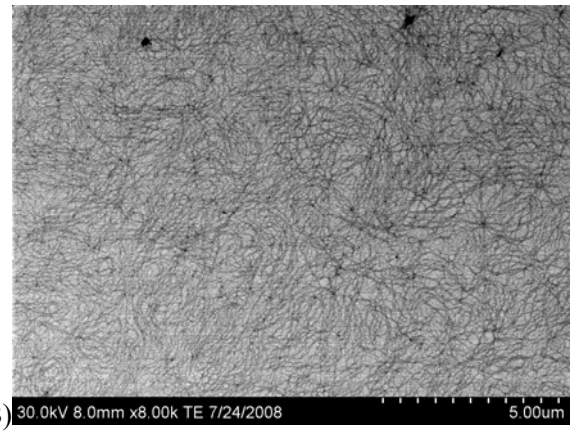

C) 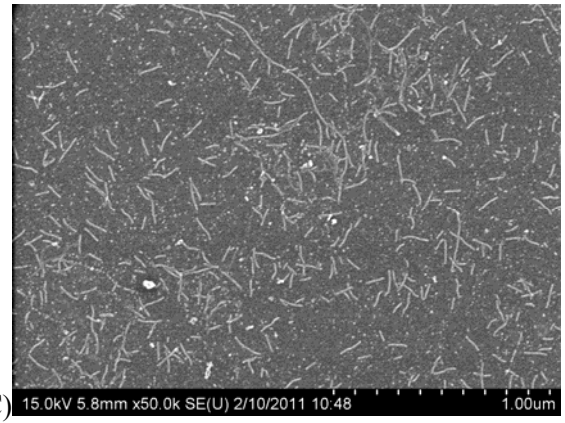
15.0kV 5.8mm x50.0k SE(U) 2/10/2011 10:48
1.00um

D) 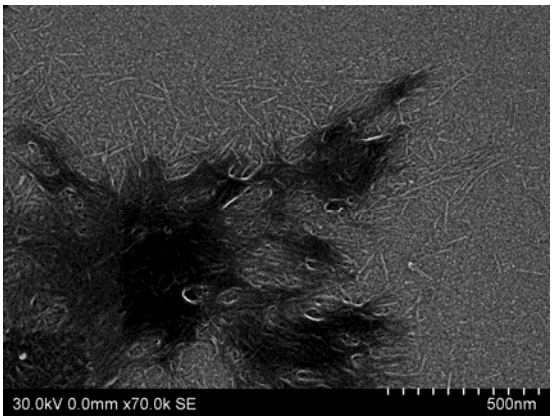
30.0kV 0.0mm x70.0k SE
500nm

E) 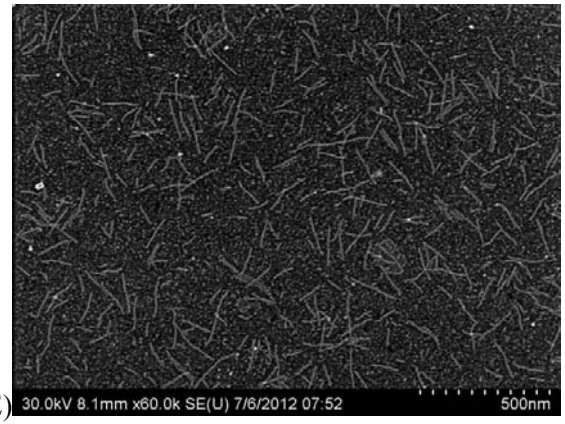
30.0kV 8.1mm x60.0k SE(U) 7/6/2012 07:52
500nm

F) 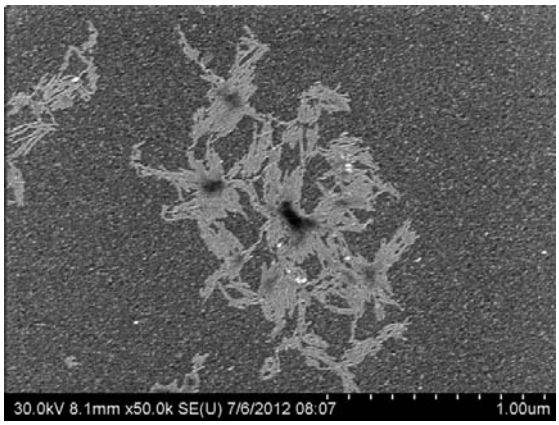
30.0kV 8.1mm x50.0k SE(U) 7/6/2012 08:07
1.00um

G) 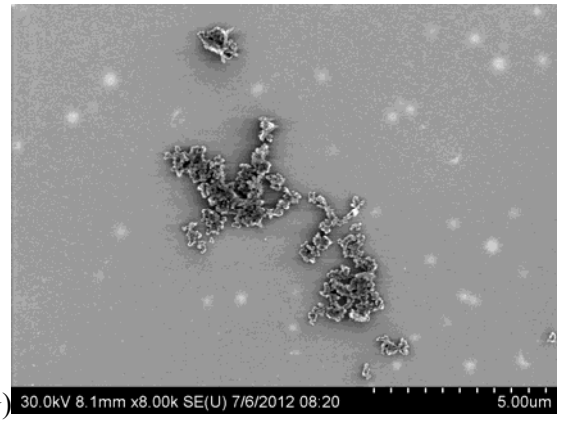
30.0kV 8.1mm x8.00k SE(U) 7/6/2012 08:20
5.00um

H) 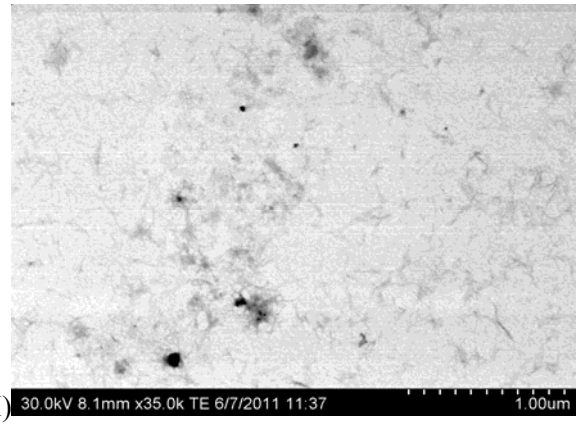
30.0kV 8.1mm x35.0k TE 6/7/2011 11:37
1.00um

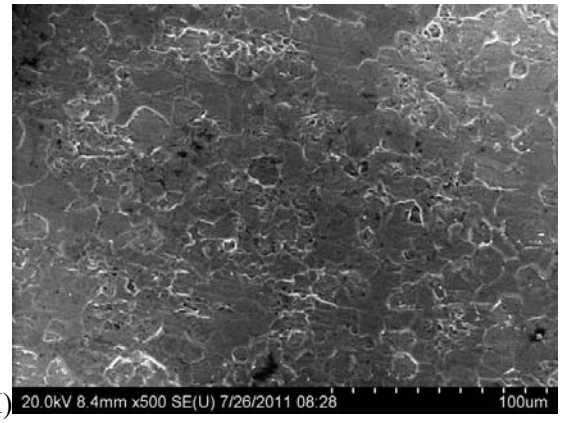

I)

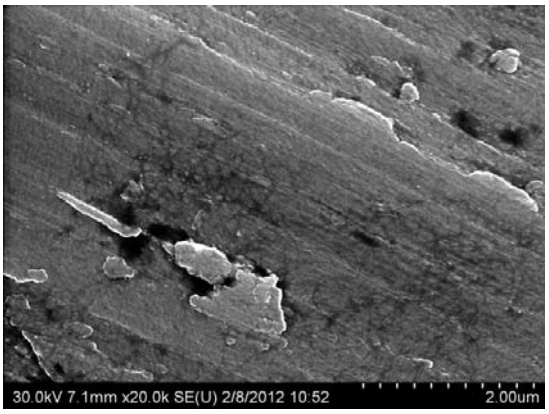

J)

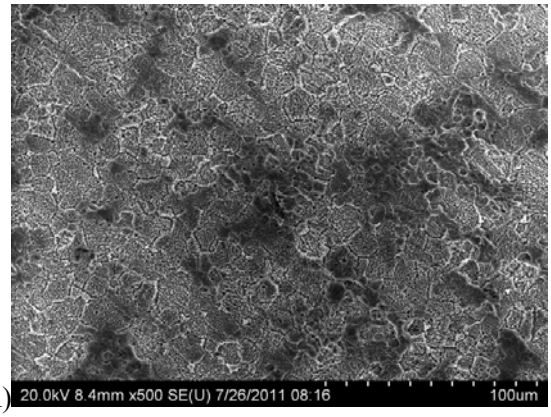

K)

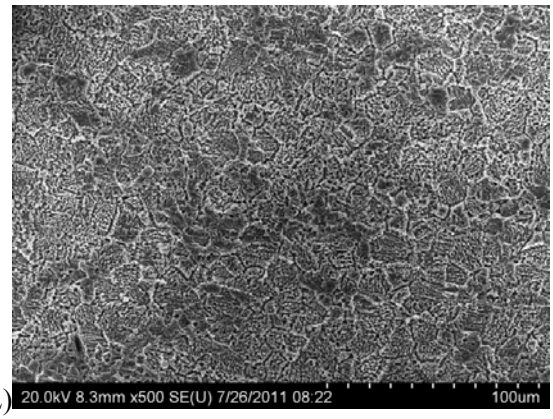

L)

Figure 3.1) SEM images of A) Twin K1 RNTs coated on carbon grid, B) Mono K1 RNTs coated on carbon grid, C) PepA-TwinG^C self-assembled RNTs coated on carbon grid, D) PepB-TwinG^C self-assembled RNTs coated on carbon grid, E) PepA:Twin K1(1:9) coassembled RNTs on carbon grid, F) PepB:Twin K1 (1:9) coassembled RNTs on carbon grid, G) PepC:Twin K1 coassembled RNTs (1:9) on carbon grid, H) PepA:Twin K1(1:1) coassembled RNTs on carbon grid, I) SEM of untreated Ti, J) SEM of Ti coated with Twin K1 RNTs, K) SEM of Ti wafer after 5 minutes of acid etching and L) SEM of Ti wafer after 8 minutes of acid etching. The magnification and scale of each image is indicated on the images

Figure 3.1A showed that Twin K1 forms long RNTs in their self-assembly. Twin G^C participate in forming the rosette of Twin K1 which stack over each other to form RNTs as shown in Figure 1.9 in the section 1.7.5. However in case of PepA-TwinG^C and PepB-TwinG^C self-assembly, their RNTs are

shorter. Twin G^C participate in the rosette formation however, the 11 amino acid side chain (as described in Figure 1.10, 1.11 in the section 1.7.5) attached with Twin G^C make the entire system bulky which affects the non-covalent stacking interactions and therefore, shorter RNTs were found in Figure 3.1B and Figure 3.1C. When PepA-TwinG^C and PepB-TwinG^C were co-assembled with Twin K1, intermediate length of RNTs were found as observed in Figure 3.1D and 3.1E. This could be attributed to co-assembly between the peptides and Twin K1, which balanced the bulky side of Peptide chain by the lysine group of Twin K1 as shown in Figure 1.11C in section 1.7.5. Figure 3.1F showed that there was no RNT formation between Peptide C-TwinG^C and Twin K1, which could be attributed to the low water solubility of Peptide C which prevented the non-covalent interactions. Figure 3.1I has shown the Twin K1 RNTs physiosorbed on Ti surface.

3.3) Cell adhesion on tissue culture treated plates coated with PepA:TwinK1(1:1) co-assembled nanotubes analyzed using a fluorescent dye

The goal of this experiment was to study the effect of Pep A:Twin K1 (1:1) co-assembled RNTs on cellular adhesion by coating them over tissue culture treated plates and compare the response with no treatment. BMP-7 at concentrations of 1 and 0.1 μg/mL were used as the positive control.

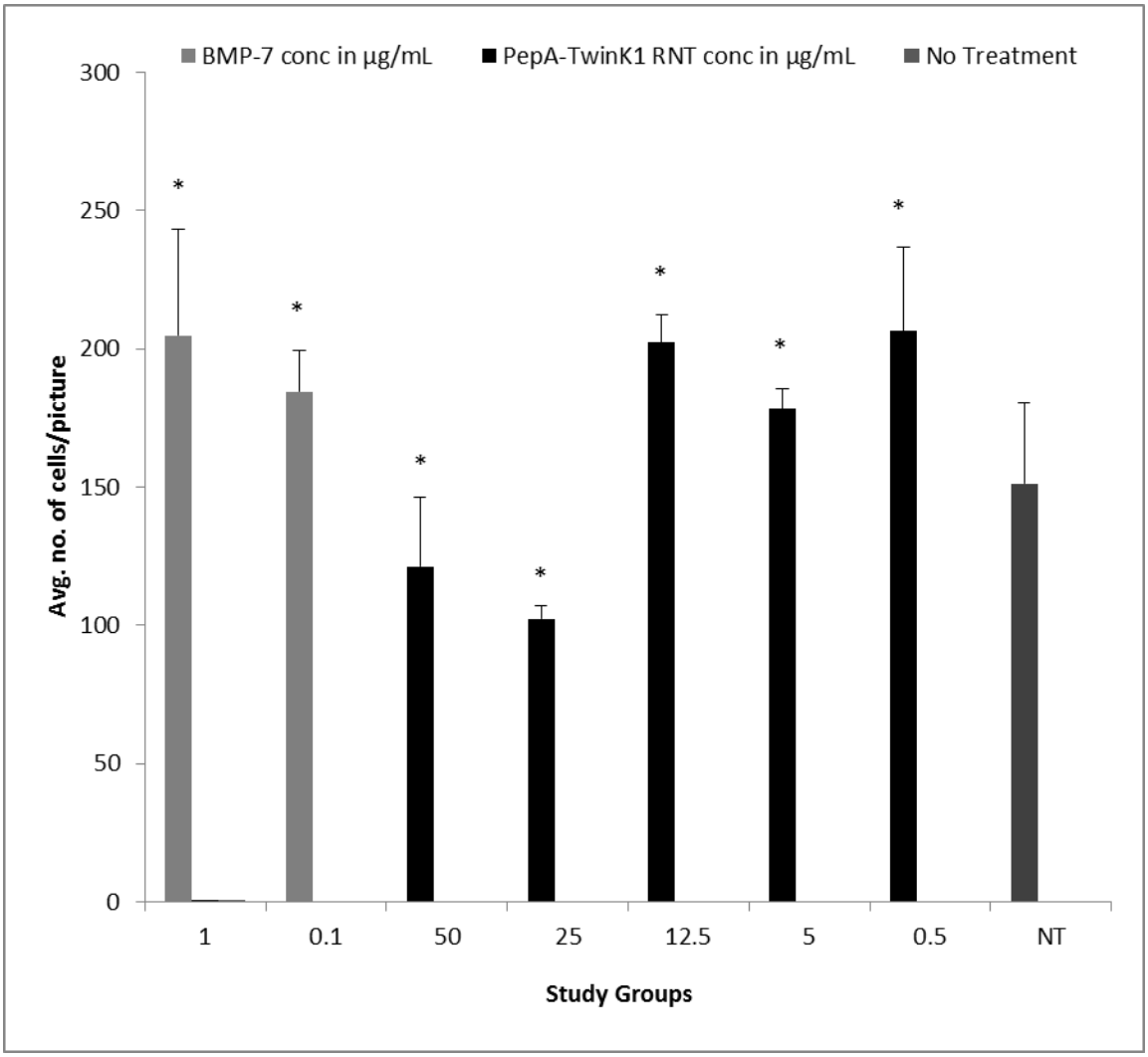

Figure 3.2) Cell attachment on tissue culture plates coated with Peptide A:Twin1 (1:1) nanotubes. The plates were coated with nanotubes and BMP-7 at indicated conentrations and cell attachment was determined by image analysis after 18 hours using Hoechst staining . Data was summarized as the average of triplicates per treatment. For statistical analysis, Two-tailed heteroscedastic t-statistic was used and statistical significance was defined by * meaning p-value<0.05 compared with no treatment

After 18 hours, the cell adhesion responses of Peptide A-TwinK1 (1:1) co-assembled RNTs and BMP-7 were compared with the No treatment group. Peptide A:Twin K1 RNT coating produced significant increase in cellular adhesion at 12.5 μg/mL, 5 μg/mL and 0.5 μg/mL concentrations. Additionally, the positive control group, BMP-7 gave a significant increase in adhesion at the concentrations of 1 and 0.1 μg/mL. However, RNTs at concentrations of 25 and 50 μg/mL lead to a decreased adhesion relative to No treatment.

The response of BMP-7 in increasing the cellular adhesion was expected. BMP-7 has proven formation and regeneration affects in bone and cartilage (Friedlaender GE, 2001) (Baylink DJ, 1993) (Reddi AH, 1993). In addition, the increase in cellular adhesion of Peptide A could be attributed to its osteogenic potential since it is a short sequence of BMP-7 (Chen Y, 2008). Moreover, Peptide A was co-assembled with Twin K1 which forms nanotubes and has been shown to be a biomimetic material which promotes human fetal osteoblast adhesion (Song S, 2012) (Zhang L, 2010). Therefore, their co-assembly should have resulted in osteogenic RNTs offering a biomimetic nanostructured material with improved surfacial properties for peptides. However, at 25 and 50 μg/mL dose, results showed a significant decrease in adhesion with the peptide nanotubes. Our research group had shown that the amount of nanotubes required to cover a substrate of 1 cm^2 is 0.5 μg (Chun, Webster, & Fenniri, 2006). Therefore, for the 2 cm^2 , used in this study, 1 μg would be enough. However, if extra material was used, multiple layers of coating could deposit on the substrate. Ther top layers would be loosely bound and therefore could leak out into the solutionand obstruct cell binding leading to a reduced cellular adhesion.

3.4) Cell Adhesion on Tissue Culture Treated plates coated with Peptide A self-assembled RNTs analyzed using a fluorescent dye:

The aim of this experiment was to study the effect on cell adhesion by coating Pep A-Twin G^C self-assembled nanotubes over tissue culture treated plates and comparing them with no treatment. The difference between this experiment and the previous experiment was the higher quantity of Peptide A present on nanotubes, because this is a self-assembly of Peptide A RNTs whereas previous experiment had a co-assembly of Peptide A RNTs and Twin K1 RNTs in 1:1 ratio.

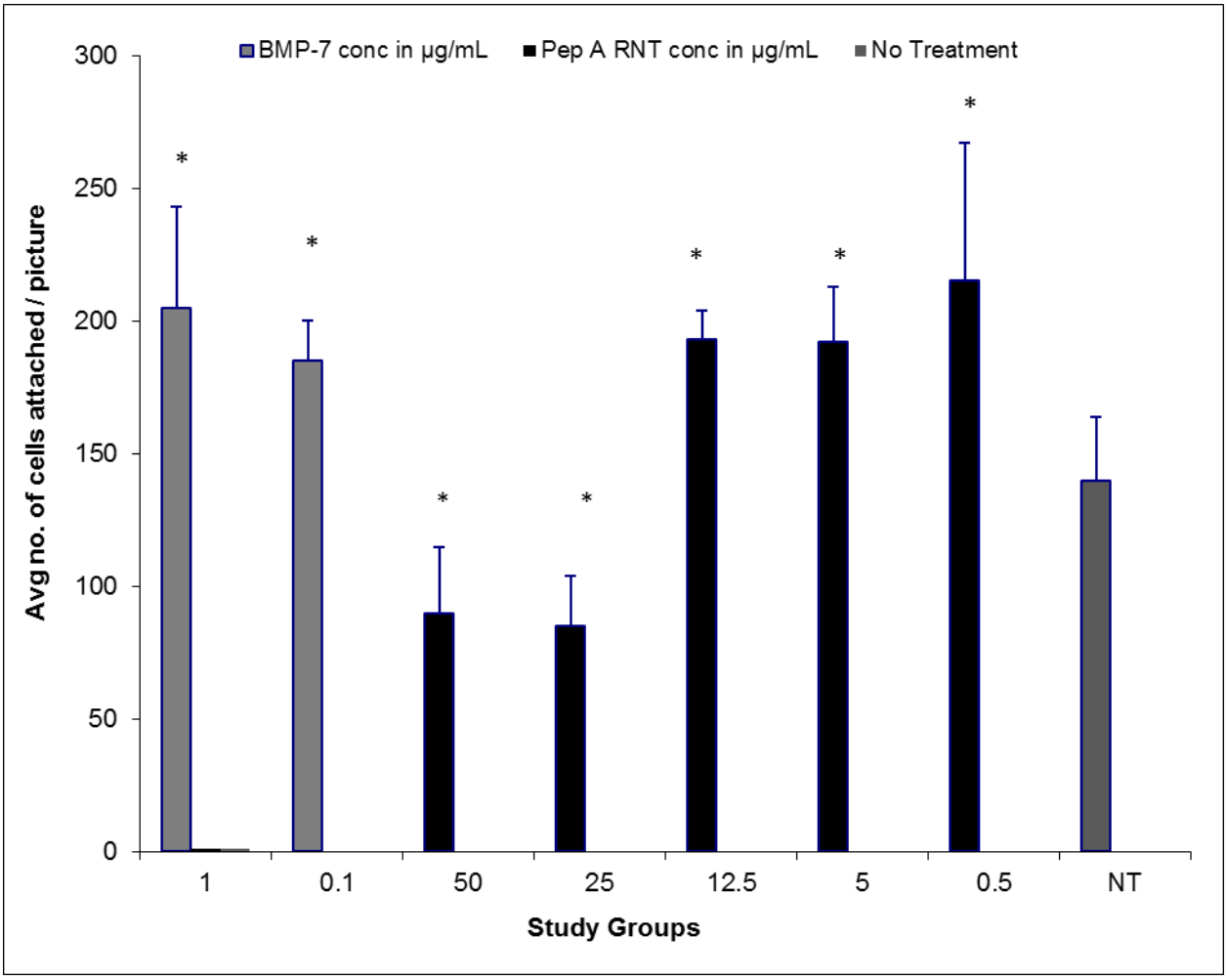

Figure 3.3) Cell attachment on tissue culture plates coated with Peptide A self assembled nanotubes. The plates were coated with nanotubes and BMP-7 at indicated conentrations and cell attachment was determined by image analysis after 18 hours. Data was summarized as the average of triplicates per treatment. For statistical analysis, Two-tailed heteroscedastic t-statistic was used and statistical significance was defined by * meaning p-value<0.05 compared with no treatment

The 18 hours adhesion study showed that hBMSCs adhered significantly better when the plates were coated with Peptide A-Twin G^C self-assembled nanotubes at doses of 0.5 µg/mL, 5 µg/mL and 12.5 µg/mL. In addition, BMP-7 (positive control group) coated plates showed significant increase in adhesion of cells. However, when the concentration of peptides reached 25 and 50 µg/mL, cellular adhesion reduced significantly.We had observed a similar trend in the previous experiment (section 3.3) where PepA:Twin K1(1:1) RNTs were helping the cells to adhere better up to a concentration of 12.5 µg/mL.Moreover, at 25 and 50 µg/mL adhesion was reduced. Therefore, we hypothesized the same reason for the outcomes as in section 3.3. Peptide A has osteogenic potential and incorporating them into biomimetic nanotubes increase their surfacial exposure to the cells thereby it improves the cellular adhesion on the substrate. However, at higher concentration of peptides, there could be multiple layers of coating where the top layers got weaker and and got pulled off with the cells attached to them. Therefore, we found a significant decrease in adhesion of cells at concentrations of 25 and 50 µg/mL.

3.5) Cell Adhesion on Tissue Culture Treated plates coated with Peptide A self assembled nanotubes analyzed using hemocytometry:

The aim of this experiment was to study the effect of Pep A self-assembled RNTs on cell adhesion by coating them on tissue culture treated plates and comparing them with the no treatment. However, the difference between this experiment and the previous experiment was the technique of analysis used (hemocytometry in this case).

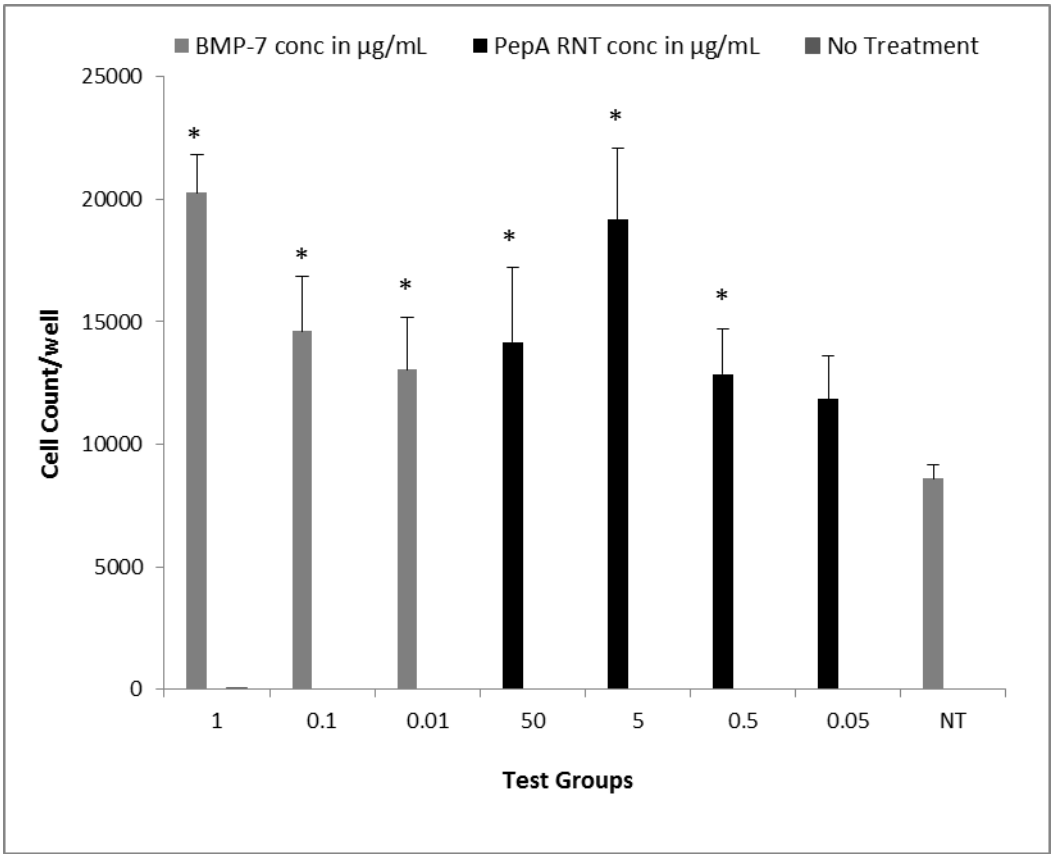

Figure 3.4) Cell attachment on tissue culture plates coated with Peptide A self assembled nanotubes. The plates were coated with nanotubes and BMP-7 at indicated conentrations and cell

attachment was determined by hemocytometry after 18 hours. Data was summarized as the average of triplicates per treatment. For statistical analysis, Two-tailed heteroscedastic t-statistic was used and statistical significance was defined by * meaning p-value<0.05 compared with no treatment

The results had shown that Pep A RNTs had helped to improve the adhesion of hBMSCs compared with no treatment. At the dose ranges of0.5, 5 and 50 μg/mL, the results were significantly higher. In addition, BMP-7 treatment had shown a dose dependent significant increase in cellular adhesion at 0.01, 0.1 and 1 μg/mL concentration.. However, cell adhesion at 0.05 μg/mL concentration of RNTs was higher but did not show statistical significance due to SD.

We decided to use hemocytometry because it provides more accurate estimation of the number of cells versus imaging the wells at 5 locations in the well as used in section 3.3 and 3.4. Based on the hemocytometer readings (which measures the actual numbers of cells on the substrate), Pep A RNTs coating showed a significant increase in cellular adhesion at 0.5, 5 and 50 μg/mL. An explanation for the increased cellular adhesion has been proposed in section 3.3. In short, PepA is a 10 amino acid long peptide chain isolated from the bioactive region of BMP-7 which has shown strong osteogenic potential. Moreover, we have linked PepA with Twin K1 RNTs which has shown the property to biomiminc the helical structure of natural collagen and has been shown to improve osteoblast adhesion. (Chen Y, 2008) (Zhang L, 2010) (Song S, 2012). Furthermore, the trend of adhesion at different doses concurs with our observation in Section 3.3 that approximately 1 μg/mL material is required to cover 2 cm^2 surface (Chun AL,

2006). In this experiment, we started with 0.025 µg (since we used 500 µL solution of 0.05 µg/mL concentration). The quantity of material was minimal and the effect was not significant. When we increased the material quantity up to 2.5 µg (500 µL of 5 µg/mL concentration), there was a consistent increase in adhesion. However, when we increased the material quantity by another ten fold, the cellular adhesion was decreased. This was expected and it could be attributed to the reason mentioned in Section 3.3. In brief, RNTs are water soluble and when there are multiple layers of material was coated over one another, the upper layers may come off with the cells or their presence in solution at such concentrations could obstruct cell binding sites to attach to the substrate.

3.6) Calibration curve of cell numbers using MTT

The aim of this experiment was to calibrate the MTT absorbance with respect to the cell numbers attached on the Ti wafer. In addition, this experiment was performed to determine whether the discrepancy in the previous two experiments were caused due to the use of Ti wafer.

A)

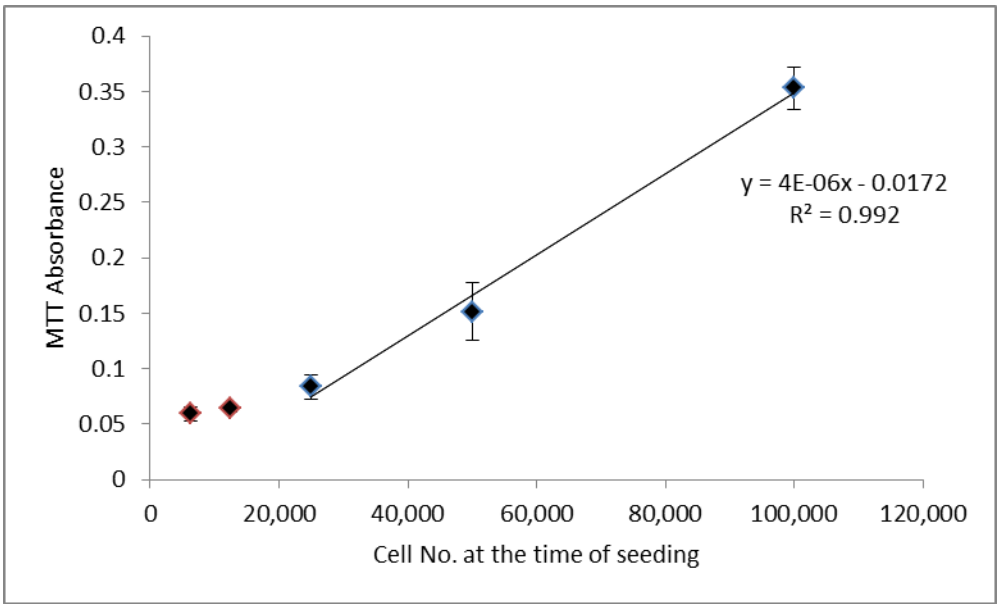

B)

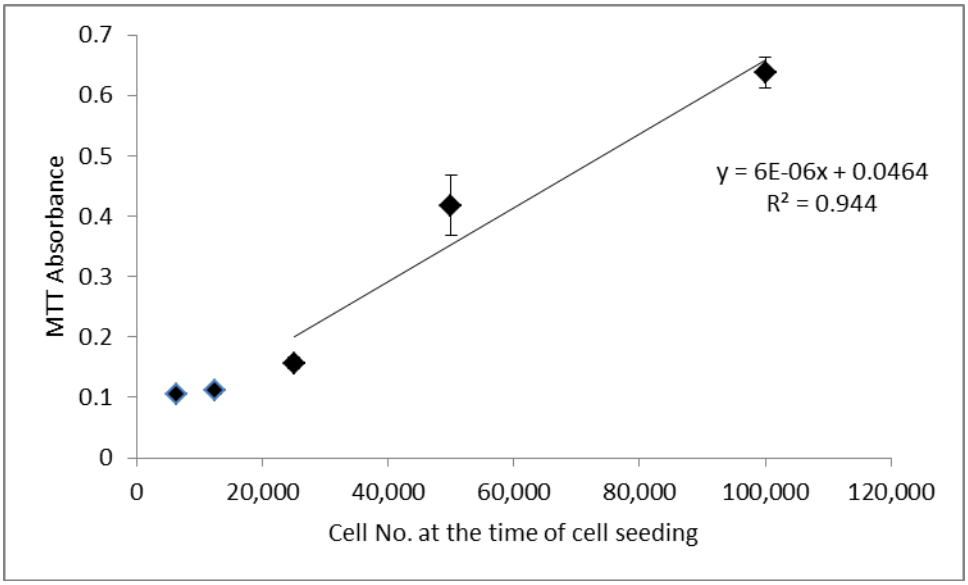

Figure 3.5) Cell attachment on Ti wafers. A) Volume of DMSO used to dissolve MTT crystals were 500 µL and B) Volume of DMSO used to dissolve MTT crystals were 300 µL. Cell attachment was determined by measuring their MTT absorbance. Incubation

period was 18 hours. Data was an average of triplicates per treatment. The curve fit was obtained using the cell numbers relevant for the adhesion experiment.

The results of A), B) showed a linear relationship between the MTT absorbance and the cell numbers. The linear co-relation value of A) was 0.992 and for B) was 0.944. In both A) and B) the MTT absorbance was highest when the seeding cell density was 100,000 cells/well in a 24 well plate. When the cell density was reduced to half, the MTT absorbace fell in the similar trend until the cell density reached to 6,250 cells/well. However, there exists a difference between the absolute value of A) and B) in their MTT absorbance. In B), the volume of DMSO was reduced to 300 μL (instead of 500 μL in A) which made the DMSO solution quiet concentrated and therefore, higher absorbance values were observed at 550 nm. The lowest chosen cell seeding density was 6,250 because below this cell density, the MTT absorbance was almost negligible.

The reason to switch to MTT was because hemocytometry (section 3.5) and imaging (section 3.3 and 3.4) could not be used when the substrate is opaque like Titanium. Therefore, among many analytical techniques, MTT was chosen to estimate cell adhesion on Ti because it is a semi-automated colorimetric assay which determines viable cell numbers and is based on the conversion by mitochondrial succinate dehydrogenase of the tetrazolium salt, to a water-insoluble purple formazan product that has been shown to be proportional to the numbers of living cells presented. The MTT assay has been demonstrated as a sensitive, precise, convenient, rapid and economical test method by many studies (Hongo T, 1990) (H. WAN, 1994) (Heo DS, 1990). These results were expected to produce a linear relationship between the number of cells attached with Ti and their MTT absorbance. The low cell seeding densities were ignored since they deviated from the linear curves.

3.7) Cell Adhesion on different substrates A) Tissue Culture treated plastic, B) Non-Tissue culture treated plastic and C) Ti coated with Twin K1 analyzed using MTT

The aim of this experiment was to determine the influence of Twin K1 RNTs on cell adhesion using different substrates, namely tissue culture treated plates, non-tissue culture treated plates and Ti wafers.

A)

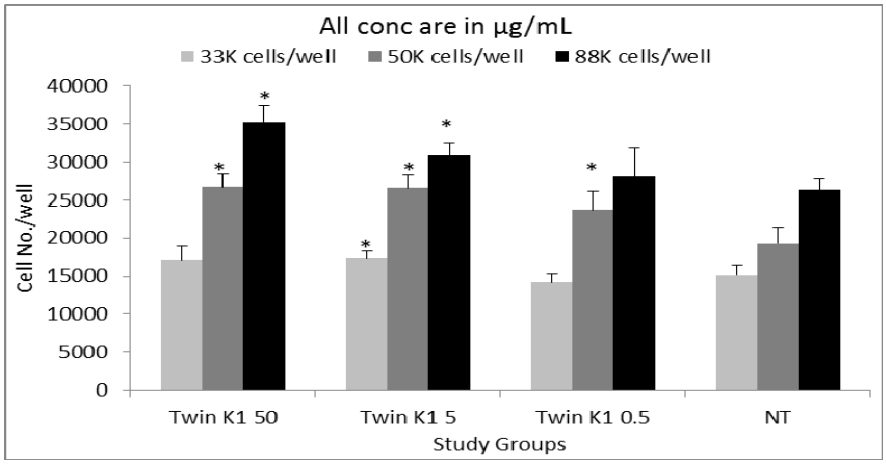

B)

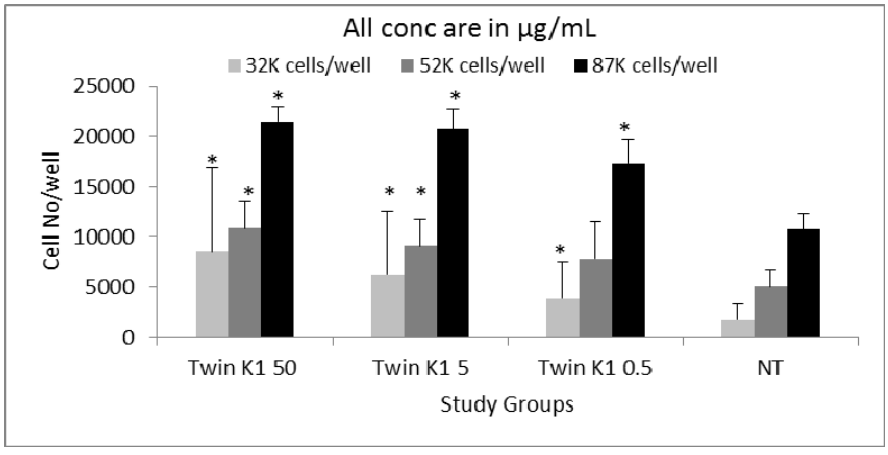

C)

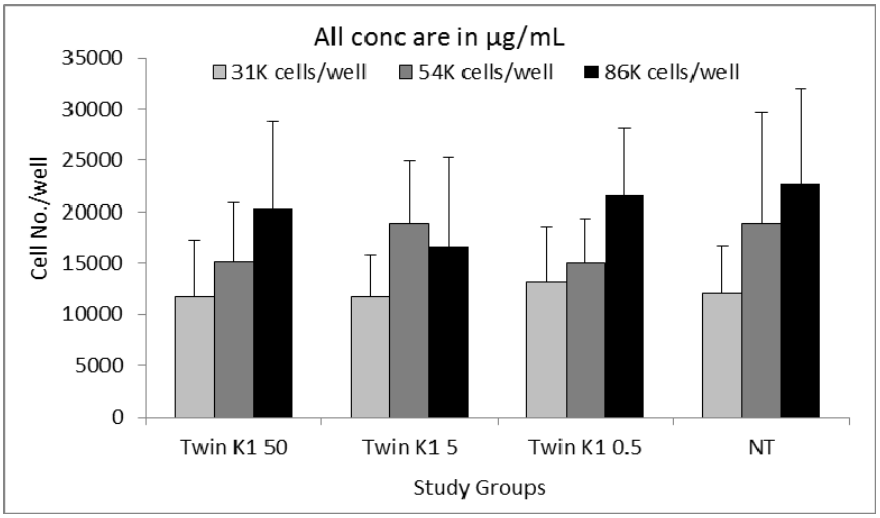

D)

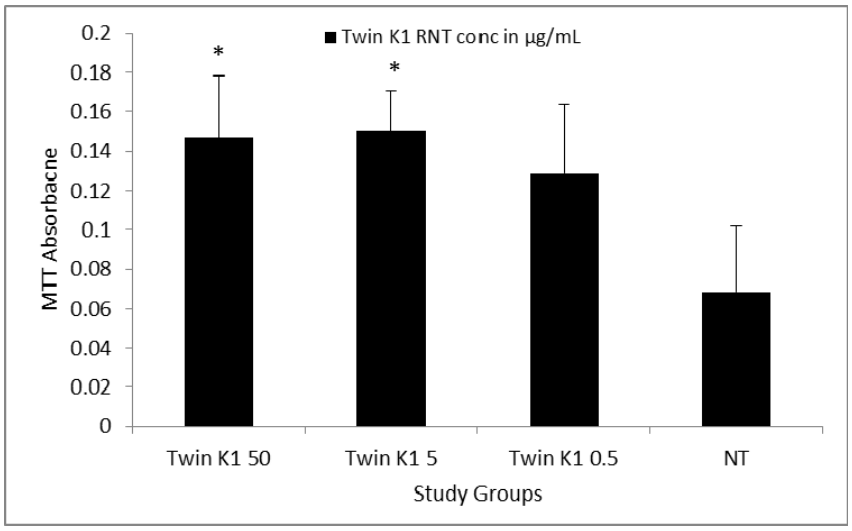

Figure 3.6) Cell attachment on different substrates, A) Tissue culture treated plates coated with Twin K1 RNTs, B) Non-tissue culture treated plates coated with Twin K1 RNTs, C) and D) Ti wafers coated with Twin K1 RNTs. Concentrations of Twin K1 and three different cell densities used are indicated in the graphs. However, for D) only one cell seeding density was used. Cell attachment was determined after 18 hours by using hemocytometry in A), B) and C) and by using MTT in C). Data was summarized as the average of triplicates per treatment. For statistical

analysis, Two-tailed heteroscedastic t-statistic was used and statistical significance was defined by * meaning p-value<0.05 compared with no treatment

The results in Figure 3.6A indicated that coating of Twin K1 RNTs increased the cell adhesion. At~33,000 cells in a 24 welled tissue culture treated plate, we observed a significant increase in cellular adhesion of Twin K1 RNTs at5 μg/mL. Second, on increasing the cell density to ~50,000 cells/well, there was a significant increase in cellular adhesion in all the three concentrations of Twin K1 RNTs (50, 5 and 0.5 μg/mL). At a cell density of 88,000 cells, results showed a significant increase in the cell adhesion at 50 and 5 μg/mL. The rest of the treatment groups showed an increase in adhesion that were not significant. Among all groups, using ~50,000 cells/well at 50 and 0.5 μg/mL concentrations of RNTs showed the highest percentage increase of hBMSCs adhesion using non-treated plastic plates: ~38.3% and 38.7% increase.

The results in Figure 3.6B have shown that, compared with tissue culture treated plates, coating of Twin K1 RNTs increased the cell adhesion. However, the number of cells adhered on the Non-tissue culture treated plate were lesser. Moreover, the results have shown greater variance in their cell numbers (particularly for low cell density seeding). While using a cell density of 32,000 cells in a 24 welled plate, all the three doses of Twin K1 showed significant increase in adhesion (50, 5 and 0.5 μg/mL). Second, in using 52,000 cells/well, two of the higher doses of Twin RNTs showed a significant increase in cell adhesion (50 and 5 μg/mL). In addition, using a cell density of 87,000 cells/well, Twin K1 RNTs showed significant increase in adhesion at all the three doses i.e. 50, 5 and 0.5 μg/mL.

The results of Figure 3.6C showed that there was not a significant difference between the Ti wafers coated with Twin K1 RNTs and the No treatment group. This could be attributed to

the employment of hemocytometry since it involves trypsinization and counting of cells which requires a transparent substrate however, Ti wafers are opaque. Therefore, we replicated the experiment using the MTT assay.

The results in Figure 3.6D were obtained with a cell density of 88,000 cells/well where each well contains a Ti wafer as a substrate. The outcomes of coating Twin K1 RNTs on the Ti wafer showed a significant increase in at RNT concentrations of 50 and 5 μg/mL.Among all the three substrates, 5 μg/mL concentration of RNTs showed the greatest increase in adhesion.

When the tissue culture treated plates were coated with Twin K1 RNTs, a synergy between the substrate (because the hydrophilic surface supports cell attachment) and the RNTs could exist for facilitating cell attachment (Zhang L, 2010). While using tissue culture treated plates, on varying the cell density from 33,000 to 88,000 cells/well, the 5 μg/mL concentration of Twin K1 RNTs gave a significant increase in cell adhesion in all the cell densities. Twin K1 RNTs are expected to increase cellular adhesion since they are biocompatible, possess a lysine chain on its periphery which carries a positive charge and can increase the surface area of the surface by modifying its nanotopography as explained in section 1.7.5 (Chun AL, 2004) (Zhang L, 2009). Moreover, it has been shown than RNTs mimic the helical structure of natural collagen which increases cellular adhesion (Chen Y, 2008) (Zhang L, 2010) (Song S, 2012). However, a higher dose of 50 μg/mL or a lower dose of 0.5 μg/mL were not consistent in rendering significant cell adhesion. This can be explained by the discussion in Sec 3.3. In brief, when the concentration of RNTs is 0.5 μg/mL, the quantity of material present is 0.25 μg/mL which is less than required (1 μg/mL, as shown in section 3.3) to cover the substrate of 2 cm^2. Moreover, when the concentration is 50 μg/mL, the quantity of material present is 25 μg/mL

which is too high for stability of coating on the substrate which may obstruct the cell binding sites.

When the Non-tissue culture treated plates were coated with Twin K1 RNTs, the cells were more dependent upon the Twin K1 RNTs coating to undergo adhesion since Non-Tissue culture treated plates are hydrophobic. Therefore, we observed a significant increase in adhesion in all the three cell densities of 32,000, 52,000 and 87,000 cells/well at almost all the doses. These outcomes could be attributed to properties of Twin K1 nanotubes as mentioned above. However, Twin K1 RNTs at a concentration of 0.5 µg/mL using 52,000 cell density, the result was insignificant. This could be attributed to the lack of material as explained in section 3.3 or due to the variation in cell numbers obtained in hemocytometry.

While coating Twin K1 RNTs on Ti wafers, the technique of analysis was switched to MTT as explained in section 3.6. Using a high cell seeding density of 88,000 cells/well, Twin K1 RNTs coating significantly increased the cell density at the two concentrations of 50 µg/mL and 5 µg/mL. This result is similar to the previous results of the experiment and can be explained in the same way as above. 5 µg/mL is an appropriate dose of the material to cover the substrate and show its response to cell adhesion. Likewise, 50 µg/mL is quite a high dose and it may have produced multiple layers of coating but if the coating is stable, it can produce significant cellular adhesion. However, at the lower concentration of 0.5 µg/mL dose, there was insufficient material to cover the entire substrate and thus we did not observe a significant increase in adhesion.

3.8) Cell Adhesion on Ti wafers by measuring the fluorescence of cellular contents quantitatively:

The aim of this experiment was to compare the attachment of hBMSCs on Ti and compare them with the No treatment. SYBR green I was used the to stain DNA of hBMSCs. The fluorescence of SYBR green I was expected to be proportional to the cells attached with Ti. Moreover, this assay was done to confirm the results obtained in Section 3.7D.

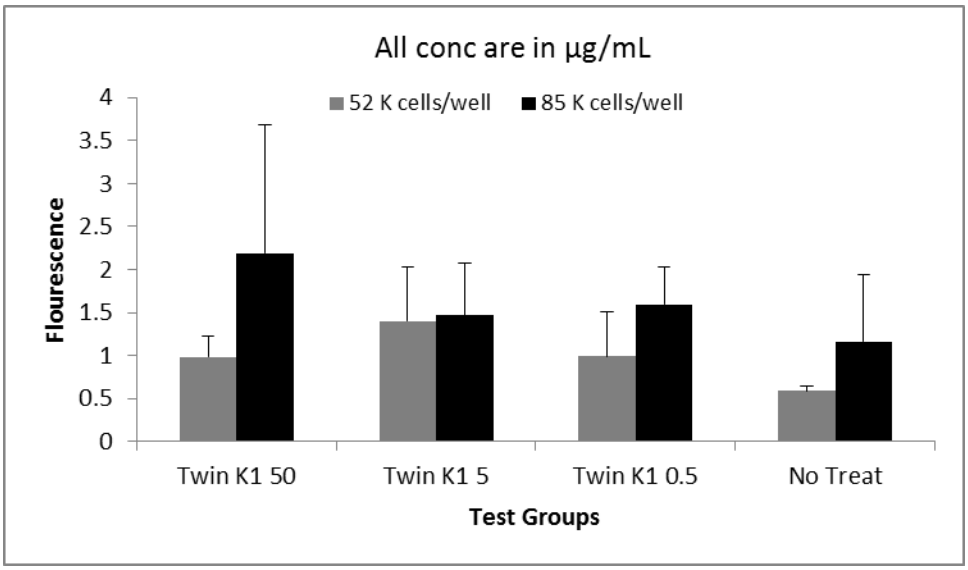

Figure 3.7) Cell attachment on Ti wafers coated with Twin K1 RNTs. Concentrations of Twin K1 used are indicated in the graphs. Cell attachment was determined by measuring the DNA content (by fluorescence) after dissolving the cellular contents. Incubation period was 18 hours. Data was summarized as the average of triplicates per treatment. For statistical analysis, Two-tailed heteroscedastic t-statistic was used and statistical significance was defined by * meaning p-value<0.05 compared with no treatment

This experiment was conducted using two cell densities, 52,000 cells/well and 85,000 cells/well. Both the cell densities, the coating of Twin K1 RNTs lead to an increase in cellular adhesion similar to previous experiments. However, none of the outcomes showed any statistical significance. The results showed a huge SD.

These results were not expected since Twin K1 had shown a significant increase in cell adhesion in the previous section 3.7 using the MTT assay. We hypothesized that the process of dissolving cells in Alkaline phosphatase buffer and then staining the celluar contents with SYBR green I (Cyanine dye) was producing a relatively large variation in the experiment. In order to confirm this, a cell density calibration experiment was performed where the cell density added to Ti wafers in 24 well plates was modified while keeping everything else constant.

3.9) Calibration curve of cells numbers attached to Ti while using automated fluorescent imaging

The aim of this experiment was to calibrate the cell numbers attached on Ti wafer at different cell seeding densities using automated fluorescent imaging.

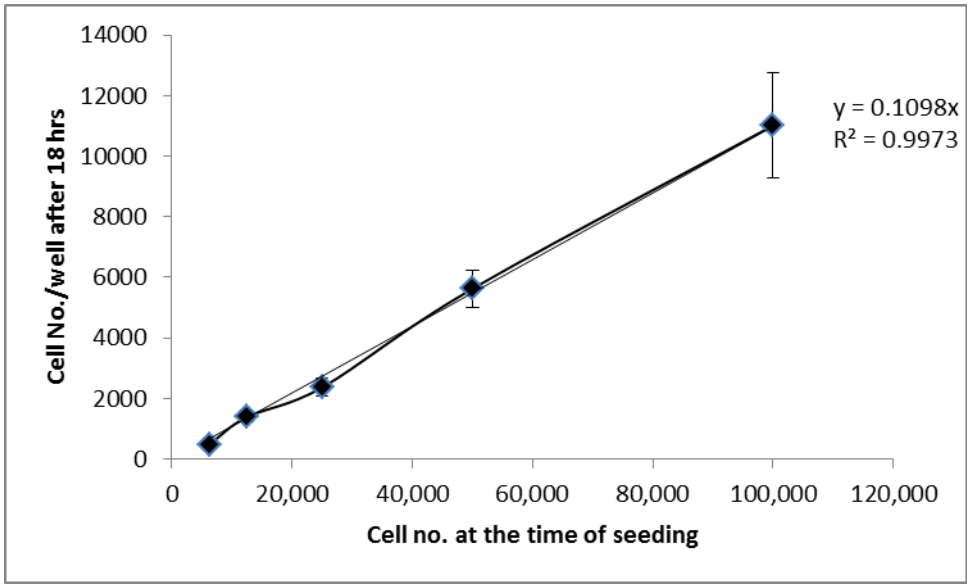

Figure 3.8) Cell attachment on Ti wafers. Cell attachment was determined by counting the cells (using an automated software) attached on the Ti wafer stained with SYBR Green I. Incubation period was 18 hours. Data was an average of triplicates per treatment.

The results showed that there was a linear relationship between the number of cells added on the wafer and the cell seeding density. The linear co-relation value is 0.9973. In brief, when the seeding cell density was 100,000, there were 12,000 cells attached to Ti wafer. Likewise, when the cell seeding density was reduced to half i.e. 50,000, there were 5,200 cells attached. Furthermore, the next lower seeding cell density was 25,000 and the number of cells attached to wafer were approx. 2,370. We chose these three cell densitites which were relevant since below the cell density of 25,000 cells/well, the cell counts were too low.

These results were in agreement with our expectations. There exists a linear relationship between the seeding cell density and the number of cells attached on Ti. Furthermore, these

results support our results in section 3.6 showing the linear relationship of seeding cell density with the number of cells attaching with the Ti wafer.

We used SYBR green I because it is a monomeric, assymetrical cyanine dye with a high binding affinity for double-stranded DNA of cells and has been used extensively for staining hBMSCs (Zipper H, 2004)(Whyte JL, 2011). This assay will be used as a complementary assay to confirm the results obtained by measuring the MTT absorbance of cell on Ti wafer. The reason to choose a complementary assay was because MTT assay measures the metabolic activity of the cells as shown in section 3.6 however, there is a possibility that cells are attached to the substrate but are metabolically inactive or over-active which may deviate the MTT absorbance. Therefore, measuring the fluorescence of live cells using SYBR green I would silent this possibility and would render more trustworthy results.

3.10) Cell Adhesion on Ti wafers analyzed through MTT assay

The aim of this experiment was to test the influence of Twin K1 RNTs on cell adhesion by coating them on Ti wafers and comparing their effect with no treatment.

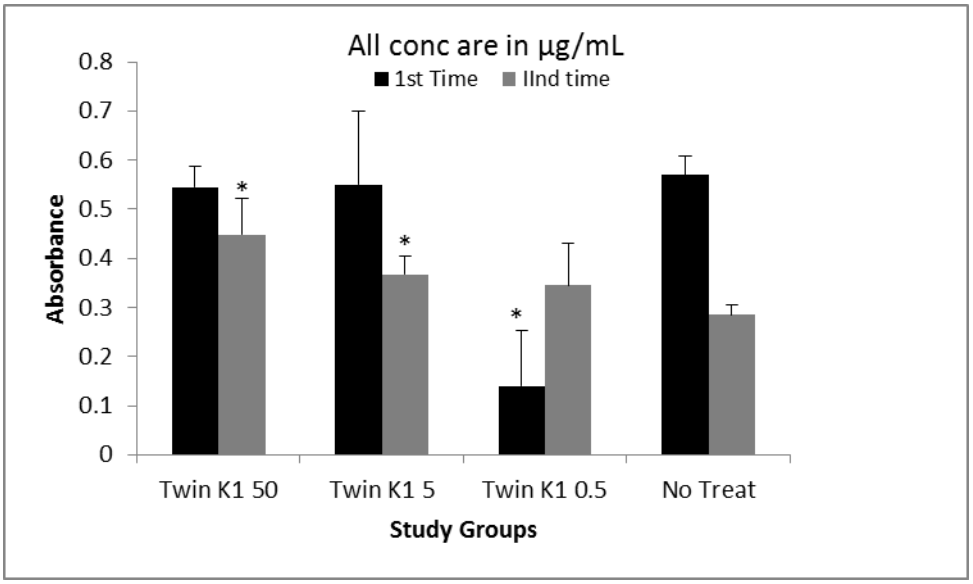

Figure 3.9) Cell attachment on Ti wafers coated with Twin K1 RNTs. Concentrations of Twin K1 are indicated in the graphs. Cell attachment was determined by using MTT after 18 hours. Data was summarized as the average of triplicates per treatment. For statistical analysis, Two-tailed heteroscedastic t-statistic was used and statistical significance was defined by * meaning p-value<0.05 compared with no treatment

The results showed that when the experiment was conducted for the first time, there was no effect at 50 and 5 µg/mL doses. Moreover, at 0.5 µg/mL dose, there was a significant negative effect on the adhesion of cells compared with the no treatment. When the same experiment was conducted for the second time, Twin K1 RNTs coating showed increase in the adhesion of cells. This response was similar to the response obtained in section 3.6D. Furthermore, when the concentration of RNTs was raised to 5 and 50 µg/mL, there was a significant increase in the adhesion of the cells. However, the difference between this experiment and 3.6D was the cell density. In this experiment, cell density was 50,000 cells/well and in 3.6D there were 88,000 cells/well.

The results obtained when the experiment was done for the first time were not expected and inexplicable. Coating of Twin K1 RNTs had been shown to increase cell adhesion in section 3.7 and it was important to check the consistency of the results. Therefore, the experiment was repeated. For the second time, the outcomes were similar to the trend obtained in Section 3.6D. These results were expected as Twin K1 RNTs 1) are biomimetic naturewhich resembles the structure of Mono K1 and mimics the structure of collagen. Moreover, it modifies the nanotopography of Ti by increasing its surface area (Lijie Zhang L, 2008) (Chun AL, 2006). Additionally, Twin K1 RNTs carry a lysine group which imparts a positive charge on its periphery which is very similar with its analog Mono K1 and has been shown to improve the adhesion of human fetal osteoblasts on Ti wafer (Song S, 2012) (Zhang L, 2010).

3.11) Cell Adhesion on Ti wafers coated with Twin K1 RNTs analyzed by counting cells using automated fluorescent imaging

The goal of this experiment was to test the influence of Twin K1 RNTs on cell adhesion on Ti wafers. The difference between this and the study described in section 3.10 is the use of analytical technique. In this experiment, the cells attached to the Ti wafer were counted using automated fluorescent imaging.

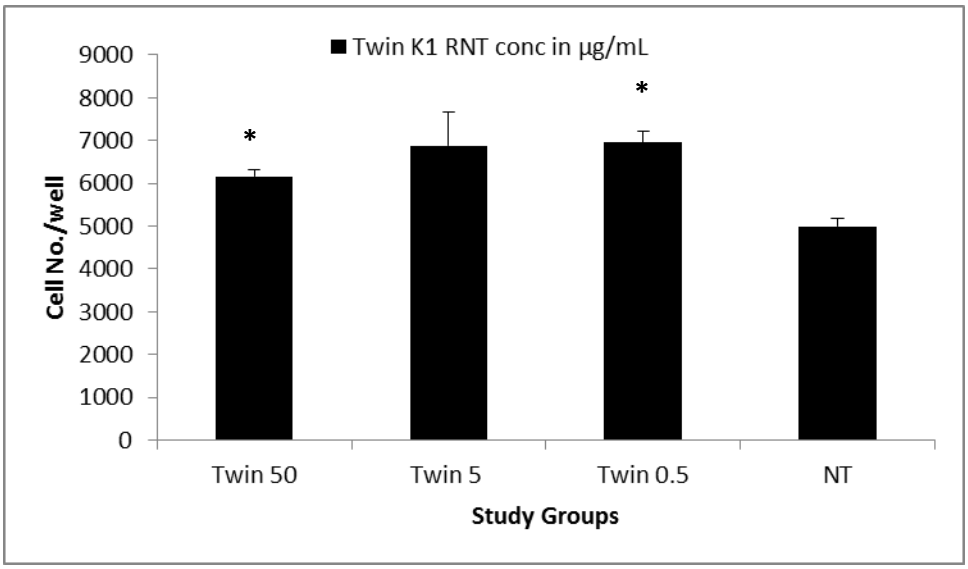

Figure 3.10) Cell attachment on Ti wafers coated with Twin K1 RNTs. Concentrations of Twin K1 are indicated in the graphs. Cell attachment was determined by counting the cells stained with SYBR Green I. Incubation period was 18 hours. Data was summarized as the average of triplicates per treatment. For statistical analysis, Two-tailed heteroscedastic t-statistic was used and statistical significance was defined by * meaning p-value<0.05 compared with no treatmentThe results of this experiment showed that Twin K1 RNTs coating on Ti wafers increased cellular adhesion which attained significance at concentrations of 0.5 and 50 µg/mL. Twin K1 RNTs at a concentration of 5 µg/mL missed significance with a small margin (due to high SD in this group). Nevertheless, these results show a similar trend with the Section 3.7 and section 3.10.

The use of analyzing the results using automated fluorescent imaging has been explained in section 3.9. In brief, imaging will complement the results obtained by using MTT (section 3.7 and 3.10) and will avoid the variable which could be possible while using MTT. The obtained

results were expected. Twin K1 RNTs have showed an increase in adhesion in sections 3.7 and 3.10 and carry the similar explanation for the outcomes. . In this study, all the concentrations of Twin K1 RNTs like 50, 5 and 0.5 μg/mL caused an increase in cellular adhesion however, the group of 5 μg/mL missed to produce significance from a small margin due to SD In section 3.13, we have tried different coating techniques in order to optimize the cellular reponse of RNTs coating on substrate. .

3.12) Cell Adhesion on Ti wafers using MTT while using Dipping method of nanotube coating

The aim of this experiment was to coat the Twin K1 nanotubes on Ti wafer by dipping them into the nanotube solution. The difference between this experiment and section 3.11 is the technique of coating the nanotubes on Ti

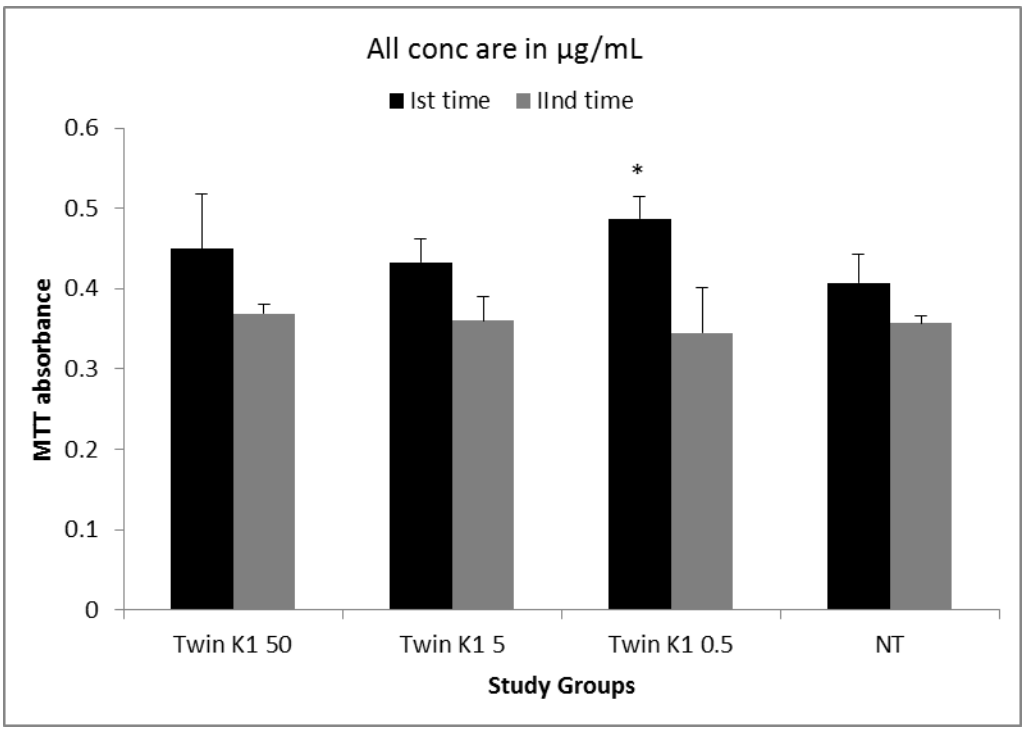

Figure 3.11) Cell attachment on Ti wafers coated with Twin K1 RNTs. Concentrations of Twin K1 are indicated in the graphs. Cell attachment was determined by measuring their MTT absorbance. Incubation period was 18 hours. Data was summarized as the average of triplicates per treatment. For statistical analysis, Two-tailed heteroscedastic t-statistic was used and statistical significance was defined by * meaning p-value<0.05 compared with no treatmentResults showed that while doing the experiment for the first time, Twin K1 at the concentration of 0.5 µg/mL had a significant effect on cellular adhesion compared with the no treatment. Although other study groups, 5 and 50 µg/mL produced an increase in adhesion but they were not statitically significant. Furthermore, when the experiment was conducted for the second time, none of the groups gave significant results.

These results were not expected. Our group has shown an increase in cellular adhesion when Ti wafers were coated with RNTs (Fine E, 2009) (Chun AL, 2004). However, there was a

possibility of insufficient response from hBMSC since two study groups could not show significant increase in adhesion from a small margin. Moreover, the cells used for this experiment were obtained from a different patient source which could be a reason for the change in reponse as obtained in sections 3.7, 3.11 and 3.12. Therefore, the experiment was repeated. In addition, the technique of coating RNTs on Ti was optimized in order to further identify the influence of RNT coating on Ti..

3.13) Comparison of coating techniques using Twin K1 RNTs and its influence on cell adhesion analyzed through MTT

Aim of this experiment was to compare three techniques of coating Twin K1 nanotubes on Ti wafers (Dipping, Drop casting, Spin coating), and comparing their cell adhesion response with the no treatment.

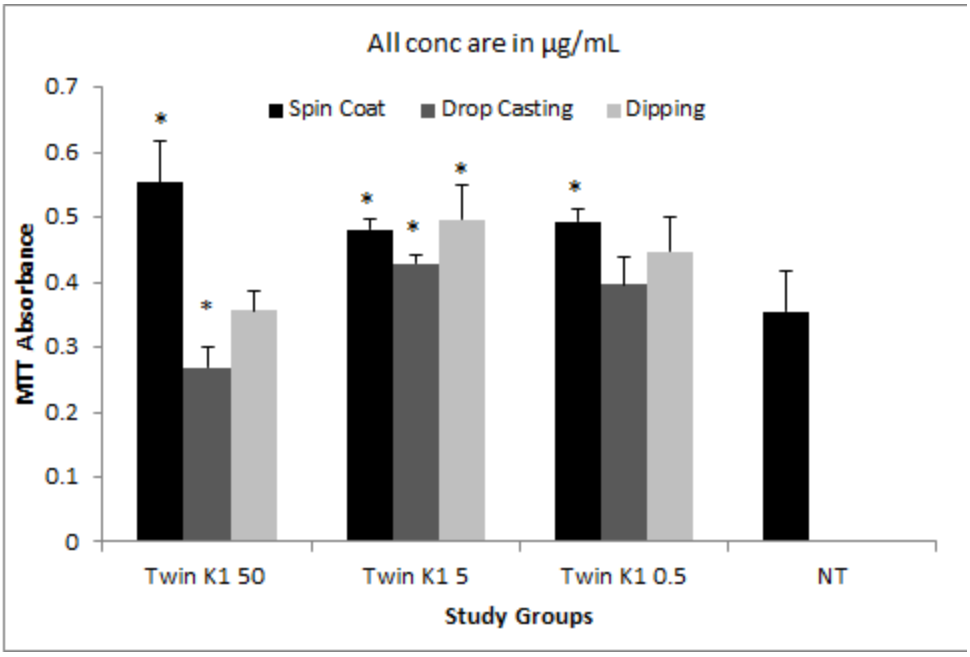

Figure 3.12) Cell attachment on Ti wafers coated with Twin K1 RNTs. Concentrations of Twin K1 are indicated in the graphs. Cell attachment was determined by measuring their MTT absorbance. Incubation period was 18 hours. Data was summarized as the average of triplicates per treatment. For statistical analysis, Two-tailed heteroscedastic t-statistic was used and statistical significance was defined by * meaning p-value<0.05 compared with no treatment

Twin K1 RNTs at a concentration of 0.5 μg/mL showed a significant increase in adhesion by using spin coating when compared with No treatment. Rest of the treatment groups produced an increase in cellular adhesion however, they were not statistically significant. Twin K1 RNTs at a concentration of 5 μg/mL produced a significant increase in adhesion using all the three techniques of coating. Furthermore, when the concentration was increased to 50 μg/mL, results were significantly higher using spin coating, significantly lower in drop casting and non significant in dipping when compared with the no treatment.

These results were expected. As described in section 3.3, when the concentration of Twin K1 RNTs was 0.5 μg/mL, the material was insufficient to cover the entire substrate which means that there will be patches of RNTs coated on Ti and therefore it was difficult to anticipate a significant increase in adhesion in all the study groups. However, when the concentraion of Twin K1 was increased to 5 μg/mL, the material was sufficient to cover the substrate and therefore there was a significant increase in adhesion using all the three techniques of coating. This trend of result was similar to section 3.7 and 3.11. Moreover, when the concentration of Twin K1 RNTs was increased to 50 μg/mL, there was excess coating material on the substrate. If the excess coating material was stable, it gave significant increase in adhesion as in case of Spin coating. However, if the coating got weak, it may not stay stable, detach from the substrate

which could block the binding site of cell adhesion as seen in case of Dipping and Drop casting. Although, these results gave an indication that there was not a significant difference in cell adhesion between the techniques of coating used but it was important to confirm these results by complementing this experiment using another analysis technique.

3.14) Comparison of coating techniques using Twin K1 and its influence on cell adhesion analyzed using automated fluorescent imaging

The aim of this experiment was to compare the Dipping and Drop casting techniques for coating Twin K1 nanotubes on the Ti wafer (Dipping and Drop Casting) and comparing their response with the no treatment. We discontinued the use of spin coating since it was difficult to maintain sterile conditions.

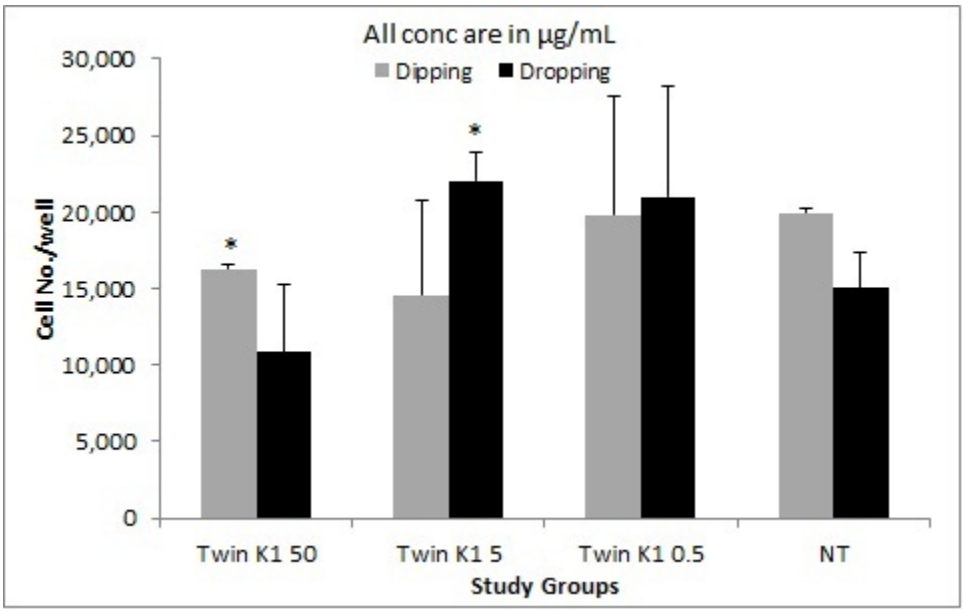

Figure 3.13) Cell attachment on Ti wafers coated with Twin K1 RNTs. Concentrations of Twin K1 are indicated in the graphs. Cell attachment was determined by counting the cells. Incubation period was 18 hours. Data was summarized as the average of triplicates per treatment. For statistical analysis, Two-tailed heteroscedastic t-statistic was used and statistical significance was defined by * meaning p-value<0.05 compared with no treatment.

Results of this experiment showed that Twin K1 RNTs at a concentration of 0.5 μg/mL did not cause a significant increase or decrease in adhesion. However, when the concentration of Twin K1 was increased to 5 μg/mL, we observed a significant increase in adhesion when using the Drop casting technique, but not with the Dipping technique. In addition, when the concentration of Twin K1 RNTs was increased to 50 μg/mL, dipping method showed a significant decrease in adhesion.

These results were expected. When the Twin K1 RNTs were coated at a concentration of 0.5 μg/mL, we saw an increase in adhesion however, the increase was not significant because there was insufficient material to cover the Ti substrate as explained in section 3.3. When the concentration of Twin K1 RNTs was increased to 5 μg/mL, there was a significant increase in cellular adhesion while using the dropping technique. Furthermore, Twin K1 RNTs at a concentration of 50 μg/mL produced a significant decrease in adhesion while using dipping technique possibly due to excess material on the substrate. This could be attributed to high concentration of RNTs which lead to either weak multilayer coating of material on Ti producing insufficient adhesion of cells or excess RNTs may have blocked the binding sites of cells to adhere with the substrate. Therefore, after this experiment and complemeting its results with the

section 3.13, we understand that there is not a significant difference between the techniques of coating used.

3.15) Test study to compare the cell adhesion on Ti via filling the well with hBMSCs cell suspension and restricting the cell suspension spreading on Ti wafer

The aim of this experiment was to compare the cell adhesion when the cell suspension was added in excess in the well containing the Ti wafer versus when the cell suspension was restricted within the boundaries of the Ti wafer.

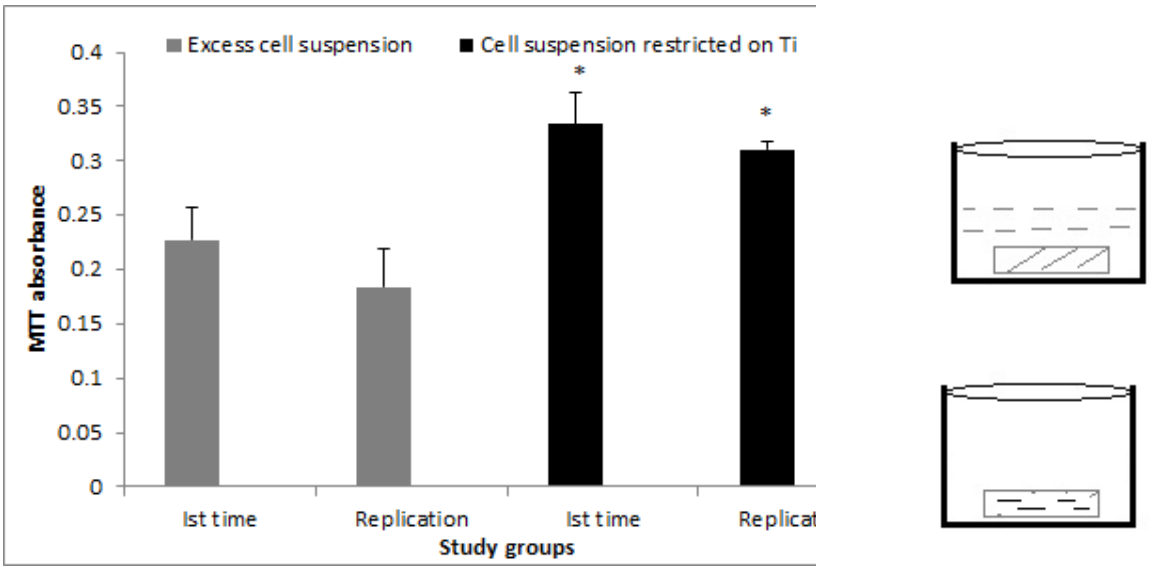

Figure 3.14) Cell attachment on Ti wafers. Cell attachment was determined by measuring their MTT absorbance. Incubation period was 18 hours. Data was summarized as the average of triplicates per treatment. For statistical analysis, Two-tailed heteroscedastic t-statistic was used and statistical significance was defined by * meaning p-value<0.05 compared with no treatment, B) Schematic representation of a Ti wafer filled with cell suspension and, C) Schematic representation of a Ti wafer on which cell suspension spread was restricted within its edges.

The results of this experiment showed that there was a significant difference in MTT absorbance when the cells were restricted on the Ti wafer versus when the wells were filled up with cell suspension.

When we added 500 µL cell suspension containing 50,000 cells in a 24 well plate containing Ti wafer, the MTT absorbance was low. We suspect that this was due to the cells falling off from the Ti wafer which covers only 1 cm^2 of surface area out of the 2 cm^2 total surface area of the well as shown in Figure 3.14 B). However, when we added a smaller volume of cell suspension on the Ti wafer while maintaining the same cell density, we found a higher MTT absorbance and less standard deviation in the values as shown in Figure 3.14 C). Moreover, both of the values of the group 'cell suspension restricted on Ti' (Ist time and replication) were statistically higher than the group 'excess cell suspension' (Ist time and replication).

3.16) Proliferation study of hBMSCs on Ti for 1, 5, 10 days

The aim of this experiment was to understand the effect of Twin K1 RNTs coated Ti wafer on cell proliferation over 10 days. The cellular response was compared with the No treatment group

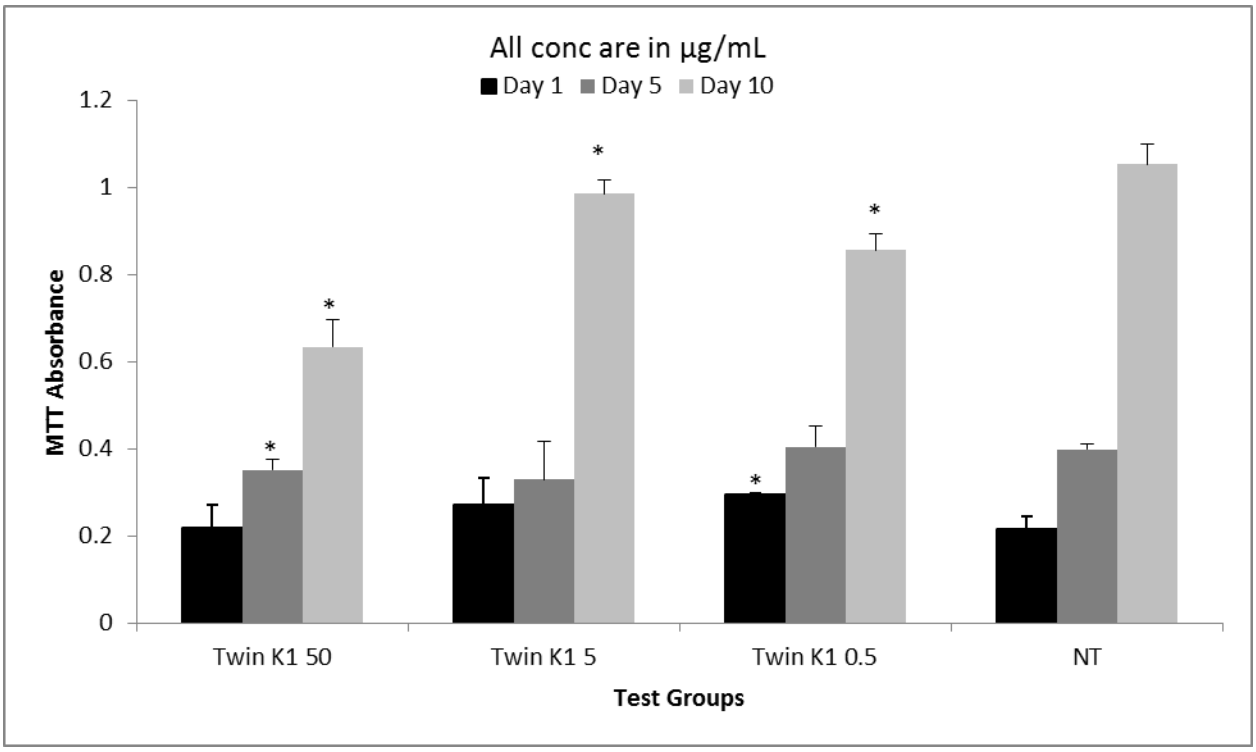

Figure 3.15) Cell proliferation on Ti wafers coated with Twin K1 RNTs. Concentrations of Twin K1 are indicated in the graphs. Cell attachment was determined by measuring their MTT absorbance. Incubation periods were 24 hours, day 5 and day 10. Data was summarized as the average of triplicates per treatment. For statistical analysis, Two-tailed heteroscedastic t-statistic was used and statistical significance was defined by * meaning p-value<0.05 compared with no treatment

Results of this experiment showed that for day 1, Twin K1 showed a significant increase in MTT absorbance only at 0.5 µg/mL concentration. On day 5, none of the peptide

concentrations showed an increase in MTT absorbance compared with day 1, except the 50 μg/mL concentration which showed a significant decrease in cell number. On day 10, all the study groups rendered a significant decrease in MTT absorbance compared with the no treatment wafers.

These results demonstrated that the Twin K1 RNT coating does not increase the adhesion for durations longer than 24 hours (i.e. proliferation). We hypothesized that decrease in cellular adhesion was attributed to the solubility of RNTs into the medium. RNTs are water soluble and when they stayed in contact with the media for 5-10 days, they may had got dissolved into the media and pulled the cells attached with the RNTs. Therefore, we observed a reduced cell adhesion as the time progressed.However, we have seen that RNTs are effective in increasing the cellular adhesion upto 24 hours and therefore, the next step was to compare the cellular adhesion caused by the coating of different peptide RNTs.

3.17) Cell Adhesion on Ti wafers coated with Peptide co-assembly RNTs and Mono K1 RNTs analyzed using MTT assay

The aim of this experiment was to test the influence of Pep A:Twin K1 (1:9) coassembled RNTs, Pep B:Twin K1 (1:9) coassembled RNTs and Mono K1 self-assembled RNTs on cell adhesion

by coating them on the Ti.

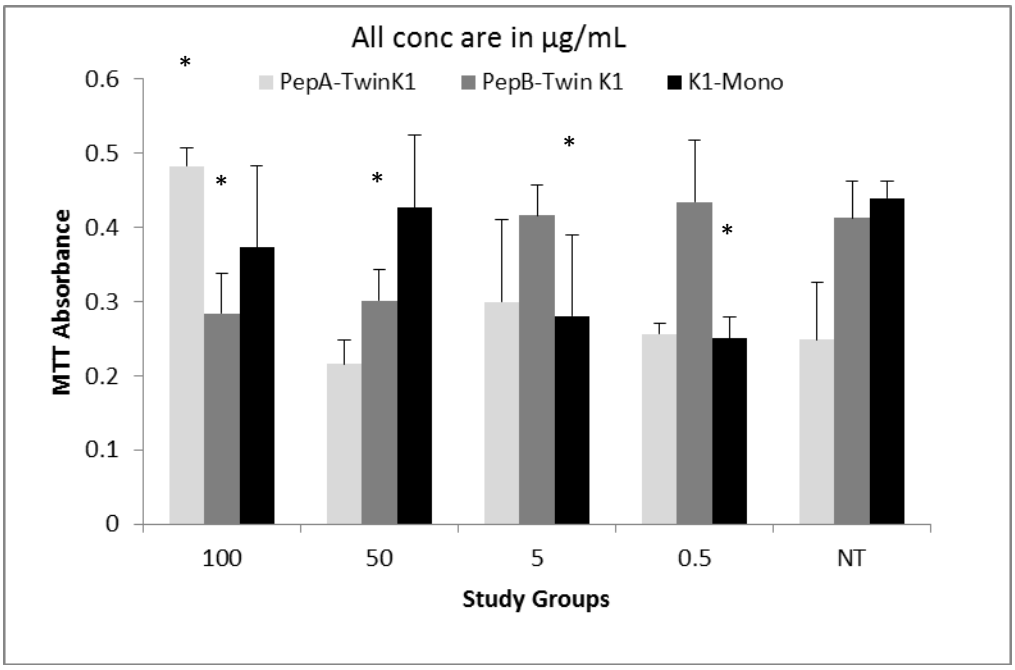

Figure 3.16) Cell adhesion on Ti wafers coated with Twin K1 RNTs. Concentrations of Twin K1 are indicated in the graphs. Cell attachment was determined by measuring their MTT absorbance. Incubation period was 18 hours. Data was summarized as the average of triplicates per treatment. For statistical analysis, Two-tailed heteroscedastic t-statistic was used and statistical significance was defined by * meaning p-value<0.05 compared with no treatment.

The results showed that Pep A:Twin K1 (1:9) coassembled RNTs showed a significant increase in MTT absorbance at 100 µg/mL concentration and none of the other concentrations of Pep A:Twin K1 RNTs gave significant results compared with the no treatment. In case of Pep B:Twin K1 (1:9) coassembled RNTs, they gave significantly reduced MTT absorbance at 100 and 50 µg/mL concentrations. The rest of the concentrations of Pep B:Twin K1 (1:9) gave non-

significant results. In addition, in the case of Mono K1 self-assembled RNTs, we observed a significant reduction in MTT absorbance at 5 and 0.5 µg/mL. Non-significant results were observed in all other concentrations of Mono K1.

The no treatment group's responses were not consistent but a similar observation was found in section 3.10. These results could be due to the instability of hBMSCs on Ti grade II wafers. Unfortunately, we could not find such report in the literature. Moreover, Pep A:Twin K1 (1:1) co-assembled RNTs gave favourable results when they were coated on Tissue culture plastic plate in section 3.3 and 3.4. Likewise, Pep A:Twin K1 (1:9) co-assembled RNTs gave significant results at 100 µg/mL. Furthermore, Mono K1 RNTs have been previously demonstrated that they improve the adhesion of human fetal osteoblasts and rat aortic endothelial cells (Zhang L, 2010) (Zhang L, 2009) (Fine E, 2009). Therefore, following these results, we hypothesized that hBMSCs are not very compatible with Ti substrate. Moreover, measuring the MTT absorbance should be complemented with another analytical technique. MTT absorbance measures the metabolic activity of the cells however, if cells interact with the RNTs they may give a higher or reduced metabolic activity (Hongo T, 1990) (Wan H, 1994) (Heo DS, 1990). In order to test these hypotheses, this experiment was repeated using a different substrate while using two analytical techniques.

3.18) Cell Adhesion on Non Treated Tissue Culture treated plastic coated with Pep A:Twin K1 (1:9) coassembled RNTs, Pep B:Twin K1 (1:9) coassembled RNTs, Twin K1 self-assembled RNTs and Mono K1 self-assembled RNTs analyzed using MTT assay

The aim of this experiment was to test the influence of Pep A:Twin K1 (1:9) coassembled RNTs, Pep B:Twin K1 (1:9) coassembled RNTs, Twin K1 self-assembled RNTs and Mono K1 self-assembled RNTs on cell adhesion on Non-Tissue culture treated plates.

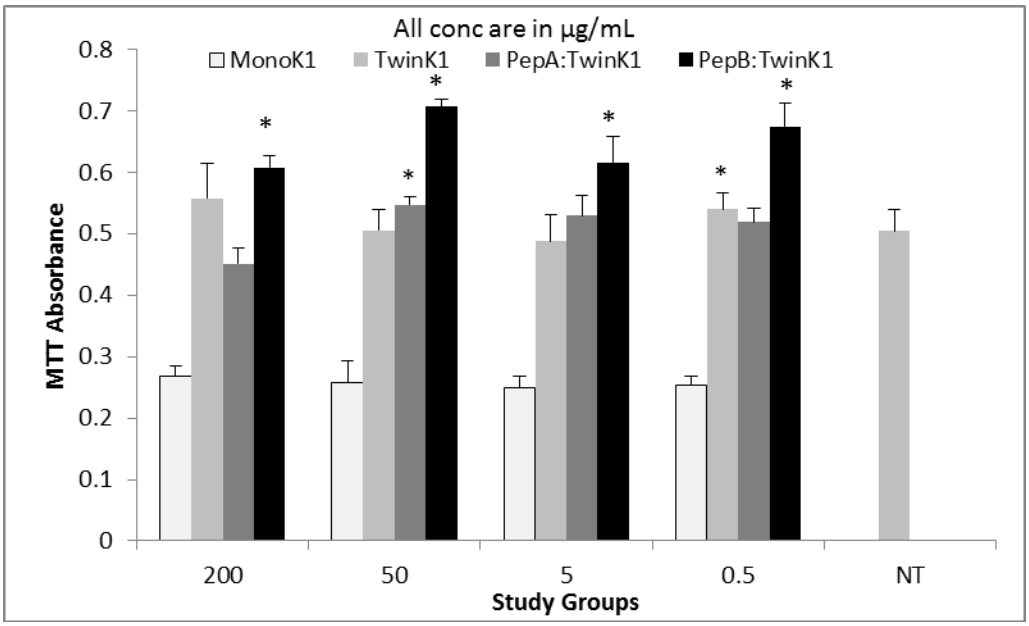

Figure 3.17) Cell adhesion on Non-tissue culture treated plastic plates coated with Pep A:Twin K1 (1:9) coassembled RNTs, Pep B:Twin K1 (1:9) coassembled RNTs, Mono K1 self-assembled RNTs and Twin K1 self-assembled RNTs. Concentrations of RNTs are indicated in the graphs. Cell attachment was determined by MTT. Incubation period was 18 hours. Data was summarized as the average of triplicates per treatment. For statistical analysis, Two-tailed heteroscedastic t-statistic was used and statistical significance was defined by * meaning p-value<0.05 compared with no treatment

Results of this experiment showed that Twin K1 RNTs coating produced a significant increase in MTT absorbance at 0.5 µg/mL and other concentrations gave non-significant results. For Pep A:Twin K1 (1:9) coassembled RNTs, a significant increase in MTT absorbance was

observed at 50_µg/mL concentration. The remainder of the Pep A:Twin K1 RNT concentrations did not produce statistical significance. For Pep B:Twin K1 (1:9) coassembled RNTs, all the study groups starting from 0.5 to 200 µg/mL concentrations lead to a significant increase in MTT absorbance. However, Mono K1 RNTs coating gave extremely low values and therefore were difficult to explain.

Twin K1 RNTs have shown increase in cellular adhesion. This could be attributed to the reasons mentioned in section 3.7 and 3.10. The increase in cellular adhesion caused by Pep A and Pep B RNTs could be attributed to their osteogenic potential because they are the short sequences of BMP-7 (Chen Y, 2008). Moreover, Peptide A and Peptide B RNTs were co-assembled with Twin K1 RNTs which has been shown to be a biomimetic material and promotes human fetal osteoblast adhesion (Song S, 2012) (Zhang L, 2010). Therefore, their co-assembly should have resulted in osteogenic RNTs offering a biomimetic nanostructured material with improved surfacial properties for peptides. However, as discussed in section 3.17, results of measuring MTT absorbance of cells should be complemented with another analytical technique. In order to confirm this set of results, this experiment was repeated using hemocytometry.

3.19) Cell Adhesion on Non Treated Tissue Culture treated plastic coated with Pep A:Twin K1 (1:9) coassembled RNTs, Pep B:Twin K1 (1:9) coassembled RNTs and Mono K1 self-assembled RNTs studied analyzed using hemocytometry

The aim of this experiment was to test the influence of coating Pep A:Twin K1 (1:9) coassembled RNTs, Pep B:Twin K1 (1:9) coassembled RNTs and Mono K1 self-assembled RNTs on cell adhesion on Non-Tissue culture treated plates.

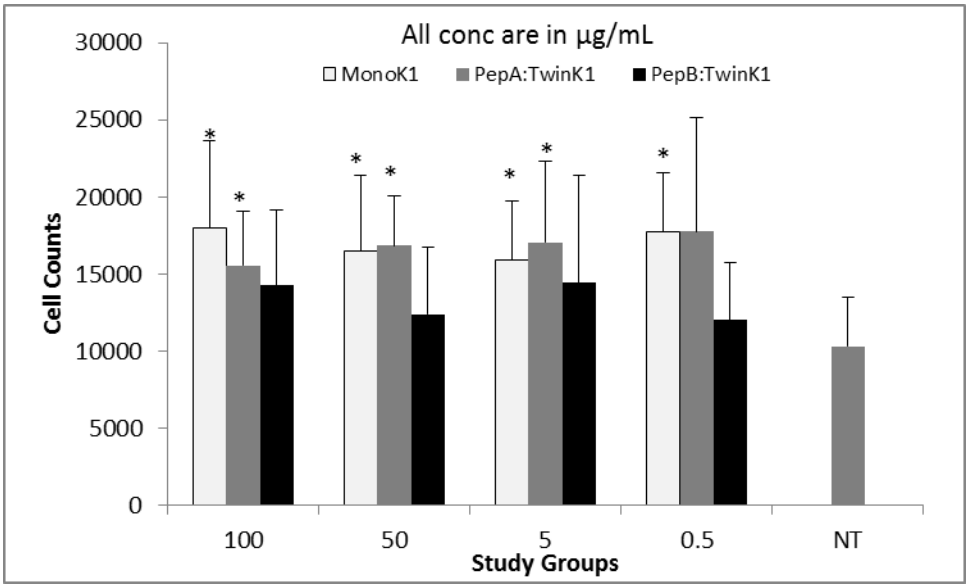

Figure 3.18) Cell adhesion on Non-tissue culture treated plastic plates coated with Pep A:Twin K1 (1:9) coassembled RNTs, Pep B:Twin K1 (1:9) coassembled RNTs and Mono K1 self-assembled RNTs. Concentrations of RNTs are indicated in the graphs. Cell attachment was determined by Hemocytometry. Incubation period was 18 hours. Data was summarized as the average of triplicates per treatment. For statistical analysis, Two-tailed heteroscedastic t-statistic was used and statistical significance was defined by * meaning p-value<0.05 compared with no treatment.

Results of this experiment showed that Pep A:Twin K1 (1:9) coassembled RNTs produced significant increase in cellular adhesion at 100, 50 and 5 µg/mL concentrations. In addition, Pep B:Twin K1 (1:9) coassembled RNTs showed some increase in adhesion, but none of the groups were statistically significant. Mono K1 showed a significant increase in adhesion in all of the study groups.

Pep A:Twin K1 (1:9) coassembled RNTs showed a significant increase in cellular adhesion. This result is in agreement with the results obtained with the Pep A self-assembled

RNTs analyzed by hemocytometry as described in section 3.5. In case of Pep B:Twin K1 (1:9) coassembled RNTs, they have shown an increase in cellular adhesion in all the study groups. However, due to the large SDs, they could not produce statistical significance. For Mono K1, we have found a significant increase in each of the study groups. These results concur with the past publications of our group where Mono K1 was used to increase the adhesion of human fetal ostroblasts (Zhang L, 2010). In brief, Mono K1 RNTs are biocompatible and possess an inner and outer diameter of 1.1 nm and 3.5 nm. Such nanometer dimension mimic dimensions of natural components of collagen (Zhang L, 2009). Furthermore, they are functionalized with lysine side chain to interact with cells (Fine E, 2009).

3.20) Cell adhesion of hBMSCs on Acid etched Ti coated with Pep A:Twin K1 (1:9) coassembled RNTs, Pep B:Twin K1 (1:9) coassembled RNTs , Mono K1 self-assembled RNTs and Twin K1 self-assembled RNTs

The aim of this experiment was to study the cellular adhesion on an acid etched surface of Ti coated with Pep A:Twin K1 (1:9) coassembled RNTs, Pep B:Twin K1 (1:9) coassembled RNTs , Mono K1 self-assembled RNTs and Twin K1 self-assembled RNTs.

A)

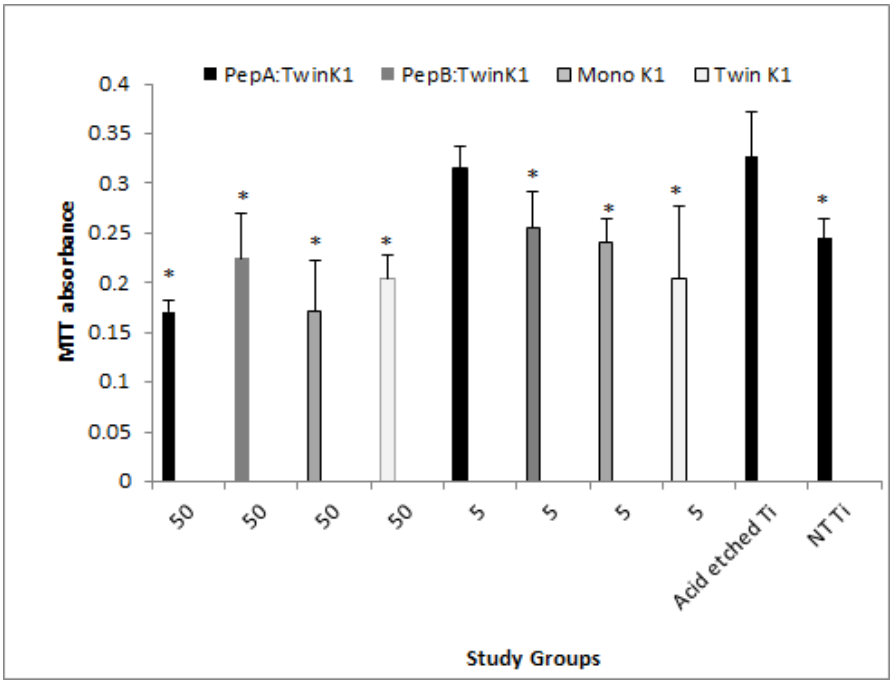

B)

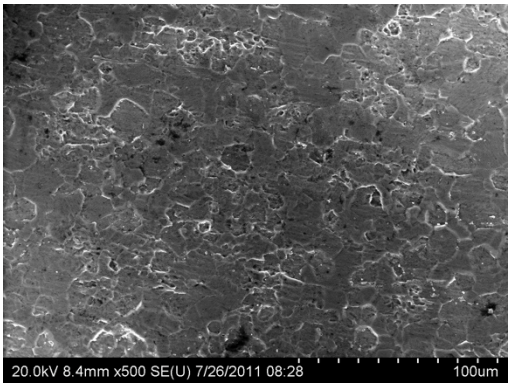

C)

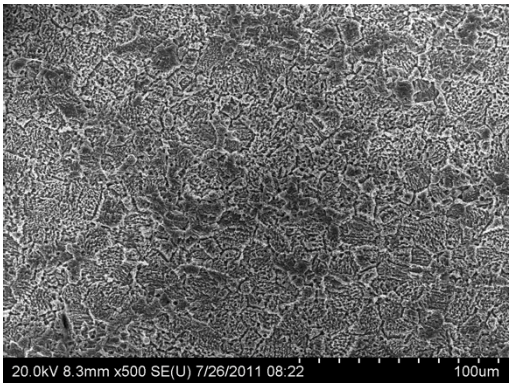

Figure 3.19) Cell adhesion on Ti and SEM images of Ti wafers a) Cell adhesion on Ti wafers coated with Pep A:Twin K1 (1:9) coassembled RNTs, Pep B:Twin K1 (1:9) coassembled RNTs, Mono K1 self-assembled RNTs and Twin K1 self-assembled RNTs. Concentrations of RNTs are indicated in the graphs. Cell attachment was determined by MTT absorbance. Incubation period was 18 hours. Data was summarized as the average of triplicates per treatment. For statistical analysis, Two-tailed heteroscedastic t-statistic was used and statistical significance was defined by * meaning p-value<0.05 compared with no treatment. b) SEM of untreated Ti, c)

SEM of Ti wafer after 8 minutes of acid etching. The magnification and scale of each image is indicated on the images

There was a significant increase in cellular adhesion on acid etched Ti as compared to untreated Ti. The Pep A:Twin K1 (1:9) coassembled RNTs showed a significant decrease in adhesion at 50 μg/mL concentration compared with acid etched Ti. However, when the concentration of RNTs were increased to 50 μg/mL, there was not a significant difference in adhesion between the treatment and the acid etched No Treatment group. In addition, Pep B:Twin K1 (1:9) coassembled RNTs, Mono K1 self-assembled RNTs and Twin K1 self-assembled RNTs showed a significant decrease in adhesion at both 50 and 5 μg/mL concentrations.

The objective of this experiment was to study whether roughening the Ti surface prior to coating them with the RNTs could further increase the cellular adhesion or not. Results showed that roughening the Ti did increase cell adhesion compared with the untreated Ti. However, RNT coating on roughened Ti reduced the cellular adhesion. It has been demonstrated in the literature that roughening the Ti surface can increase cellular adhesion of hBMSCs and our results showed a similar trend (Camilla C. G. Moura, 2010).

3.21) Cytotoxicity (MTT) assay of TwinK1

The aim of this experiment was to study the biocompatibility of Twin K1 self-assembled RNTs, PepA:Twin K1 (1:9) co-assembled RNTs and PepB:Twin K1 (1:9) co-assembled RNTs. Results of this experiment showed that there was no effect on the cell viability when Twin K1 and

PepB:Twin K1 (1:9) RNTs concentration was varied from 0.2 to 200 µg/mL. Moreover, in case of PepA:TwinK1 RNTs, they showed increased cellular viability at 100 and 10 µg/mL doses and showed no reduction in viability up to 200 µg/mL concentration.

A)

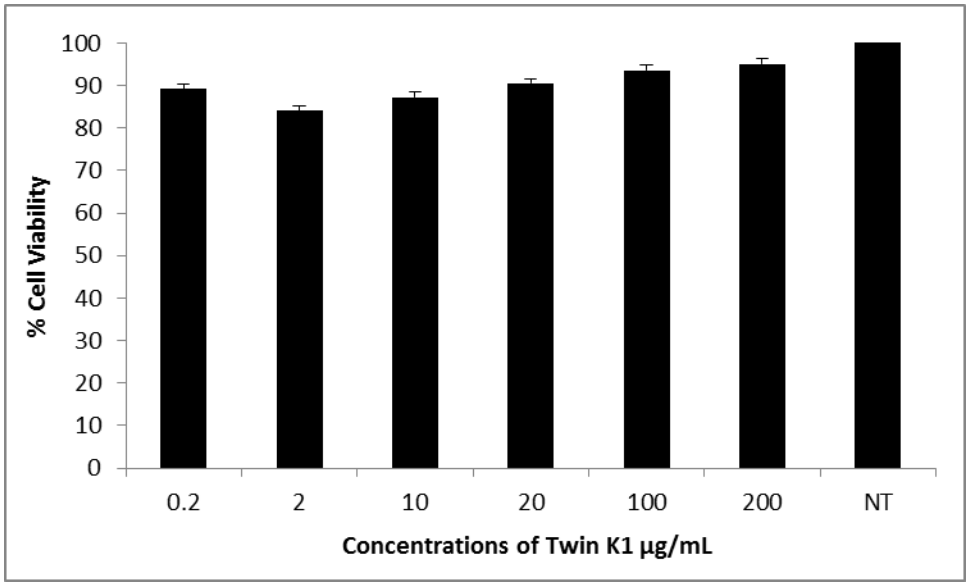

B)

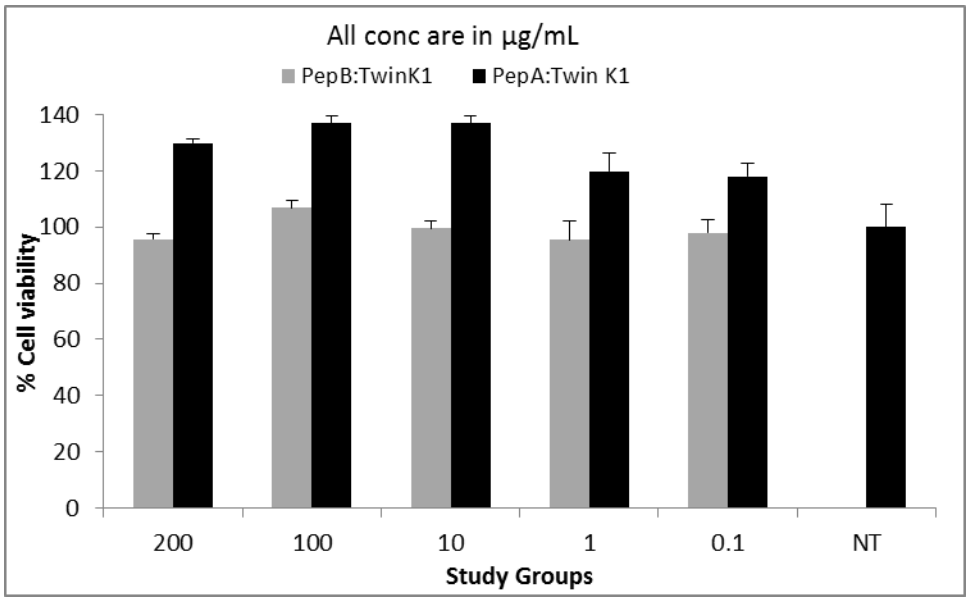

Figure 3.20) Cellular viability after treatment with a) Twin K1 self-assembled RNTs and b) PepA:Twin K1 (1:9) co-assembled RNTs and PepB:Twin K1 (1:9) co-assembled RNTs. MTT

assay was performed to determine cell viability. Incubation period was 24 hours. Data was an average of triplicates per treatment.

These results were expected and showed that Twin K1, PepA:TwinK1(1:9) and PepC:TwinK1(1:9) RNTs were biocompatible. In case of the groups treated with PepA:TwinK1(1:9) RNTs, there was a possibility of cell proliferation which could produce higher MTT absorbance than the No treatment group. In addition, there is another possibility that cells interacted with RNTs which increased their metabolic activity and caused an increase in MTT absorbance.

3.22) Osteogenic Differentiation studies of hBMSCs using PepB:TwinK1 (1:9) co-assembled RNTs by coating them onto the plate:

The aim of this experiment was to study the osteogenic differentiation of hBMSCs when PepB:TwinK1(1:9) RNTs were coated onto Tissue culture plates. BMP-7 was used as the positive control in this experiment.

A)

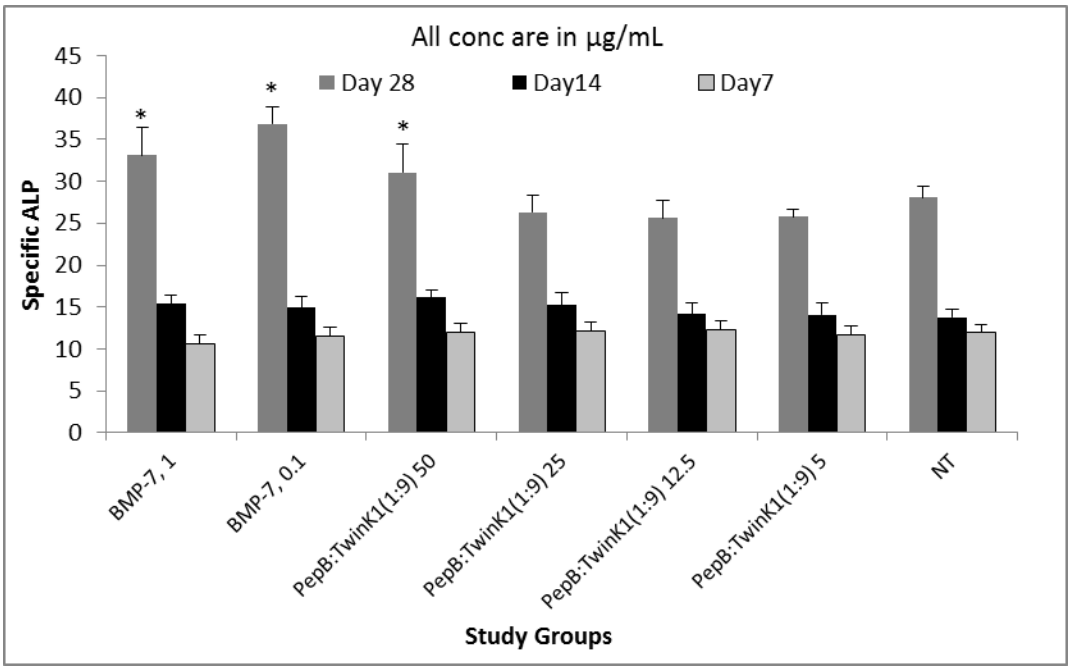

B)

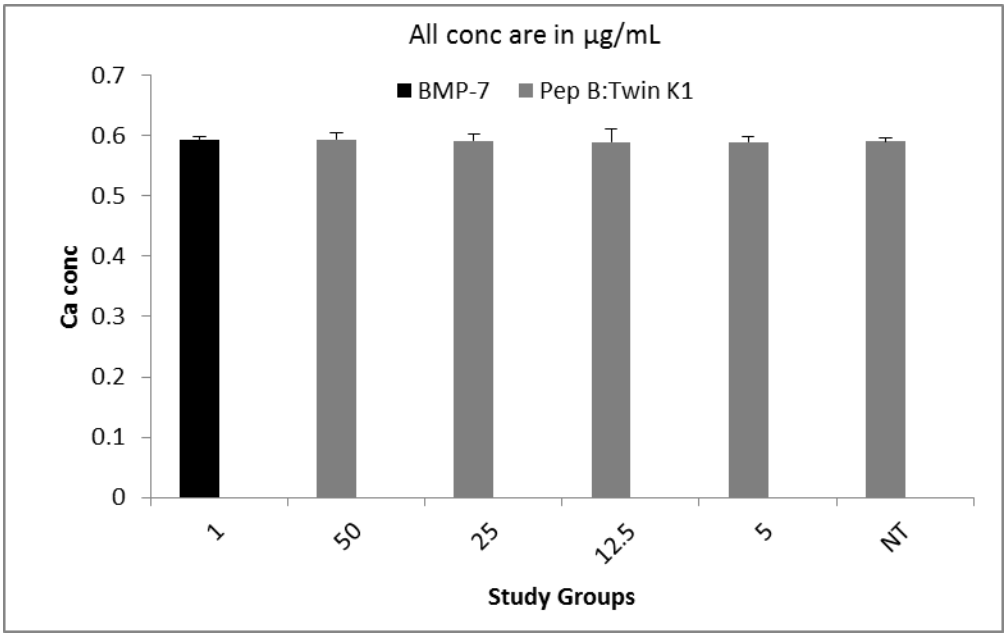

Figure 3.21) A) Specific ALP (ALP/DNA) activity of PepB:TwinK1 (1:9) co-assembled RNTs. B) Calcium concentrations obtained in hBMSCs as treated by PepB:TwinK1 (1:9) co-assembled RNTs. Specific ALP activity was calculated by taking the ratio of ALP (alkaline phosphatase activity) with the DNA content and Calcium assay was conducted by measuring

calcium absorbance in the respective groups in order to calculate Ca concentrations. Concentrations of RNTs are indicated in the graphs. Incubation periods were 7, 14 and 28 days. Data was summarized as the average of triplicates per treatment. For statistical analysis, Two-tailed heteroscedastic t-statistic was used and statistical significance was defined by * meaning p-value<0.05 compared with no treatment. Results of this experiment showed that on day 7, there was not a significant difference between the specific ALP activity of the cells treated with the peptide co-assembly or BMP-7, and no treatment groups. On day 14, a small difference in specific ALP was observed, which was not significant. On day 28, we observed a significant increase in specific ALP activity of the groups treated with BMP-7 (1 and 0.1 μg/mL) and the group treated with PepB:TwinK1(1:9) co-assembled RNTs at 50 μg/mL concentration. However, there was no significant calcium deposition in any of the groups.

These results were not expected. Specific ALP is an early marker of differentiation however, we observed its significance on the fourth week of incubation. There can be two possible reasons for this. One, the quantity of peptide physiosorbed on the plate was too small to stimulate osteogenic differentiation in the cells at an early stage. Two, the cells were slow in responding since the positive control in the study, BMP-7 also caused a significant increase in specific ALP activity on week 4. In line with slow induction of specific ALP, was the low level of calcium deposition. ALP augments calcification through the hydrolysis of pyrophosphate and ATP, which inhibit calcification, and is crucial for phosphate production, needed for the crystallization of hydroxyapatite (Mostafa NZ, 2011). In our study, peptide co-assembly groups took 4 weeks to show a significant increase in specific ALP activity and may have required another couple of weeks to show a significant difference in calcium. We found that it is difficult

to incubate hBMSC in plates under such conditions, since they tend to grow fungus around the fourth week, and thus the cells had to be harvested on day 28. In order to understand whether coating of peptides was the best practice for osteogenic differentiation or not; we designed another experiment where peptide assemblies were added into the solution.

3.23) Osteogenic Differentiation studies of hBMSCs using 'Soluble' PepA self-assembled RNTs, PepA:TwinK1 (1:1) co-assembled RNTs, PepA:TwinK1 (1:9) co-assembled RNTs

The aim of this experiment was to study the osteogenic differentiation when 'soluble' PepA self assembled RNTs, PepA:TwinK1(1:1) co-assembled RNTs and PepA:TwinK1(1:9) co-assembled RNTs were treated with hBMSCs. BMP-7 was used as the positive control in this experiment. The difference between this experiment and section 4.23 was the peptides were added in solution in this experiment.

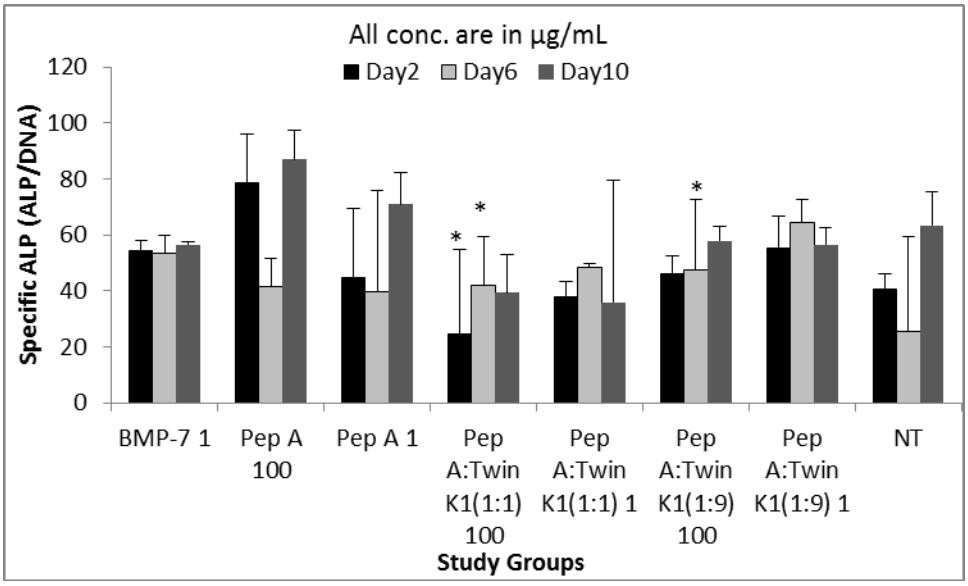

Figure 3.22) Specific ALP activity of PepA:TwinK1(1:9) RNTs. Specific ALP activity was obtained by taking the ratio of ALP (Alkaline Phosphatase) activity with the DNA content of the respective groups. Concentration of the peptide co-assemblies were indicated in the graphs. Incubation periods were 2, 6 and 10 days. Data was summarized as the average of triplicates per treatment. For statistical analysis, Two-tailed heteroscedastic t-statistic was used and statistical significance was defined by * meaning p-value<0.05 compared with no treatment.

Results of this experiment showed that on Day 2, there was no significant difference in specific ALP activity of the peptide assemblies, except the PepA:TwinK1(1:1) 100 μg/mL which was significantly less compared with the no treatment. On day 6, PepA:TwinK1(1:1) and PepA:TwinK1(1:9) both at a concentration of 100 μg/mL produced significantly higher specific ALP activity. In addition, on day 10, there was no significant difference in ALP activity as compared with the no treatment.

The lack of ALP induction after 2 days could be attributed to the limited amount of time allowed for induction after RNT treatment. However, on day 6, we observed an increase in specific ALP activity in two co-assemblies of PepA:TwinK1(1:1) and PepA:TwinK1(1:9). This response could be attributed to the osteogenic potential of peptide co-assembled RNTs. Peptide A is an eleven amino acid long sequence isolated from BMP-7 which has shown alkaline phosphatase activity in human fetal osteoblasts (Chen Y, 2008). Moreover, Twin K1 RNTs have a biomimetic structure which improves human osteoblast adhesion. Therefore, considering these results, another experiment was designed where the incubation period was extended to include Ca studies as well as other peptide co-assemblies.

3.24) Osteogenic Differentiation studies of hBMSCs using 'soluble' PepA:TwinK1 (1:9) co-assembled RNTs, PepB:TwinK1 (1:9) co-assembled RNTs and PepC:TwinK1 (1:9) co-assembled RNTs

The aim of this experiment was to study the osteogenic potential of soluble PepA:TwinK1 (1:9) co-assembled RNTs, PepB:TwinK1 (1:9) co-assembled RNTs and PepC:TwinK1 (1:9) co-assembled RNTs by measuring their ALP activity and Ca deposition.

A)

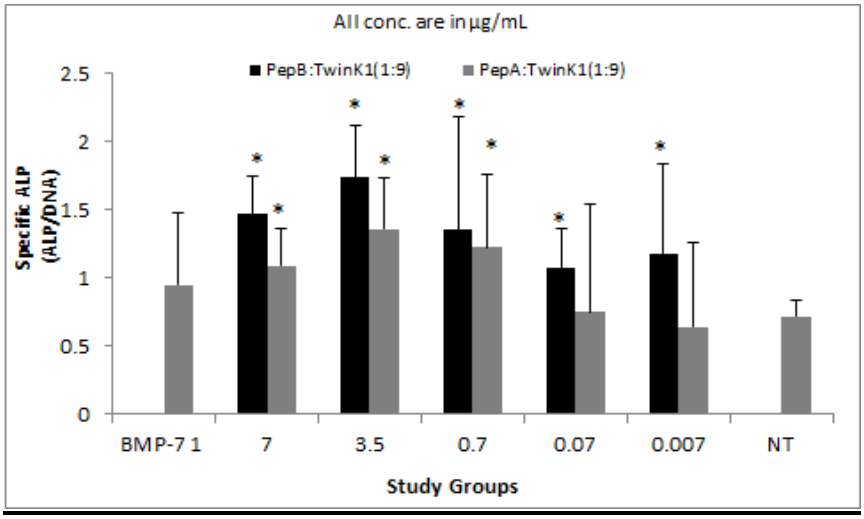

B)

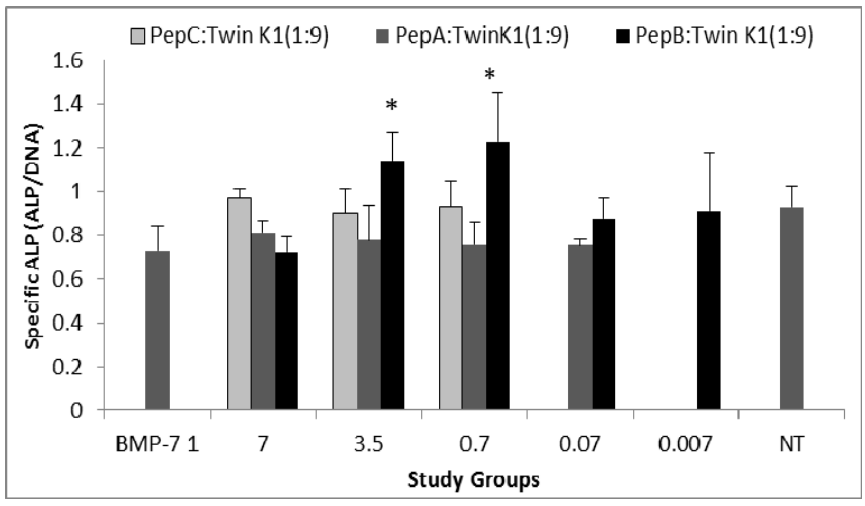

C) 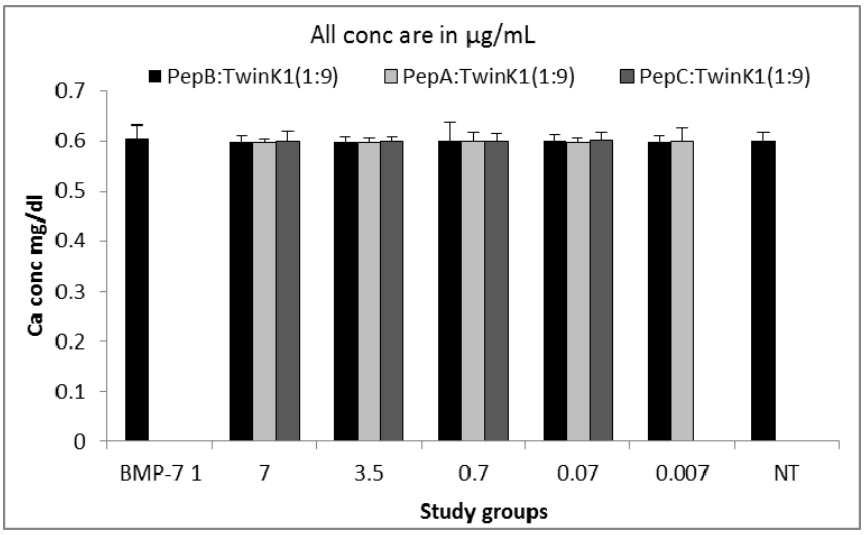

Figure 3.23) A) Day 7 and B) Day 14 Specific ALP activity of PepA:TwinK1(1:9) RNTs, PepB:TwinK1 (1:9) co-assembled RNTs and PepC:TwinK1 (1:9) co-assembled RNTs. C) Calcium concentrations obtained in hBMSCs as treated by peptide co-assemblies. Specific ALP activity was obtained by taking the ratio of ALP (alkaline phosphatase activity) with the DNA content. A Calcium assay was conducted by measuring the calcium absorbance in the respective groups in order to estimate Ca concentration. Concentration of the peptide co-assemblies are indicated in the graphs. Data is summarized as the average of triplicates per treatment. For statistical analysis, Two-tailed heteroscedastic t-statistic was used and statistical significance was defined by * meaning p-value<0.05 compared with no treatment.

Results of this experiment showed that on day 7, PepA:TwinK1 (1:9) co-assembled RNTs showed significantly higher specific ALP activity at 7, 3.5 and 0.7 µg/mL concentrations compared with the no treatment. In addition, PepB:TwinK1 (1:9) co-assembled RNTs produced significant specific ALP activity in 7, 3.5, 0.7, 0.07 and 0.007 µg/mL concentrations. However, PepC:TwinK1 (1:9) co-assembled RNTs produced extremely high and unexpected results on

Day 7 which were difficult to explain and therefore were included in appendix. On day 14, only PepB:TwinK1 (1:9) co-assembled RNTs produced specific ALP activity on 3.5 and 0.7 μg/mL concentrations. The remainder of the study groups gave insignificant results. On Day 30, a Ca assay was conducted which produced insignificant results in all the study groups.

ALP results of this experiment were in line with expected osteogenesis of these peptides, however, the Ca deposition results were unexpected. ALP is an early osteogenic differentiation marker and Peptide A,B's co-assemblies have produced a significant increase in specific ALP activity which could be attributed to their osteogenic potential as described in section 3.23. On day 14, the induced specific ALP had a natural trend of falling down and in spite of that, PepB:TwinK1(1:9) RNTs could sustain a significant increase of specific ALP activity from the No treatment group. These results prove one of our hypothesis proposed in section 3.22 that adding the RNTs in medium was a better practice than coating them over the plate. However, we could not observe a significant change in Ca deposition. One of the possible reasons could be the low cell density. There was a likelihood that if the cells attched to the plate were at a sub optimal density, their proliferation to cover the surface could delay their differentiation. We could not extend our studies any further since hBMSCs started growing fungus during the middle of third week. In order to investigate this further, we performed another experiment with tripling the cell seeding density for the Ca studies.

3.25) Osteogenic Differentiation studies of hBMSCs using soluble Peptide A, Peptide B, Peptide C, PepA:TwinK1 (1:1) co-assembled RNTs, PepB:TwinK1 (1:9) co-assembled RNTs and PepC:TwinK1 (1:9) co-assembled RNTs

The aim of this experiment was to study the osteogenic differentiation of hBMSCs when treated with soluble peptides with and without co-assemblies. The difference between this experiment and section 3.24 was adding extra groups of peptides A, B and C which did not contain co-assembled RNTs. Moreover, the cell density in the Ca deposition studies were tripled.Results of Day 7 of this experiment showed that quite a few study groups produced a significant increase in specific ALP activity when compared with the No treatment groups as shown in table 3.2.

A)

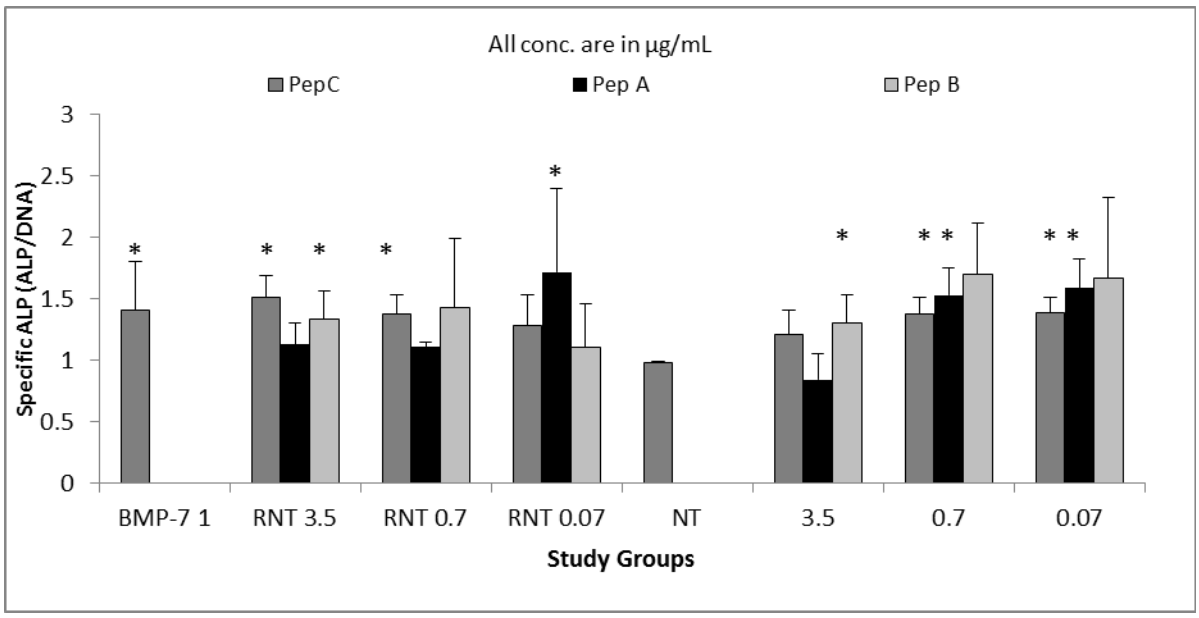

B)

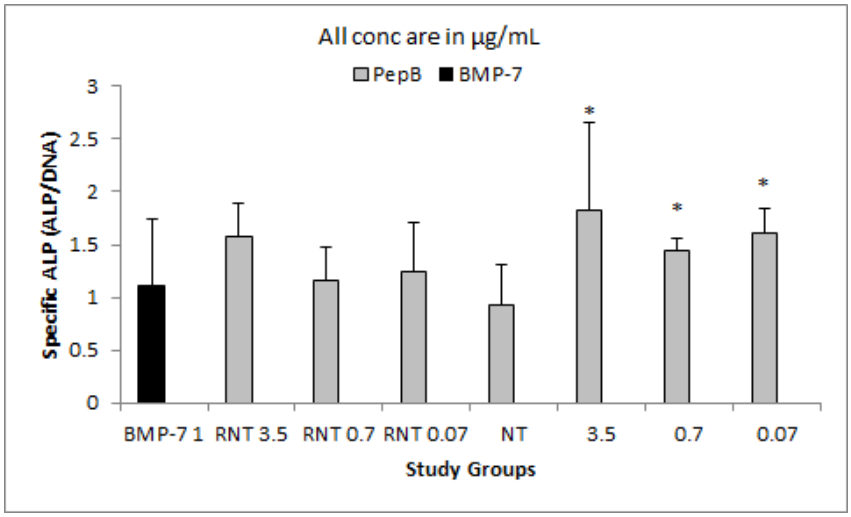

C)

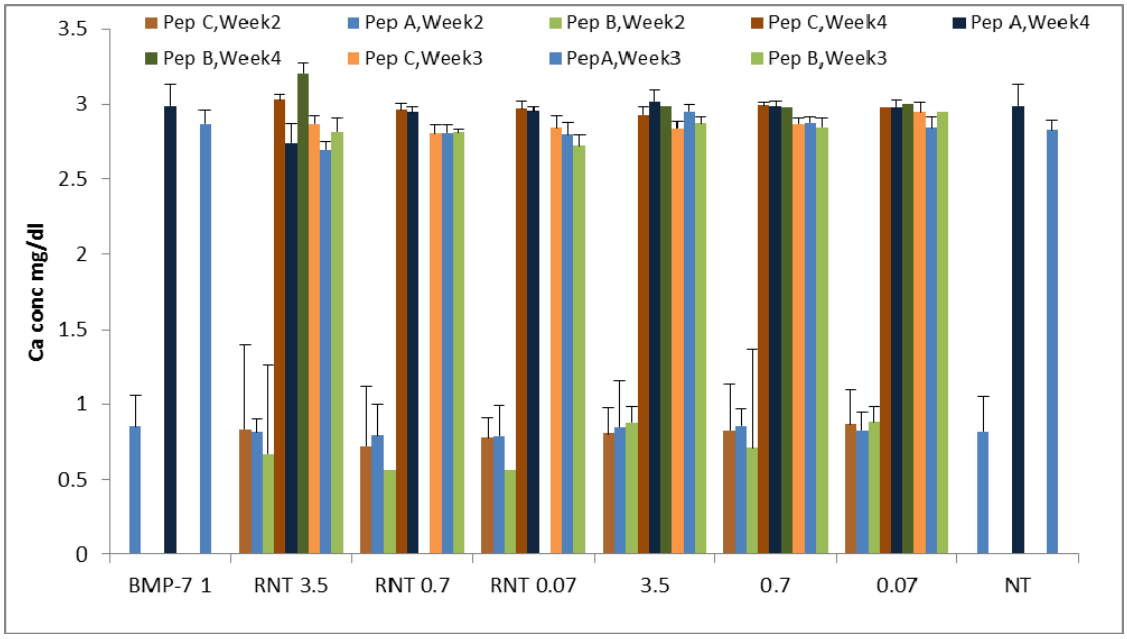

Figure 3.24) A) Day 7 and B) Day 14 Specific ALP activity of peptide assemblies. C) Calcium concentrations obtained in hBMSCs as treated by peptide assemblies. Specific ALP activity was obtained by taking the ratio of ALP (alkaline phosphatase activity) with the DNA content and Calcium assay was conducted to measure the calcium absorbance in the respective groups in order to estimate Ca concentration. Concentration of the peptide assemblies were indicated in the graphs. Data was summarized as the average of triplicates per treatment. For

statistical analysis, Two-tailed heteroscedastic t-statistic was used and statistical significance was defined by * meaning p-value<0.05 compared with no treatment.

Table 3.2) The study groups which produced significantly higher Specific ALP activity on Day 7 when compared with the no treatment group.

Study Groups	**Concentrations in µg/mL**
Pep A	0.7, 0.07
PepA:TwinK1(1:9) RNTs	0.7
PepB:TwinK1(1:9) RNTs	3.5
Pep C	0.7, 0.07
PepC:TwinK1(1:9) RNTs	3.5, 0.7
BMP-7	1

On Day 14, in the results of PepB, there was a graudual fall in specific ALP activity among all the groups and only PepB without RNTs sustained significant increase in specific ALP activity at 3.5, 0.7 and 0.07 µg/mL concentration. In addition, results of PepA and PepC on Day 14 were extremely high which were difficult to explain and therefore were included in the Appendix. However, none of the treatment groups produced a significant difference in the Ca deposition studies on all the time points.

ALP and calcium results of this experiment were not expected. On Day 7, Peptide co-assemblies gave a similar response as compared with the peptides without a co-assembled RNTs.

Initially, we thought that incorporating a biomimetic co-assembly of Twin K1 to the osteogenic peptides A, B and C would further improve the osteogenic potential of the cells. However, we did not find such a trend since the values of specific ALP were quite close. This meant that Twin K1 RNTs did not promote the osteogenic differentiation of hBMSCs. Moreover, Ca deposition studies showed that there was no difference among the treatment groups. Furthermore, the BMP-7 positive control group also rendered insignificant outcomes. This showed that hBMSCs did not respond to the stimulation under the osteogenic environment which could be due to the inactivity of the cells.

3.26) References

1. Ai Lin Chun, J. H. (2004). Helical rosette nanotubes: a more effective orthopaedic implant material. *Nanotechnology, 15*, s234-s239.
2. Baylink DJ, F. R. (1993). Growth factors to stimulate bone formation. *J Bone Mineral Res, 8*, s565-s572.
3. Camilla C. G. Moura, M. A.-B. (2010). The effect of a nanothickness coating on rough titanium substrate in the osteogenic properties of human bone cells. *Journal of Biomedical Materials Research Part A, 94*(1), 103-111.
4. Chun, A. L., Webster, T. J., & Fenniri, H. (2006). Helical Rosette Nanotubes: Topographical and Chemical Roles in Osteoblast Attachment. *Adv. Sci. Technol, 53*, 1-8.
5. Dae Seog Heo, J.-G. P. (1990). Evaluation of Tetrazolium-based Semiautomatic Colorimetrie Assay for Measurement of Human Antitumor Cytotoxicity. *CANCER RESEARCH, 50*, 3681-3690.
6. Eli Fine, L. Z. (2009). Enhanced endothelial cell functions on rosette nanotube-coated titanium vascular stents. *International Journal of Nanomedicine, 4*, 91-97.
7. Friedlaender GE, P. C. (2001). Osteogenic protein-1 (bone morphogenetic protein-7) in the treatment of tibial nonunions. *J Bone Joint Surg Am, 83*, 151-158.

8. H. WAN, R. W. (1994). A study of the reproducibility of the MTT test. *JOURNAL OF MATERIALS SCIENCE: MATERIALS IN MEDICINE, 5*, 154-159.

9. Hongo T, F. Y. (1990). An in vitro chemosensitivity test for the screening for anti-cancer drugs in childhood leukemia. *Cancer, 65*, 1263-1272.

10. Jemima L. Whyte, S. G. (2011). Density of human bone marrow stromal cells regulates commitment to vascular lineages. *Stem Cell Res, 6*(3), 238-250.

11. Lijie Zhang, F. R. (2009). Arginine-glycine-aspartic acid modified rosette nanotube–hydrogel composites for bone tissue engineering. *Biomaterials, 30*, 1309-1320.

12. Lijie Zhang, J. R. (2009). Biologically inspired rosette nanotubes and nanocrystalline hydroxyapatite hydrogel nanocomposites as improved bone substitutes. *Nanotechnology, 20*, 175101-175113.

13. Lijie Zhang, U. D. (2010). Tuning cell adhesion on titanium with osteogenic rosette nanotubes. *J Biomed Mater Res A, 95*(2), 550-563.

14. Nesrine Z. Mostafa, H. U.-B. (2011). In Vitro Osteogenic Induction Of Human Gingival Fibroblasts For Bone Regeneration. *The Open Dentistry Journal, 5*, 139-145.

15. Reddi AH, C. N. (1993). Initiation and promotion of bone differentiation by bone morphogenetic proteins. *J Bone Mineral Res, 8*, s499-s502.

16. Shang Song, Y. C. (2012). Self-assembled rosette nanotubes for incorporating hydrophobic drugs in physiological environments. *Nanotechnology, 6*, 101-107.

17. Yupeng Chen, T. J. (2008). Increased osteoblast functions in the presence of BMP-7 short peptides for nanostructured biomaterial applications. *J Biomed Mater Res A, 91*(1), 296-304.

18. Zipper H, B. H. (2004). Investigations on DNA intercalation and surface binding by SYBR Green I, its structure determination and methodological implications. *Nucleic Acids Res, 32*(12), e103.

4) CONCLUSIONS & FUTURE PROSPECTS

Health statistics show that the number of patients requiring joint replacements has been increasing in the past decade and is projected to continue rising in the future. Success in surgical joint replacements in the 60's has resulted in a huge demand amongst patients but 12-16% of the total joint replacements performed constitute revisions which is an implication of implant failure rate. The increasing demand for more durable implants have led to new formulations of high performance nanomaterials that can improve implant fixation to juxtaposed bone.

Rosette Nanotubes (RNTs) are a new class of soft organic nanomaterials composed of a guanine-cytosine building block that self-assembles in aqueous environments into stable nanotubular structures. RNTs can be functionalized with biologically active short bone morphogenic protein-7 peptides. The work here-within represents the purification, characterization and first investigation of RNTs using hBMSCs.

Our studies began with the purification of the following peptides using HPLC. Obtained yields were in a range of 12-20%.

a) PepA:Twin K1 (1:9) co-assembled nanotubes

b) PepB:Twin K1 (1:9) co-assembled nanotubes

c) PepC:Twin K1 (1:9) co-assembled nanotubes

d) PepA

e) PepB

f) PepC

This was followed by the SEM characterization of Twin K1 and Peptide RNTs which showed their nanotubular morphology and changes in their length as self-assembled RNTs were co-assembled. This observation was missing with PepC and PepC:Twin K1 (1:9) co-assembled nanotubes because of their water insolubility.

The second phase focussed on the cytocompatibility studies of Twin K1, PepA:TwinK1 (1:9) and PepB:TwinK1 (1:9) and hBMSCs. We found that the minimum cell viability was 83% and most of the groups produced more than 95% cell viability. This indicated that the materials were inherently non-toxic. In addition, we observed that the percent cell viability of PepA:TwinK1 (1:9) and PepB:TwinK1 (1:9) were more than 100% in a few study groups. We hypothesized that this could be due to the interaction of RNTs with the cells which increased its metabolic activity.

The third phase focussed on the cell adhesion studies using hBMSCs. We coated Twin K1 self-assembled RNTs, PepA:TwinK1 (1:1) co-assembled and PepA self-assembled RNTs on Tissue-

culture treated plates which produced a significant increase in cellular adhesion. Later, we replaced the tissue culture treated plates with Non-tissue culture treated plates. TwinK1, Mono K1 self-assembled RNTs, PepA:TwinK1 (1:9) and PepB:TwinK1 (1:9) co-assembled RNTs coating produced a significant increase in cellular adhesion on Non-tissue culture treated plates. This was observed upto a concentration range of RNTs; for excess concentrations, a reduction in cell adhesion was evident. In addition, we replaced the Non-tissue culture treated plates with Ti wafers and studied the effect on cellular adhesion by coating RNTs on them. While using the Ti substrate, we performed a set of optimization experiments like improving the cell spreading on Ti, coating techniques (spin coating, drop casting and dipping) and modification of Ti surface but none of these experiments rendered a consistent increase or decrease in cellular adhesion compared with the no treatment and we hypothesized that hBMSCs were not stable on Ti which was responsible for such outcomes.

The fourth and final phase of the studies was the osteogenic differentiation studies of peptide co-assemblies where we found that PepA:TwinK1 (1:9), PepB:TwinK1 (1:9) and PepC:TwinK1 (1:9) co-assembled RNTs produced a significant increase in the specific ALP activity of hBMSCs. None of the above mentioned studies showed a significant difference in the Calcium deposition which is going to be the next phase of studies.

These results are important for 1) optimizing the purification parameters of peptide co-assemblies, 2) understanding the characteristics of RNTs when they were attached with growth factor mimicking peptides such as the peptides for BMP-7, 3) for product development where the initial biocompatibility screening data of novel biomaterial was promising, 4) understanding the cell adhesion profile on different substrates when coated with RNTs (and especially

concentration effects), and 5) understanding the early phase osteogenic differentiation studies of hBMSCs when treated with RNTs.

Future Work:

For future prospects, there are a few studies that would contribute to complement the investigation for RNT's commercialization:

1) Long term osteogenic differentiation studies (Ca deposition) of RNTs using hBMSCs. This study will show the potential of RNTs for bone repair.
2) The above study could be complemented with the assessment of mRNA expression level of osteogenic cytokines using Real time-Polymerase Chain Reaction (RT-PCR).
3) For orthopedic applications, RNT degradation and metabolism studies could be helpful to identify the long term influence of RNTs to cells and organs. For example, in the *in vivo* studies, the histology of livers and kidneys of pigs could be evaluated for toxicities, and RNT units could be isotope labeled to determine their pathological tracks.

5) Appendix

5.1) The following exhibits are the unmodified HPLC chromatograms and MS spectrums of Section 3.1

A) HPLC chromatogram of Peptide A, B) MS spectrum of Peptide A, C) HPLC chromatogram of Peptide A-Twin G^C, D) MS spectrum of Peptide A-Twin G^C, E) HPLC chromatogram of Peptide B, F) MS spectrum of Peptide B, G) HPLC chromatogram of Peptide B-Twin G^C, H) MS spectrum of Peptide B-Twin G^C, I) HPLC chromatogram of Peptide C, J) MS spectrum of Peptide C, K) HPLC chromatogram of Peptide C-Twin G^C, L) MS spectrum of Peptide C-Twin G^C

A)

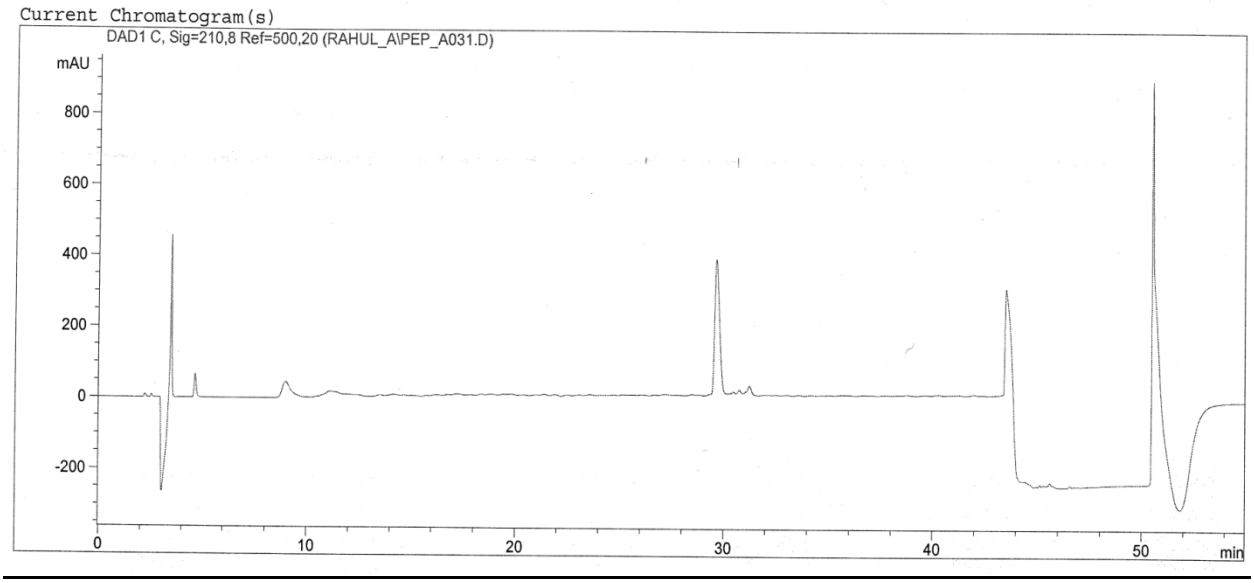

B)

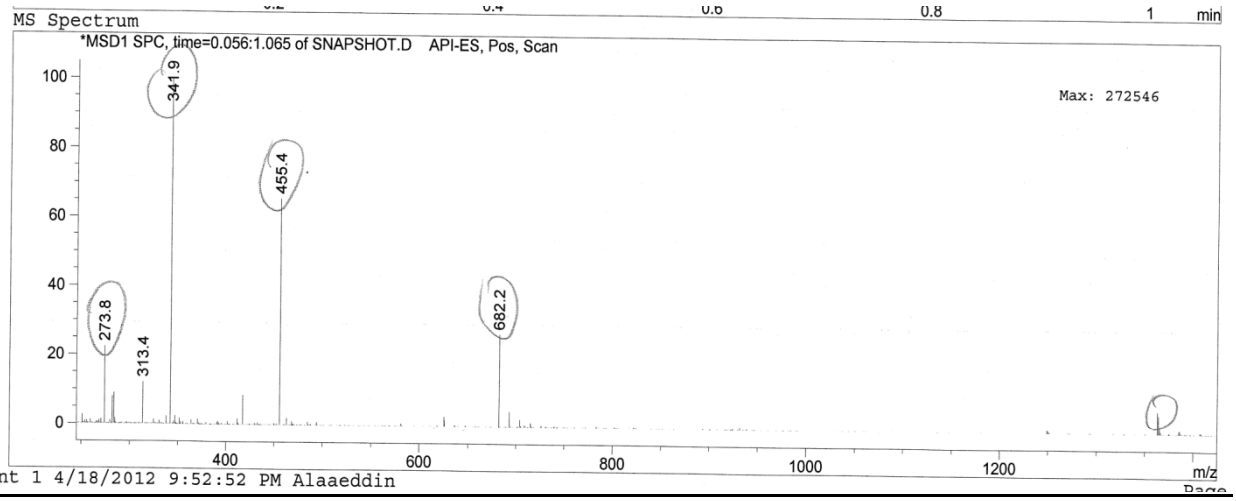
MS Spectrum
*MSD1 SPC, time=0.056:1.065 of SNAPSHOT.D API-ES, Pos, Scan
Max: 272546
341.9
455.4
273.8
313.4
682.2
m/z
ient 1 4/18/2012 9:52:52 PM Alaaeddin

C)

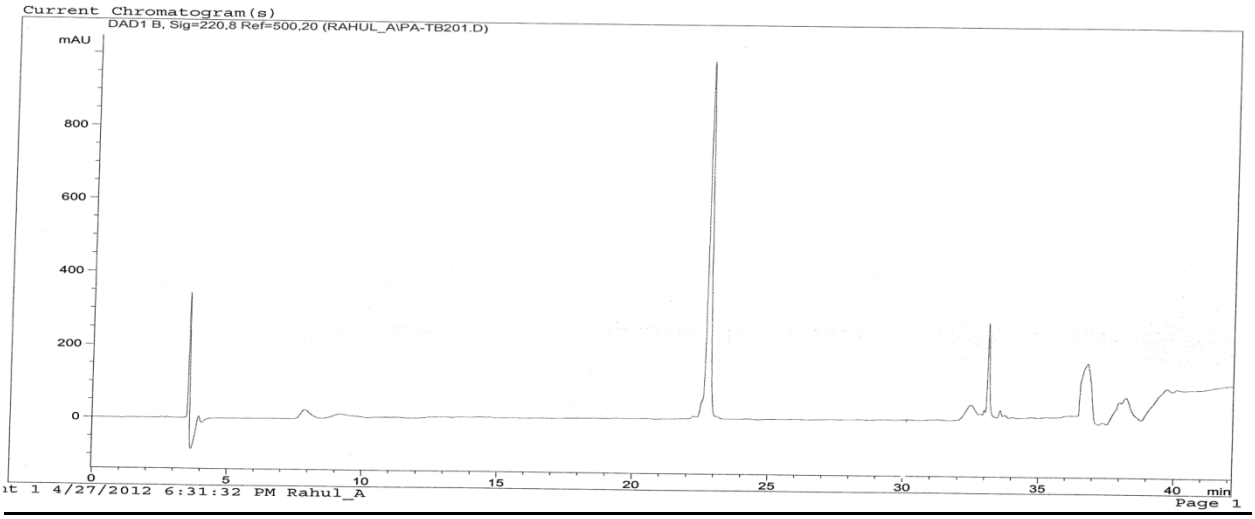
Current Chromatogram(s)
DAD1 B, Sig=220,8 Ref=500,20 (RAHUL_A\PA-TB201.D)
mAU
min
Page 1
t 1 4/27/2012 6:31:32 PM Rahul_A

D)

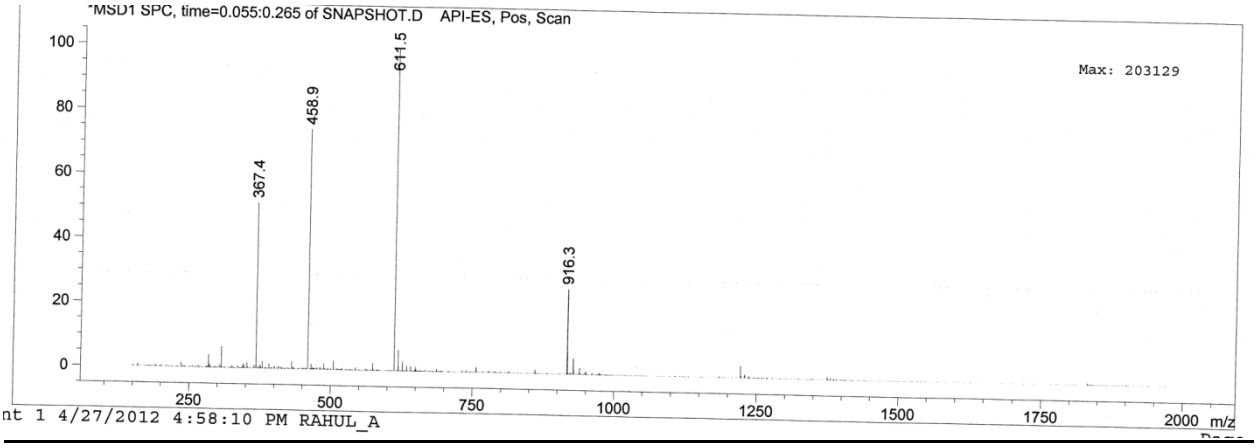
*MSD1 SPC, time=0.055:0.265 of SNAPSHOT.D API-ES, Pos, Scan
Max: 203129
611.5
458.9
367.4
916.3
m/z
nt 1 4/27/2012 4:58:10 PM RAHUL_A

E)

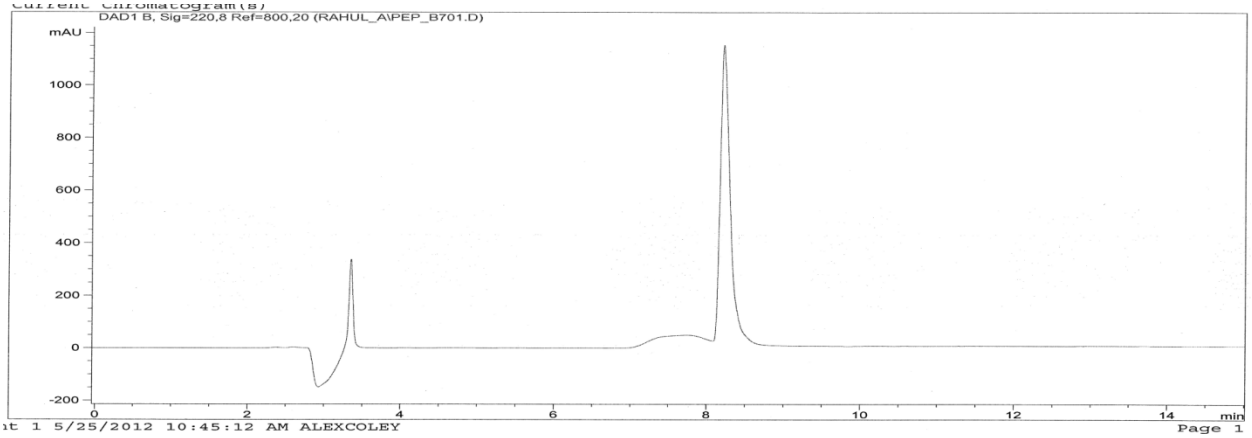
DAD1 B, Sig=220,8 Ref=800,20 (RAHUL_A\PEP_B701.D)
mAU
1000
800
600
400
200
0
-200
0
2
4
6
8
10
12
14
min
Page 1

F)

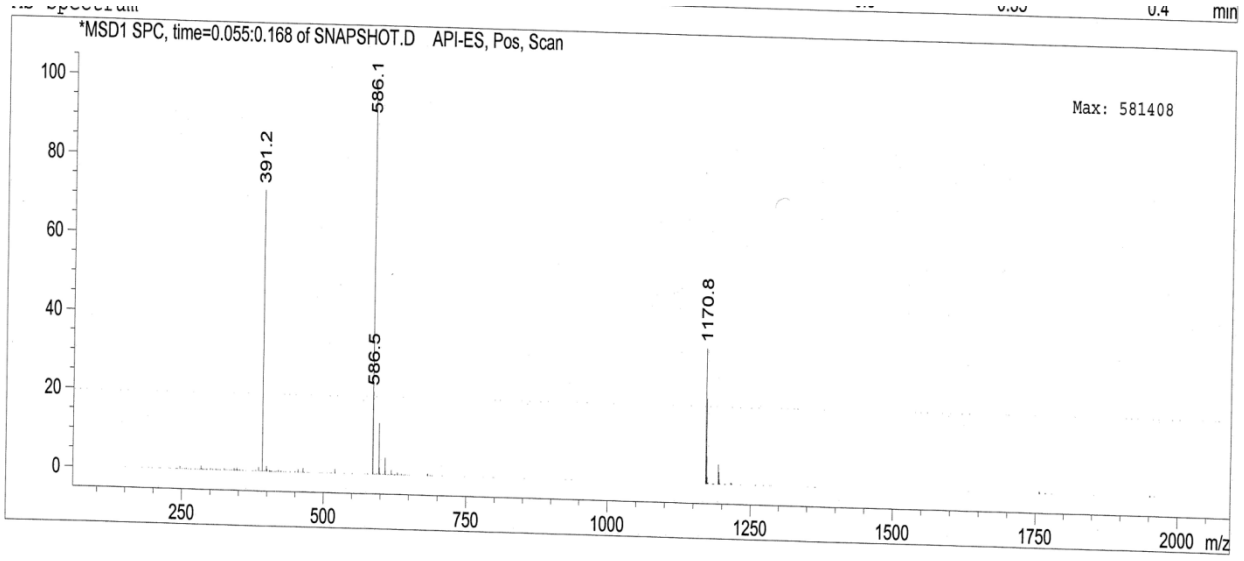
*MSD1 SPC, time=0.055:0.168 of SNAPSHOT.D API-ES, Pos, Scan
Max: 581408
586.1
391.2
586.5
1170.8
100
80
60
40
20
0
250
500
750
1000
1250
1500
1750
2000 m/z

G)

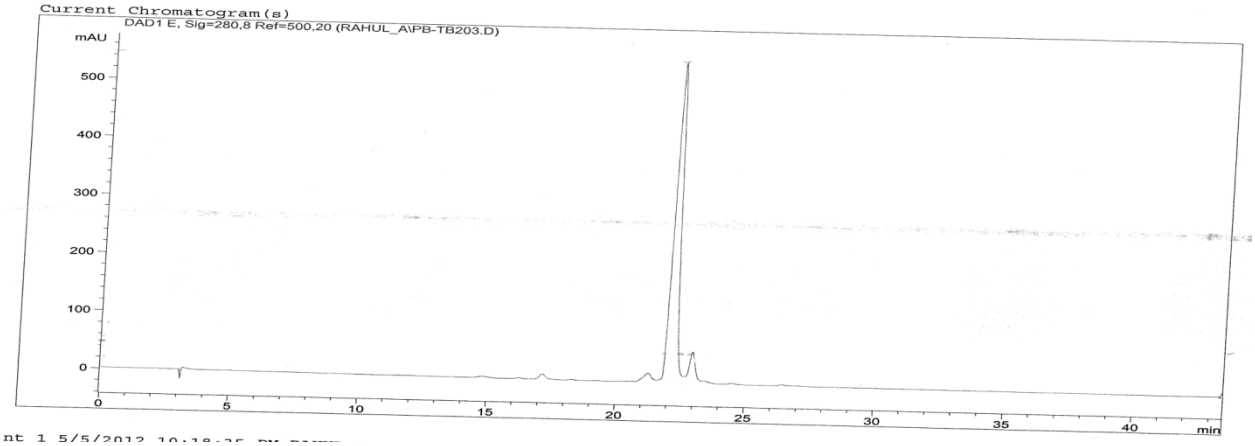
Current Chromatogram(s)
DAD1 E, Sig=280,8 Ref=500,20 (RAHUL_A\PB-TB203.D)
mAU
500
400
300
200
100
0
0
5
10
15
20
25
30
35
40
min

H)

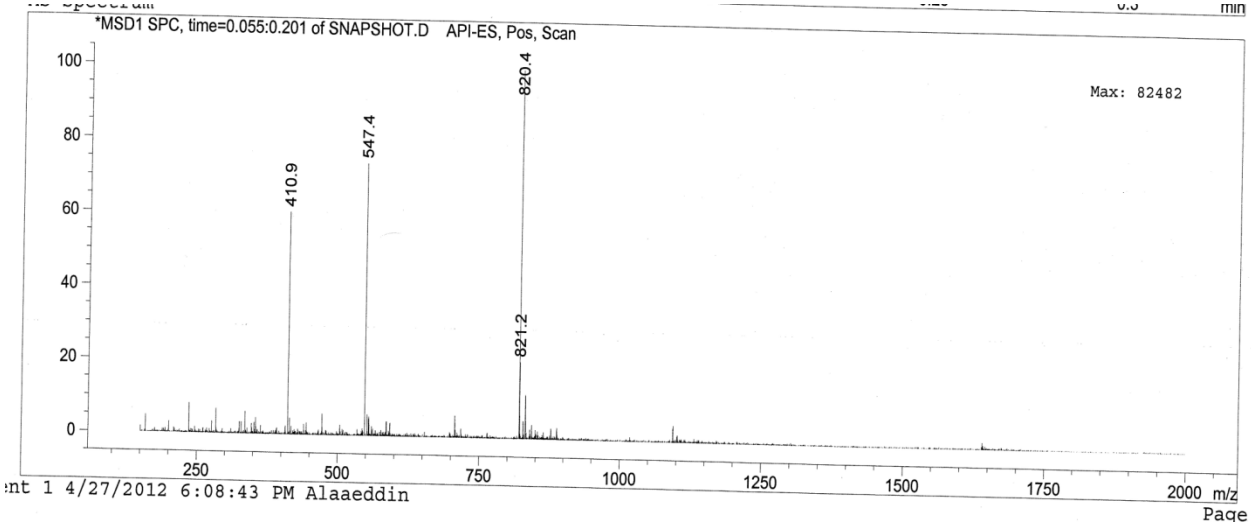
*MSD1 SPC, time=0.055:0.201 of SNAPSHOT.D API-ES, Pos, Scan
Max: 82482
820.4
547.4
410.9
821.2
m/z
nt 1 4/27/2012 6:08:43 PM Alaaeddin

I)

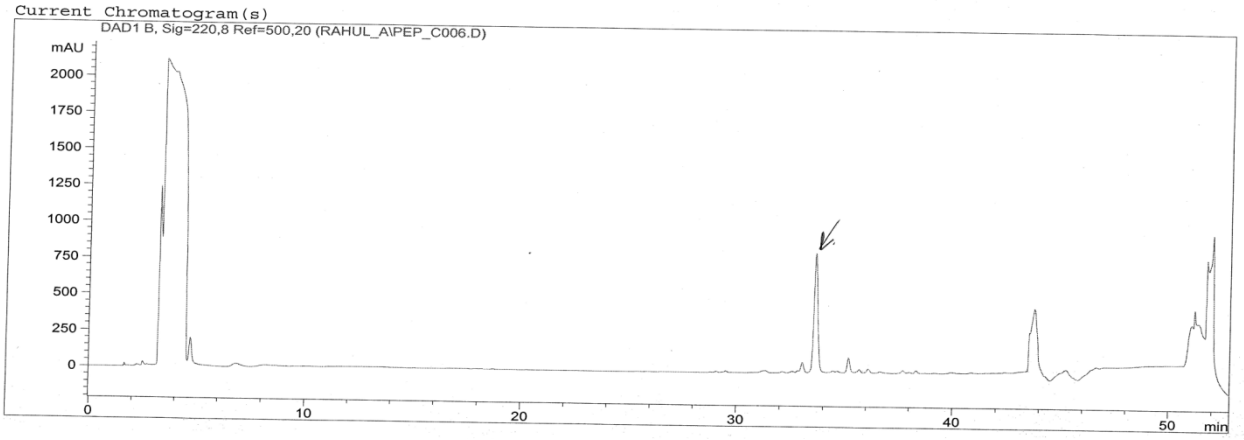
Current Chromatogram(s)
DAD1 B, Sig=220,8 Ref=500,20 (RAHUL_A\PEP_C006.D)
mAU
min

J)

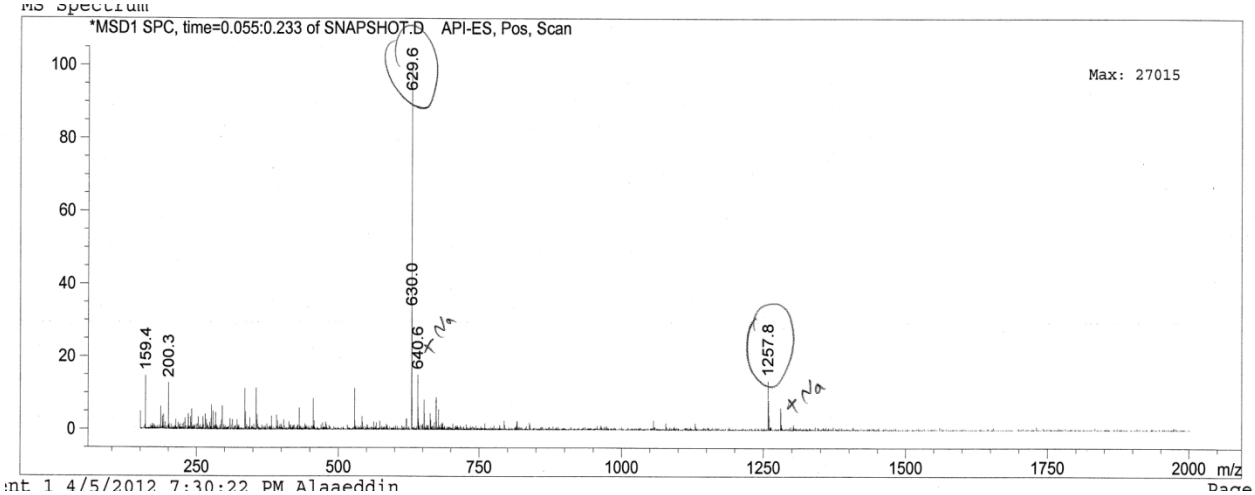
*MSD1 SPC, time=0.055:0.233 of SNAPSHOT.D API-ES, Pos, Scan
Max: 27015
629.6
630.0
640.6
159.4
200.3
1257.8
m/z

K)

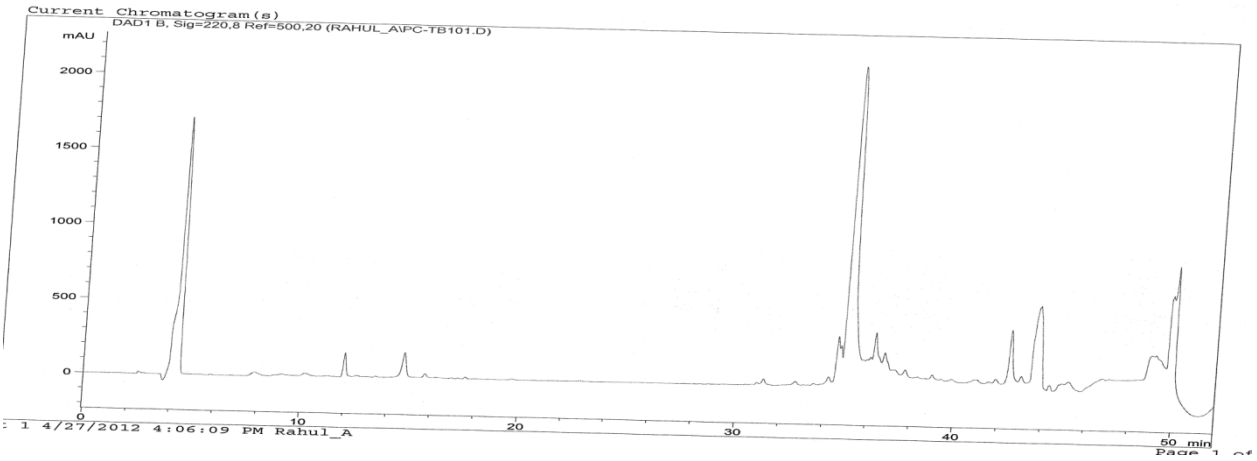

L)

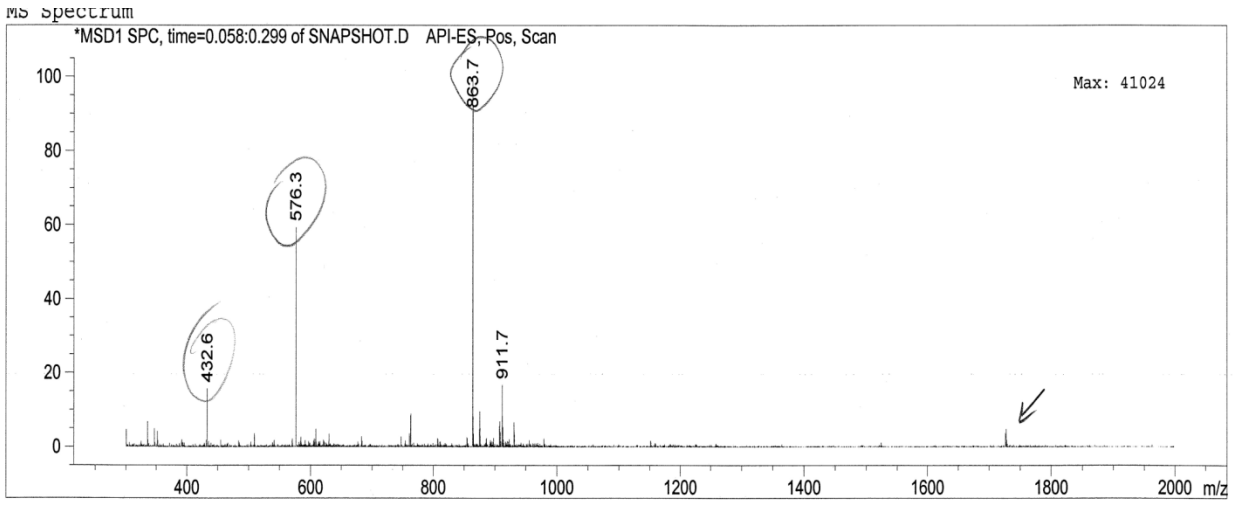

5.2) The following exhibits are the unmodified result of Section 3.8

Figure 5.1) Cell attachment on Ti wafers. Cell attachment was determined by measuring the fluorescence after dissolving the cell contents. Incubation period was 18 hours. Data was an average of triplicates per treatment.

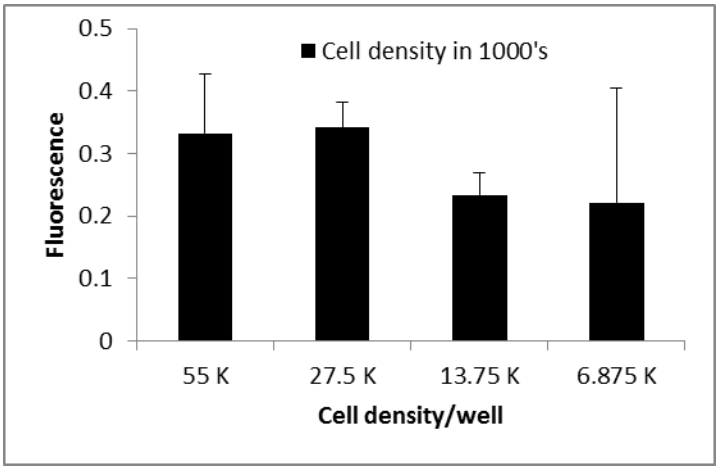

5.3) The following exhibit is the unmodified results of Section 3.22

Figure 5.2) A) DNA content of PepB:Twin K1 (1:9) RNTs and BMP-7 treated groups with respect to time, B) Alkaline phosphatase activity of PepB:Twin K1 (1:9) RNTs and BMP-7 treated groups with respect to time. Concentration of RNTs and incubation periods are mentioned in the figure Data was an average of triplicates per treatment.

A)

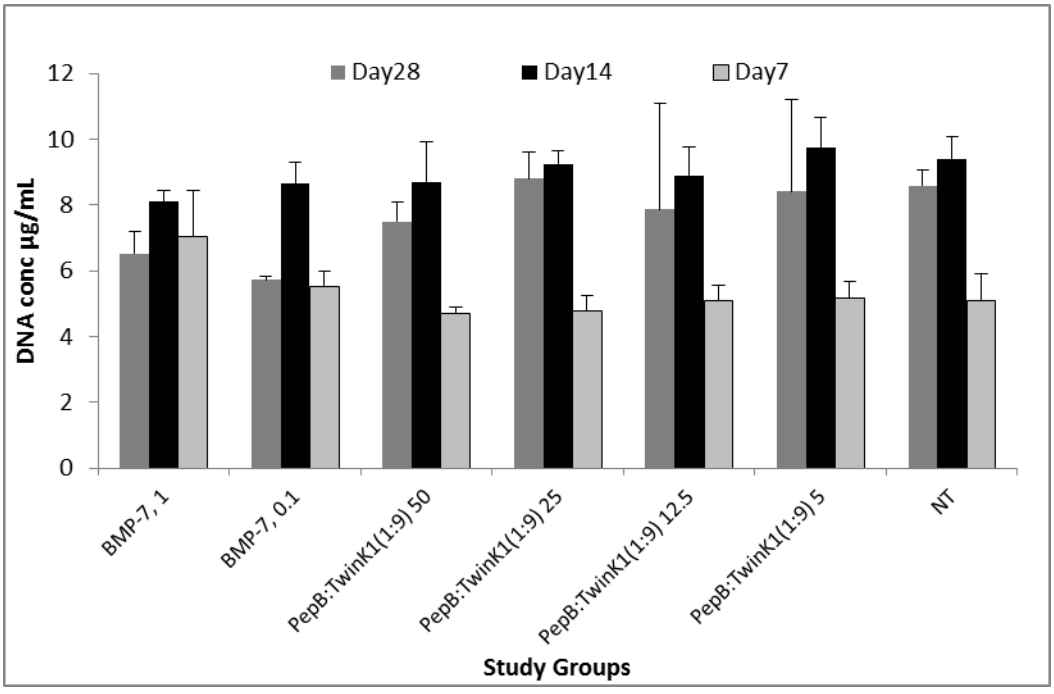

B)

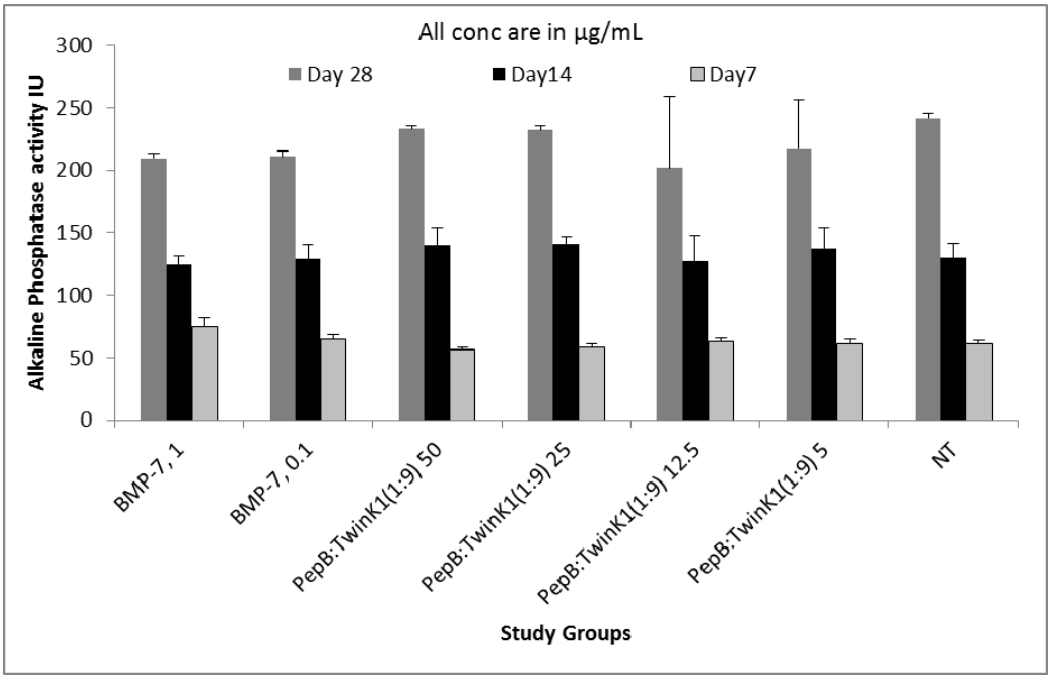

5.4) The following exhibits are the unmodified results of Section 3.23

Figure 5.4) A) DNA content of PepA self-assembled and co-assembled RNTs and BMP-7 treated groups with respect to time, B) Alkaline Phosphatase activity of PepA self-assembled and co-assembled RNTs and BMP-7 treated groups with respect to time. Concentration of RNTs and incubation periods are mentioned in the figure. Data was an average of triplicates per treatment.

A)

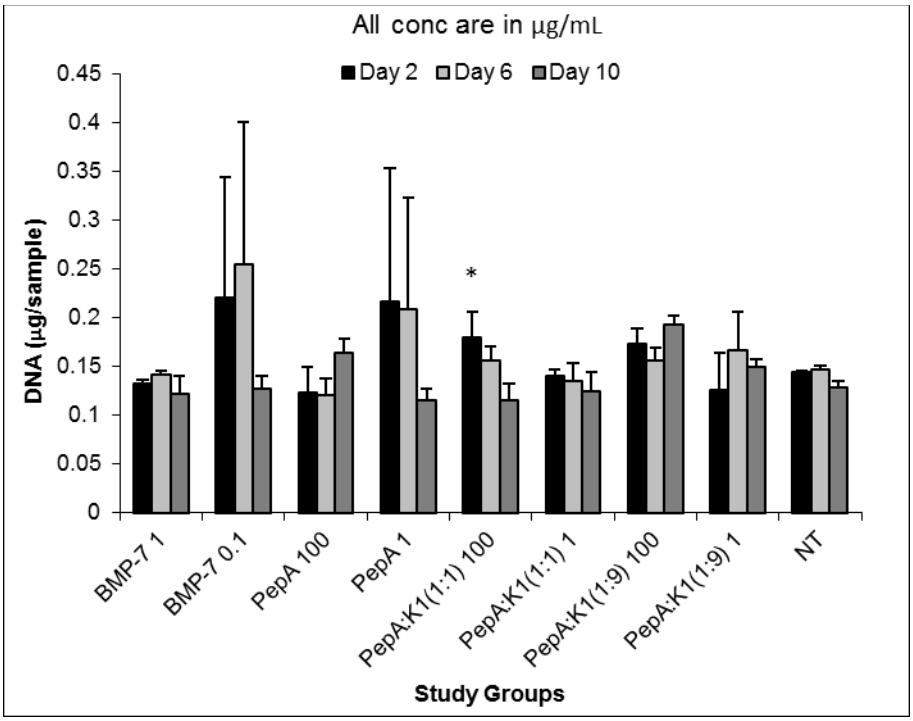
All conc are in µg/mL
Day 2
Day 6
Day 10
DNA (µg/sample)
0.45
0.4
0.35
0.3
0.25
0.2
0.15
0.1
0.05
0
*
BMP-7 1
BMP-7 0.1
PepA 100
PepA 1
PepA:K1(1:1) 100
PepA:K1(1:1) 1
PepA:K1(1:9) 100
PepA:K1(1:9) 1
NT
Study Groups

B)

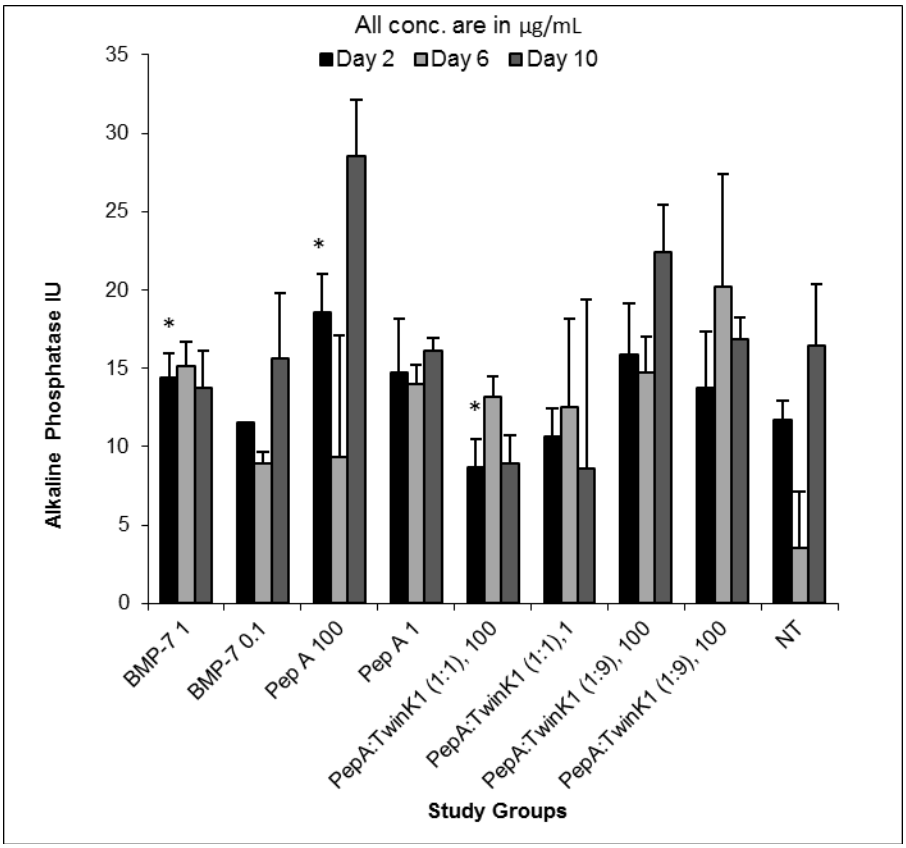
All conc. are in µg/mL
Day 2
Day 6
Day 10
Alkaline Phosphatase IU
35
30
25
20
15
10
5
0
*
*
*
BMP-7 1
BMP-7 0.1
Pep A 100
Pep A 1
PepA:TwinK1 (1:1), 100
PepA:TwinK1 (1:1), 1
PepA:TwinK1 (1:9), 100
PepA:TwinK1 (1:9), 100
NT
Study Groups

5.5) The following exhibits are the unmodified results of Section 3.24

Figure 5.5) DNA content of PepB:TwinK1 (1:9) co-assembled RNTs, PepC:TwinK1 (1:9) co-assembled RNTs, PepC:TwinK1 (1:9) co-assembled RNTs and BMP-7 treated groups on A) day 7, C) day 14. Alkaline Phosphatase activity of PepA self-assembled and co-assembled RNTs and BMP-7 treated groups on B) day 7, D) day 14. Concentration of RNTs are mentioned in the figure. Data was an average of triplicates per treatment.

A)

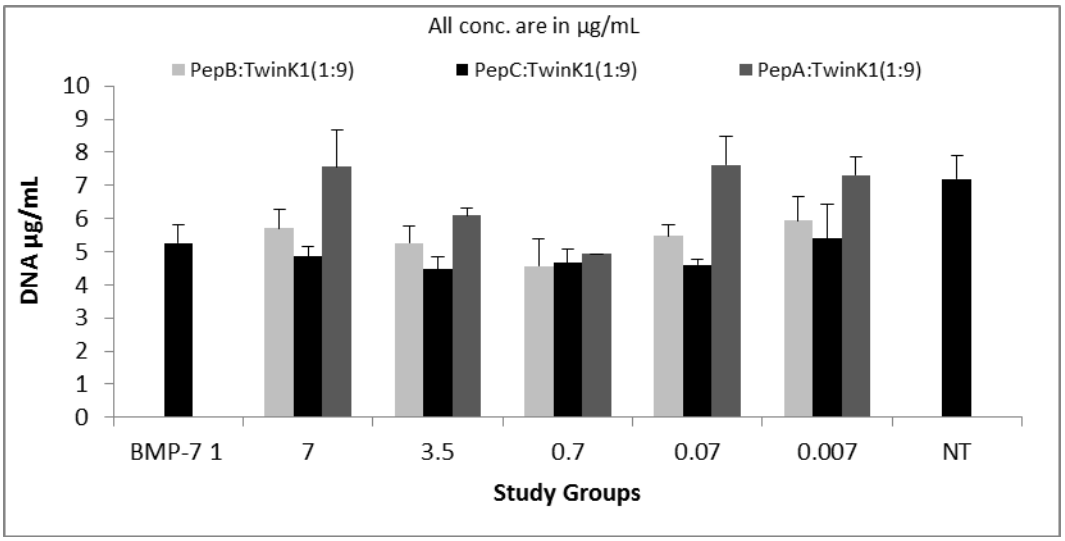

B)

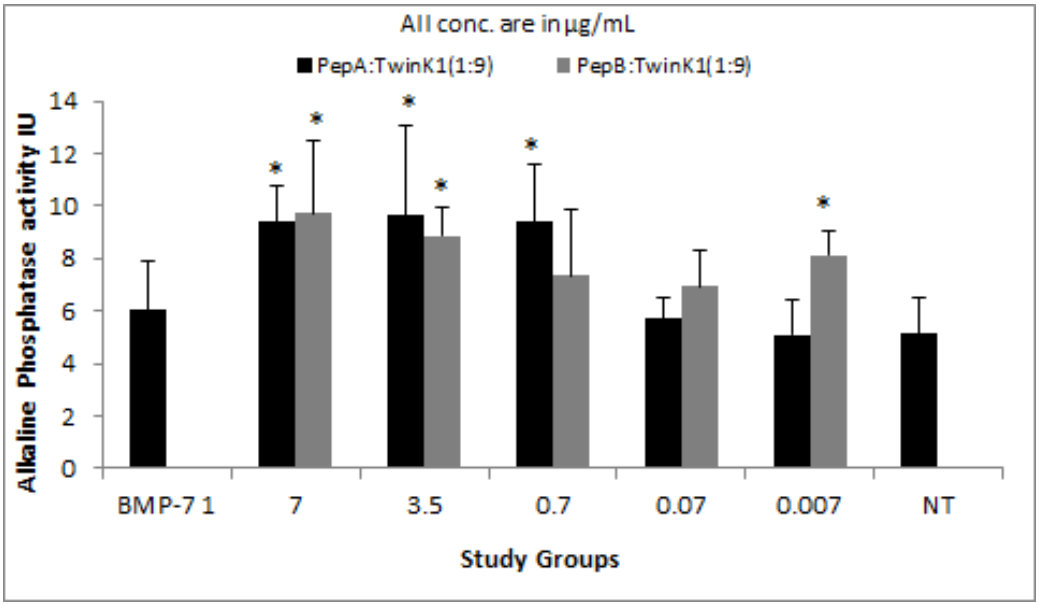
All conc. are in µg/mL
PepA:TwinK1(1:9)
PepB:TwinK1(1:9)
Alkaline Phosphatase activity IU
14
12
10
8
6
4
2
0
BMP-7 1
7
3.5
0.7
0.07
0.007
NT
Study Groups

C)

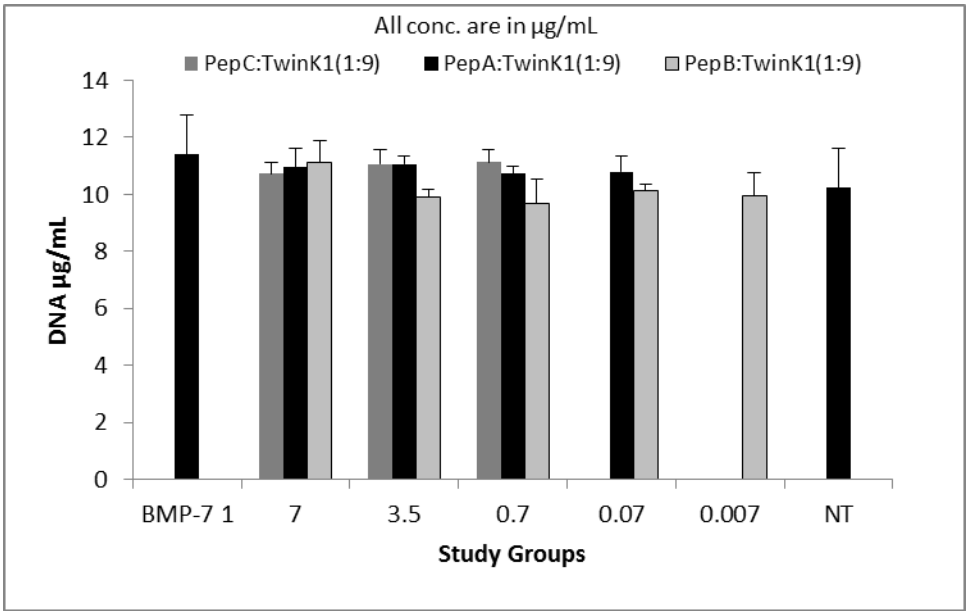
All conc. are in µg/mL
PepC:TwinK1(1:9)
PepA:TwinK1(1:9)
PepB:TwinK1(1:9)
DNA µg/mL
14
12
10
8
6
4
2
0
BMP-7 1
7
3.5
0.7
0.07
0.007
NT
Study Groups

D)

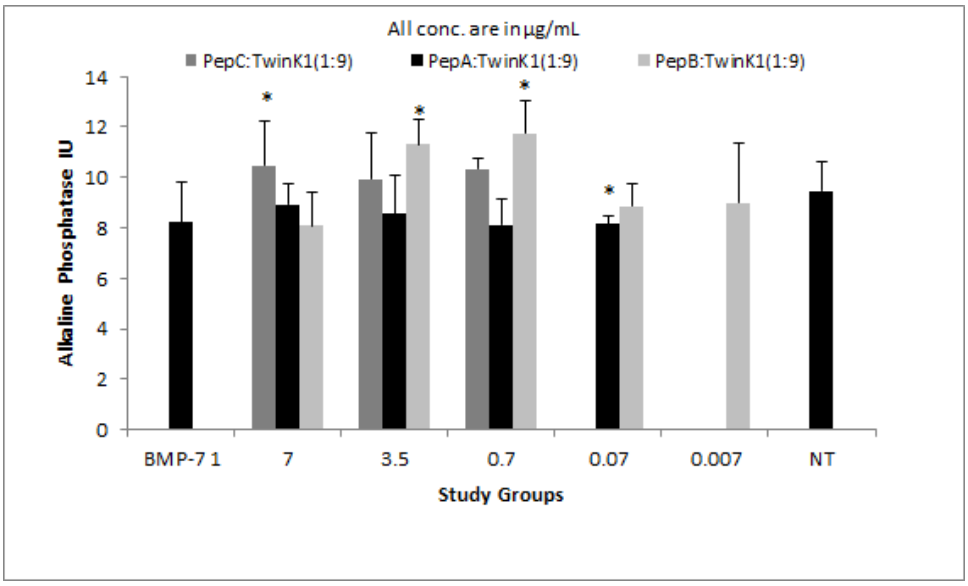

5.6) The following exhibits are the unmodified results of Section 3.25

Figure 5.6) Specific ALP activity of Pep A:TwinK1(1:9) RNTs and Pep C:TwinK1(1:9) RNTs on day 14